Università degli Studi di Milano

PhD Course in Experimental Medicine

CYCLE XXXVIII
PhD thesis

Dissecting the role of the tetraspanin MS4A4A in modulating macrophage plasticity and function

---

Candidate: **Dr. Alessia Troilo**
Matr. ID: R13814
Orcid ID: 0000-0001-9295-655X

Tutor: **Prof. Massimo Locati**

Supervisor: **Prof. Elena Monica Borroni**

Director: **Prof. Nicoletta Landsberger**

Academic Year 2024-2025

INDEX

ABSTRACT 3
DISCLOSURE FOR RESEARCH INTEGRITY 5
ABBREVIATIONS 6
INTRODUCTION 8
1. Macrophages 8
1.1 Macrophage origin 8
1.2 Macrophage functions 9
1.3 Macrophage activation state 11
1.4 Dynamic of macrophages: from inflammation to resolution 13
2. MS4A protein family 15
2.1 MS4A protein structure 15
2.2 MS4A proteins expression 16
2.3 MS4A proteins functions 18
2.3.1 MS4A proteins as ion channel 18
2.3.2 MS4A proteins as immunomodulator 18
3. MS4A4A 20
4. MS4A4A in pathology 22
4.1 MS4A4A in Rheumatoid Arthritis 22
4.2 MS4A4A in Alzheimer's disease 22
4.3 MS4A4A in cancer 23
AIM OF THE THESIS 25
MATHERIALS AND METHODS 26
1. Mice 26
2. Human monocyte-derived macrophages 26
3. MS4A4A silencing by siRNA in human macrophages 26
4. BMDM isolation and cell culture 27
5. RNA extraction, transcription and Real-Time PCR 28
6. Enzyme-Linked Immunosorbent Assay (ELISA) 28
7. Western Blot 28
8. Co-immunoprecipitation 29
9. Flow Cytometry 29
10. Calcium flux assay 30
11. Confocal microscopy 30

12. Sample Preparation for LC-MS/MS analysis 31
13. Liquid Chromatography and Mass Spectrometry 32
14. Data Analysis for LC-MS/MS 32
15. Bulk RNA-seq 34
16. Ingenuity Pathway Analysis (IPA) and Comparative Pathway Analysis 35
17. Statistics 35
RESULTS 36
1. Characterization of the structure and subcellular localization of MS4A4A 36
1.1 Tertiary structure prediction and intrinsic disorder analysis of MS4A4A 36
1.2 Identification and Characterization of Ligand-Binding Pockets in MS4A4A 38
1.3 Structural and Functional Supports for MS4A4A as an Ion Channel 41
1.4 MS4A4A localization in macrophage 45
2. Identification of MS4A4A interacting partners 48
3. Functional characterization of MS4A4A in inflammatory conditions 52
3.1 MS4A4A modulation upon LPS stimulation 52
3.2 Characterization of the impact of MS4A4A on macrophage basal phenotype 54
3.3 Transcriptional profile of MS4A4A KO macrophages after LPS stimulation 54
3.4 Functional role of MS4A4A in LPS-induced macrophages response 61
4. Role of MS4A4A in modulating dexamethasone response in rheumatoid arthritis 75
DISCUSSION 85
ACKNOWLEDGMENTS 94
REFERENCES 95
LIST OF FIGURES AND TABLES 101
APPENDIX 109
DISSEMINATION OF RESULTS 114

ABSTRACT

MS4A4A belongs to the membrane-spanning 4A (MS4A) family, whose proteins show preferential expression in distinct cell types and structural similarities to tetraspanins, including the ability to interact with and modulate the activity of various immunoreceptors, such as pattern recognition receptors (PRRs) and Ig receptors. MS4A4A is selectively expressed by macrophages, and its expression is upregulated upon treatment with Interleukin-4 (IL-4) and glucocorticoids (Dexamethasone, Dex). However, the molecular mechanisms by which MS4A4A exerts its biological function in macrophages remains largely uncharacterised.

MS4A4A has been increasingly studied in relation to several diseases with inflammatory components. Specifically, it has been implicated in Alzheimer's disease, potentially affecting microglial activation. In the context of cancer, we have previously reported that MS4A4A is required for the macrophage-dependent activation of NK cell anti-metastatic functions. Recently, we have shown that MS4A4A+ macrophages are detected in the synovial tissue of rheumatoid arthritis (RA) patients. Although less extensively studied, MS4A4A expression was associated with inflammatory diseases such as sepsis, atherosclerosis, and inflammatory bowel disease. Macrophages are key players in the pathogenesis of these diseases due to their ability to shift between pro-inflammatory and anti-inflammatory phenotypes, allowing them to drive tissue damage or promote repair.

In this context, the present study aimed to characterize the biological function of MS4A4A in macrophages and its involvement in macrophage activation and function.

Firstly, the structure of MS4A4A was investigated and characterised via artificial intelligence analysis and molecular dynamics simulation, to clarify its role in cellular signaling and potentially linking its structure to specific biological outcomes. Then, having observed only minimal differences in the transcriptional profiles between WT and KO macrophages, further investigation focused on the role of MS4A4A in macrophage activation. This led to the identification of two potential partners: the γ-chain of Fc gamma receptors (FcγRs) and Toll-like receptor 2 (TLR2), suggesting a possible involvement of MS4A4A in their inflammatory signaling. In the context of RA, where macrophages show altered FcγRIII expression, MS4A4A expression was found to be upregulated and positively correlated with disease pathogenesis, as well as with FcγRIII and the FcγR γ-chain expression in RA patients. Notably, both MS4A4A and FcγRIII are induced by Dex. MS4A4A was shown to limit the anti-inflammatory effects of Dex during FcγR-mediated inflammation by affecting the release

of TNF-α and CXCL2. This modulatory role of MS4A4A appears to be independent on direct influence on FcγR signaling, and the precise mechanism remains to be defined.

To dissect the role of MS4A4A in macrophage activation mediated by TLR-2, we found that MS4A4A regulates the surface expression of TLR2 and affects the release of the anti-inflammatory cytokine IL-10. This impairment in IL-10 release is not limited to TLR2 stimulation but is also observed with other TLR agonists. Notably, during LPS stimulation, the reduced IL-10 release persists over time, starting as early as 2 hours post-stimulation. Further analysis showed that LPS induces MS4A4A expression and led to the identification of an IL-10 storage pool in resting macrophages. The defect in IL-10 release may result from a role of MS4A4A in regulating IL-10 de novo synthesis and/or the mobilization of this intracellular IL-10 pool. This study provides a valuable contribution to the field, expanding the current knowledge of MS4A4A's role in macrophage activation and its impact on inflammatory response.

DISCLOSURE FOR RESEARCH INTEGRITY

The research was conducted following the European Code of conduct for research integrity.

ABBREVIATIONS

AD = Alzheimer’s disease

Agg-IviG = Aggregated intravenous immunoglobulin G

Dex = Dexamethasone

BMDM = Bone Marrow Derived Macrophages

Co-IP = Co-Immunoprecipitation

CS = Corticosteroid

DMARDs = Disease-Modifying Anti-Rheumatic Drugs

ELISA = Enzyme-linked immunosorbent assay

ER = Endoplasmic Reticulum

FcγR = Fc gamma Receptor

FCER1G = Fc Receptor Gamma-Chain gene

FCGR3A = FcγRIIIa, Fc gamma Receptor III A

FcεRI = Fc Receptor Gamma-Chain

H-89 = H-89 dihydrochloride

IL- = Interleukin-

IPA = Interpretative Phenomenological Analysis

KO = MS4A4A Knock Out

LPS = Lipopolysaccharide

M-CSF = Macrophage Colony Stimulating Factor

MS4A = Ganulocyte-macrophage colony stimulating factor

NT = Not Treated

PAMPs = Pathogen Associated Molecular Patterns

PCA = Principal Component Analysis

PKA = Protein Kinase A

P3C4 = Pam3CysSerLys4 (PAM3CSK4)

qPCR = Quantitative real time Polymerase Chain Reaction

RA = Rheumatoid Arthritis

RNAseq = RNA sequencing

ROS = Reactive Oxygen Species

STIA = Serum Transfer-Induced Arthritis

TGN = Trans-Golgi Network

TLR- =Toll Like Receptor-

WB = Western Blot

WT = Wild Type

INTRODUCTION

1. Macrophages

Macrophages are innate immune cells that belong to the mononuclear phagocyte system, which also includes monocytes and dendritic cells. The term "macrophage" is derived from the Greek roots *macro-* (large) and *-phage* (eater), reflecting their phagocytic activity. Although macrophages are distributed throughout virtually all tissues, they are particularly abundant in the gastrointestinal tract, liver, spleen, upper respiratory tract and central nervous system. These cells can sense a wide array of stimuli, including viral, bacterial, and microbial antigens, immune complexes, apoptotic and necrotic cells, as well as soluble mediators released by other immune and non-immune cells. Signals from the surrounding microenvironment are integrated by macrophages to elicit context-dependent responses. Through this capacity, macrophages play essential roles in host defence, tissue remodelling and the maintenance of homeostasis. However, dysregulation of macrophage functions can contribute to the development and progression of various pathological conditions, including cancer, obesity, and fibrosis (1).

1.1 Macrophage origin

For many years, it was widely accepted that tissue-resident macrophages originated exclusively from circulating monocytes, which in turn derive from multipotent hematopoietic stem cells (HSCs) located in the bone marrow. These stem cells give rise to both myeloid and lymphoid lineages, with monocytes specifically developing from the myeloid lineage. Upon encountering inflammatory signals, monocytes are recruited from the bloodstream into affected tissues, where they differentiate into macrophages (2). However, several studies have challenged this traditional view, demonstrating that a significant proportion of tissue macrophages originate from embryonic progenitors. Indeed, fate-mapping studies demonstrated that certain tissue-resident macrophages establish their niches before birth and can sustain their populations independently of bone marrow-derived progenitors throughout adult life (3). Supporting this, numerous mouse studies have confirmed adult tissue-resident macrophages such as Kupffer cells, Langerhans cells, microglia and alveolar macrophages(4–6). Research has demonstrated that erythroid-myeloid progenitors (EMPs) originate from Tie2+ cells in the yolk sac, migrate to the fetal liver, and there expand and differentiate into various blood cell types including erythrocytes, megakaryocytes,

macrophages, monocytes, granulocytes and mast cells(7). Furthermore, Schulz et al. showed that mice lacking c-Myb are still capable of generating fetal F4/80^{bright} macrophages and sustaining the adult F4/80^{bright} macrophage population independently of bone marrow-derived progenitors (8). All these data support the theory that tissue-resident macrophages are derived from yolk-sac progenitors and not from bone marrow hematopoietic stem cells. Although some of tissue-resident macrophages can be replaced by bone marrow progenitors, they possess the capacity for self-maintenance via local proliferation, a process known as *self-renewal*. This mechanism is regulated by cytokines and growth factors such as CSF1, CSF2, IL-4 and estrogens (9).

Functionally, monocyte-derived macrophages are primarily involved in immune defence and responses to injury or infection, contributing minimally to tissue homeostasis. In contrast, embryonically derived tissue-resident macrophages play essential roles in maintaining tissue homeostasis, supporting organ function, and facilitating tissue remodelling.

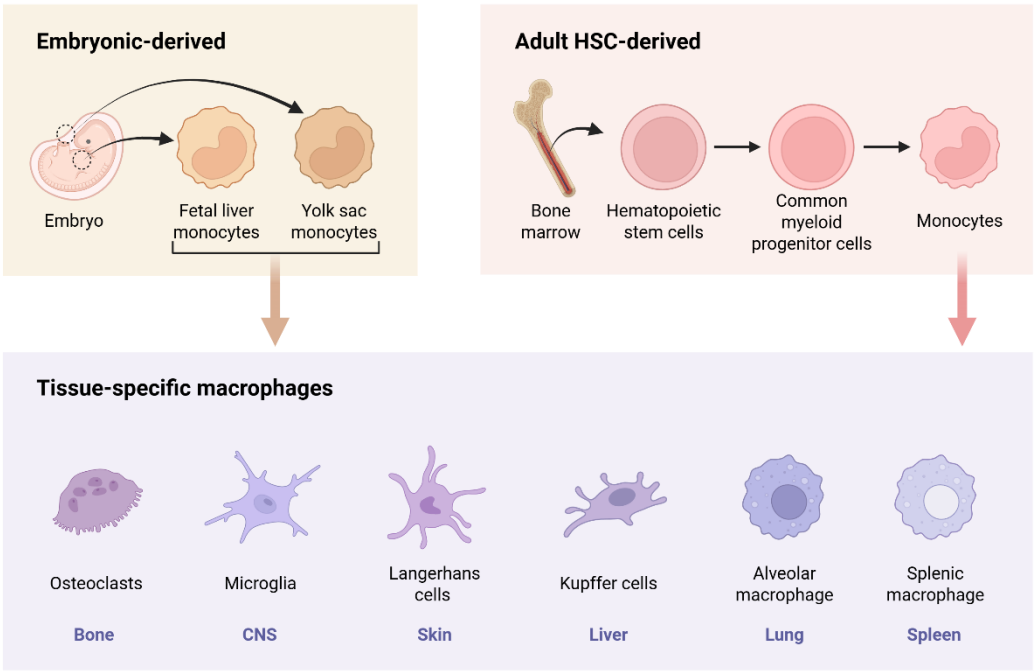

Figure 1. Origin and development of macrophages. Created with BioRender.

1.2 Macrophage functions

Macrophages are highly versatile immune cells that adapt dynamically to environmental signals. They play essential roles in preserving tissue homeostasis, regulating immune responses, promoting tissue repair, and, in some contexts, contributing to disease progression.

Despite their morphological and functional diversity, macrophages carry out four key activities:

1. Phagocytosis is a key mechanism by which macrophages internalize and break down pathogens, apoptotic cells and cellular debris. Macrophages recognize their targets via specific surface receptors (pattern recognition receptors – PRRs - and opsonin) that bind microbial structures or opsonized materials. Once recognition occurs, the target enters in a membrane-bound compartment known as a phagosome. The phagosome then merges with lysosomes to form a phagolysosome, where hydrolytic enzymes mediate the breakdown of the internalized material. Phagocytosis triggers a pro-inflammatory response characterizing bye degradation of pathogenic components that results in the release of pro-inflammatory molecules that recruit and activate other immune cells (10,11).
2. Efferocytosis represents a specialized subset of phagocytosis focused on the removal of apoptotic cells. It is an anti-inflammatory response that supports tissue regeneration and immune tolerance. The identification of apoptotic cells occurs through two primary mechanisms involving either direct or indirect recognition of phosphatidylserine (PS), a key "eat-me" signal exposed on the outer leaflet of the apoptotic cell membrane. Following recognition and binding, apoptotic cells are internalized in a tightly regulated manner, thereby preventing secondary necrosis and the subsequent release of damage-associated molecular patterns (DAMPs), which could otherwise initiate an immune response (10).
3. Secretion of cytokines and chemokines. Macrophages release cytokines, chemokines, growth factors and enzymes that shape immune responses and affect the other cells. Pro-inflammatory mediators, such as TNF-α and IL-1β, play a key role in initiating and sustaining inflammation, while anti-inflammatory cytokines (e.g. IL-10 and TGF-β) help to suppress inflammation and support resolution. Through these secretory activities, macrophages contribute to host defence against pathogens and to processes of tissue remodelling and repair (12). Cytokine secretion is regulated at multiple steps: including gene transcription, protein translation and processing within cellular organelles like the ER and Golgi. Macrophages release cytokines through the continuous (constitutive) secretion pathway or via alternative routes. Proteins destined for secretion are transported from the ER to the Golgi, then sorted in the trans-Golgi network (TGN), and finally delivered to the cell surface either directly or through recycling endosomes. However, non-traditional cytokine release mechanisms are still not fully understood.

4. Antigen presentation is a vital mechanism that links innate and adaptive immunity. Macrophages, as professional antigen-presenting cells (APCs), play a central role by capturing, processing and presenting antigens to T cells. They interact with $CD4^+$ helper and $CD8^+$ cytotoxic T cells influencing activation and regulation of the immune response. Macrophages present antigens to T cells via major histocompatibility complex: MHC class II displays extracellular antigens to $CD4^+$ T cells, while MHC class I presents intracellular antigens to $CD8^+$ T cells, helping responses against both external and internal threats. The antigen uptake from macrophages is followed by their degradation into peptides in the endolysosome. These peptides are then loaded onto MHC molecules and transported to the cell surface for recognition by T-cell receptors (TCRs). Co-stimulatory molecules like CD80 and CD86 further enhance T-cell activation and differentiation. Macrophages can also perform cross-presentation, where extracellular antigens are presented on MHC class I molecules (12).

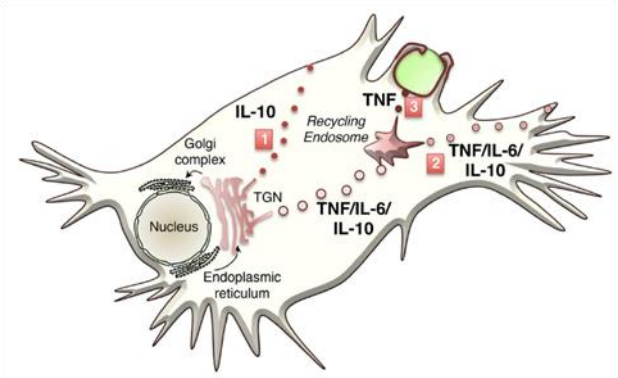

B

Protein	TNF	IL-6	IL-10
iRhom2	+	NA	NA
p230	+	+	+
Golgin-97	–	–	+
CCTα	+	+	ND
PI3K p110δ	+	ND	–
Dynamin 2	+	ND	ND
Stx4	+	ND	+
Stx6	+	+	+
Vti1b	+	+	+
VAMP3	+	+	+
SNAP23	+	ND	+
SCAMP5	+	+	ND
Rab6	+	ND	ND
Rab11	+	ND	+
Rab37	+	ND	ND
Munc13-1	+	ND	ND
AP-1	+	ND	ND
Syt XI	+	+	ND
PKA	ND	ND	+
Rac1	+	ND	ND
CDC42	+	ND	ND

NA, not applicable; ND, not determined.

Figure 2. Classical transport pathways used to secrete macrophage cytokines. (A) Three major transport pathways for cytokine secretion have been identified to date. The first involves direct transport to the cell surface (IL-10) from the TGN, the second pathways routes cytokines via the recycling endosome and the out to the cell surface (TNF, IL-6 and IL-10), and the 3 rd pathway occurs during phagocytosis where cytokine (TNF) is routed from the recycling endosome to the phagocytic cup. (B) Trafficking machinery that regulate cytokine secretion in macrophages.

1.3 Macrophage activation state

While macrophage developmental origins determine their tissue distribution and longevity, their functional specialization is dynamically regulated by polarization states - a continuum

bridging embryonic programming and environmental cues. Historically and schematically, macrophages have been divided into two forms of macrophage activation, often referred to as M1 (or classic) and M2 (or alternative) (**Figure 3**). M1 macrophages may be induced in vitro by bacterial products and interferons produced during type 1 immune responses driven by type 1 T helper and innate lymphoid cells, whereas M2 macrophages are induced by cytokines produced during type 2 immune responses driven by type 2 T helper and innate lymphoid cells, such as IL-4 and IL-13(13). M1 macrophages are primarily associated with pro-inflammatory responses, tissue damage and anti-tumor activity. They secrete a broad range of inflammatory cytokines, including TNF-α, IL-1α, IL-1β, IL-6, IL-12, IL-18 and IL-23, and express chemokines such as CX3CL1 that enhance Th1 responses. In the tumor microenvironment, M1 macrophages contribute to anti-tumor immunity by recruiting NK cells and $CD8^+$ T lymphocytes through their cytokine output. They are characterized by high expression of surface and intracellular markers including CD40, CD80, CD86, iNOS, Ly6C, TLRs, ROS, COX-2, CCL5, and MHC class II molecules (14).

In contrast, M2 macrophages promote tissue repair, remodelling and resistance to parasites. They secrete anti-inflammatory cytokines such as IL-10 and TGF-β and support angiogenesis and regeneration through the release of growth factors like VEGF. Their phenotype is defined by the expression of markers such as dectin-1, DC-SIGN, mannose receptor, scavenger receptors A and B1, CD163, CCR2, and CXCR1/2. While beneficial for wound healing, M2-like activity can also contribute to tumor growth and fibrosis (14,15). Furthermore, the M2 phenotype can be subdivided into four distinct subclasses:

1. M2a macrophages, induced by IL-4, IL-10, IL-13, and PPARγ, are involved in parasite clearance and are marked by the expression of CD45, CD206, YM1, RELMα, IGF1, DCIR, Stabilin-1 and factor XIII-A.
2. M2b macrophages, generated by stimulation with LPS and IL-1β, play key roles in immunoregulation and are identified by markers such as CD86 and SPHK1.
3. M2c macrophages, which arises following exposure to glucocorticoids and/or IL-10, is implicated in tissue repair and extracellular matrix remodelling, and expresses markers including MerTK, CD136, and CD206.
4. M2d macrophages, often associated with tumor-associated macrophages (TAMs), exhibit angiogenic properties. They can be induced by stimuli such as LPS, TLR ligands, TNF-α, IL-6 and IL-10(15).

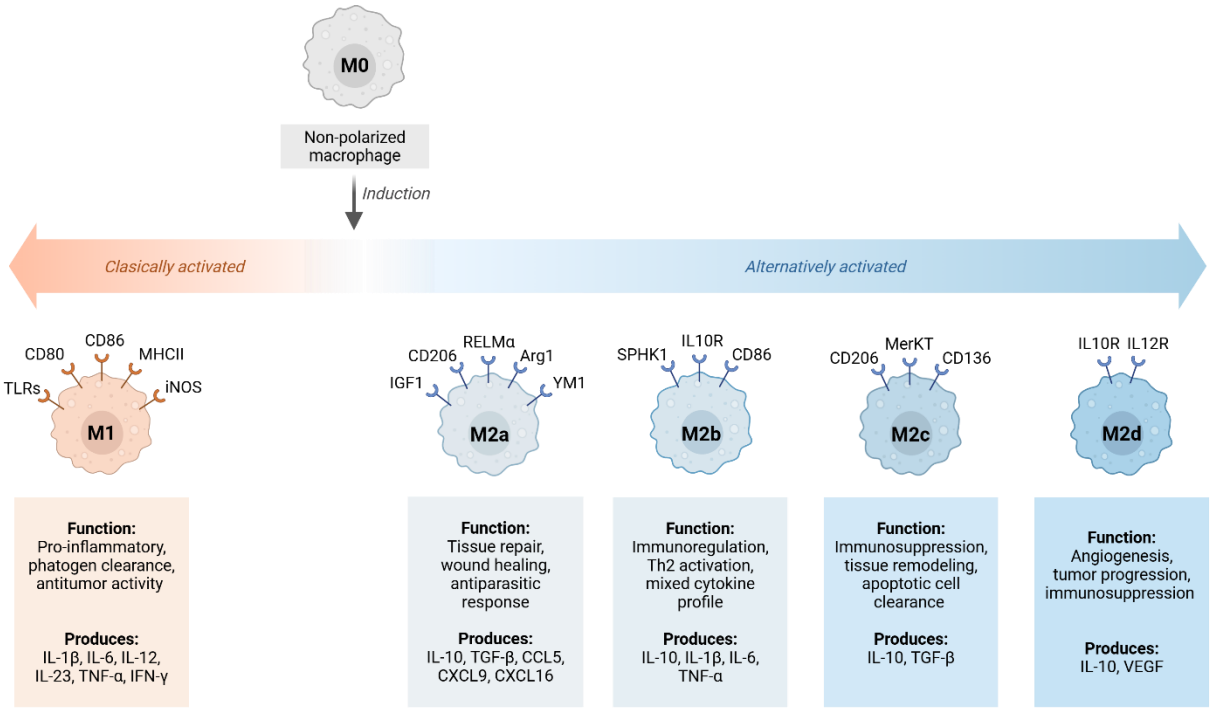

Figure 3. Spectrum of macrophage polarization from M0 to M1 and M2 phenotype. Created with BioRender.

Macrophage polarization is a dynamic and flexible process that allows macrophages to adopt a range of functional profiles in response to environmental signals. While the classical M1/M2 model highlights two opposing activation states, recent studies have identified numerous intermediate phenotypes that fall outside this traditional framework (12,13) . For instance, M4 macrophages, induced by platelet factor 4 (CXCL4), display both pro-inflammatory and foam cell-like features and are involved in atherosclerosis (16). Mox macrophages, generated under oxidative stress, exhibit unique transcriptional profiles driven by NRF2-dependent gene expression and contribute to tissue remodeling (17). During the resolution of inflammation resolving macrophages (Mres) remove apoptotic cells and release anti-inflammatory mediators to promote tissue repair and restore homeostasis (18). These specialized subtypes highlight the complexity of macrophage biology and support a shift toward a more context-dependent classification system beyond the traditional M1/M2 dichotomy.

1.4 Dynamic of macrophages: from inflammation to resolution

Following injury or infection, damage-associated molecular patterns (DAMPs) from necrotic cells and pathogen-associated molecular patterns (PAMPs) are recognized by innate immune receptors like Toll-Like receptors (TLRs) on tissue-resident cells. This detection

triggers the release of proinflammatory chemokines (e.g., CXCL1, CXCL2, CXCL5, CXCL8, CX3CL1) and cytokines (e.g., TNF, IFN-γ, IL-1β, IL-6, IL-33, and various growth factors). These chemokines recruit immune cells to the injury site, including monocytes from the bone marrow that enter the tissue and differentiate into proinflammatory, classically activated (M1-like) macrophages. Together with neutrophils, they clear dead cells and debris while releasing proinflammatory mediators and reactive oxygen species (ROS) to prevent pathogen spread and promote further immune cell recruitment (15).

Inflammation resolution is triggered by effector cells that induce inhibition of pro-inflammatory profiles and transition toward tissue repair and homeostasis. Initially, dampening of acute inflammation starts only once the injurious agents responsible for triggering the inflammatory response are eliminated. Afterward, the production of pro-inflammatory mediators stops, and any remaining mediators are degraded and cleared. This results in the downregulation of proinflammatory signaling and arrestin further leukocyte recruitment and edema formation (19,20).

Resolution is an active process involving:

1. Clearance of dying immune cells through efferocytosis by macrophages.
2. A shift in macrophage function toward anti-inflammatory activity.
3. Production of mediators that promote repair and tissue regeneration.

During this phase, classically activated macrophages (M1) shift to alternatively activated anti-inflammatory (M2) phenotype. Efferocytosis enables this transition, resulting in a decrease in pro-inflammatory cytokines and increased levels of anti-inflammatory mediators such as IL-10 and TGF-β(21). These pro-resolution macrophages also express regulatory molecules (e.g., PDL1, ICOS ligand), produce fewer inflammatory cytokines (e.g., TNF, IL-1β, IL-18), and generate specialized pro-resolving lipid mediators (SPMs), promoting tissue recovery and restoration of homeostasis (21).

2. MS4A protein family

In the early 2000s, Ishibashi and colleagues formally designated a group of genes encoding tetraspanin-like proteins as the *membrane-spanning four-domains subfamily A* (MS4A), although individual members of this family had been identified several years earlier(22). The first three members - CD20 (MS4A1), MS4A2 (FcεRIβ), and MS4A3 (HTm4) - were cloned between the late 1980s and early 1990s, revealing a high degree of sequence homology (23–25). Currently, the MS4A family comprises 18 genes located on chromosome 11q12 in the human genome, and 23 orthologous genes mapped to chromosome 19 in mice (22). Although MS4A proteins are increasingly recognized as a novel class of regulators in immune cell activation, the expression patterns, interaction networks, and biological functions of most family members remain poorly understood.

2.1 MS4A protein structure

The structure of MS4A proteins shares topological similarities with the well-characterized tetraspanin superfamily; however, the two families do not exhibit significant sequence homology (**Figure 4**). MS4A proteins are typically defined by four predicted hydrophobic transmembrane domains connected by one intracellular and two extracellular loops, with both the N- and C-termini located on the cytoplasmic side (26). Unlike tetraspanins, the second extracellular loop in MS4A proteins is considerably longer - approximately 20–90 amino acids, compared to 8–21 in tetraspanins. Moreover, MS4A proteins lack the conserved cysteine-cysteine-glycine motifs found in tetraspanins, which facilitate disulfide bond formation in their extracellular regions (27). Their transmembrane domains also lack the polar residues characteristic of tetraspanins (28).

Most MS4A members share a moderate degree of sequence similarity with MS4A1 (approximately 20–32%), with the highest conservation found in the first three transmembrane domains, which contain several conserved motifs. This conservation suggests that these transmembrane segments play a critical and common role in MS4A protein function. By contrast, the most variable regions are found in the N- and C-terminal cytoplasmic domains and in the second extracellular loop, likely contributing to functional diversity among MS4A proteins. Additionally, the cytoplasmic termini of MS4A proteins are rich in proline residues. Although their exact role remains unclear, proline-rich domains are commonly involved in key cellular processes such as cytoskeletal organization, transcriptional regulation and signal transduction. These regions are also known to bind SH3

domains, suggesting they may facilitate protein-protein interactions through adaptor functions (29).

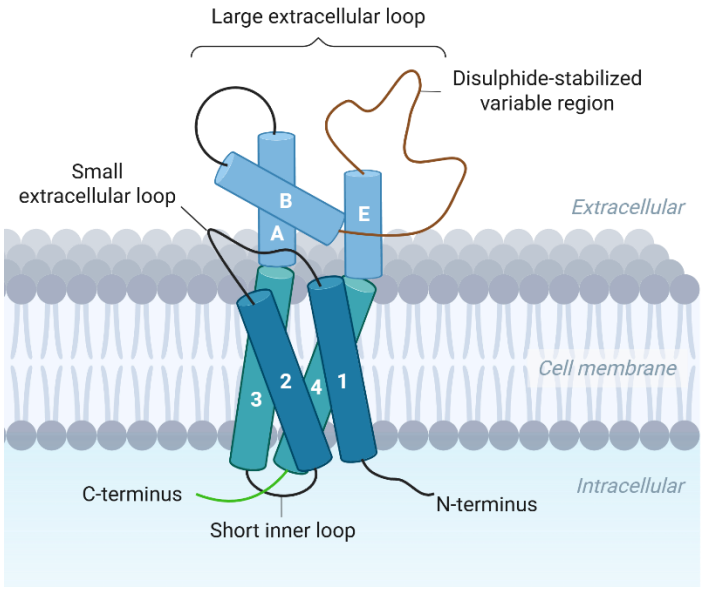

Figure 4. The tetraspanins structure. The full-length protein adopts a compact, rod-like conformation composed of four transmembrane (TM) helices (shown in light and dark grey, labelled 1–4). Connecting TM domains 3 and 4 is a large extracellular loop (spanning 70–130 amino acids), which includes a conserved helical segment (comprising helices A, B, and E, shown in blue) and a variable region (depicted in dark red, located between helices B and E). This variable region often plays a key role in interacting specifically with partner proteins. Although not illustrated, this segment is usually stabilized by two to four conserved disulfide bonds. A smaller extracellular loop (13–30 amino acids) links TM helices 1 and 2. Tetraspanins generally feature short cytoplasmic tails at both the amino and carboxy termini (6–19 amino acids) and possess a small intracellular loop of approximately 4 amino acids (30). Created with BioRender.

2.2 MS4A proteins expression

While some members - such as MS4A1 (CD20), MS4A2 (FcεRIβ), and MS4A3 (HTm4) - exhibit expression largely restricted to the hematopoietic system, other MS4A family members are found in diverse non-hematopoietic tissues (**Figure 5**).

In both humans and mice, MS4A1 is primarily expressed by B cells, MS4A2 by mast cells and basophils, and MS4A3 by progenitor cells of the myeloid and lymphoid lineages (23–25,31). Correspondingly, MS4A1 is highly expressed in lymphoid tissues such as the spleen and lymph nodes, while MS4A2 and MS4A3 show enriched expression in the bone marrow, where hematopoietic precursors reside. MS4A5 is expressed only in a specific myelomonocytic cell line, and MS4A13 and MS4A14 expression is confined to the testis.

Additionally, MS4A12 has been identified on the apical membrane of colon epithelial cells in healthy human tissues (32).

Two distantly related genes, TMEM176A (HCA112) and TMEM176B (LR8/TORID), share 10–20% sequence identity with other MS4A proteins but are located on a different chromosomal locus (chromosome 7q36.1 in humans). Unlike most MS4A family members, TMEM176A and TMEM176B are broadly expressed, including in immature and resting dendritic cells (particularly $CD4^+$ DCs) in both rats and humans, and similar patterns have been described in mice. More recent studies also report TMEM176 expression in $ROR\gamma t^+$ lymphocytes, which include both Th17 cells and group 3 innate lymphoid cells (ILC3s), in humans and mice (32).

A novel dimension of MS4A gene distribution emerged from the discovery that a subset of MS4A genes is expressed in mammalian olfactory sensory neurons (OSNs) (33). Among them MS4A8, MS4A10, and MS4A15, MS4A4A, MS4A6A, and MS4A7 are included. Within the hematopoietic system, transcriptional profiling of human macrophages revealed high expression of MS4A4A and MS4A6A (34). MS4A4A expression has also been observed in human mast cells, and its expression has been validated in macrophages across various tissues such as colon, lungs and skin (35,36). Both MS4A4A and MS4A6A are expressed in human microglia, and MS4A7 has been proposed as a marker distinguishing HSC-derived microglia-like macrophages in mice (37). Ms4a8a, the murine homolog of MS4A8, has been identified in TAMs (38).

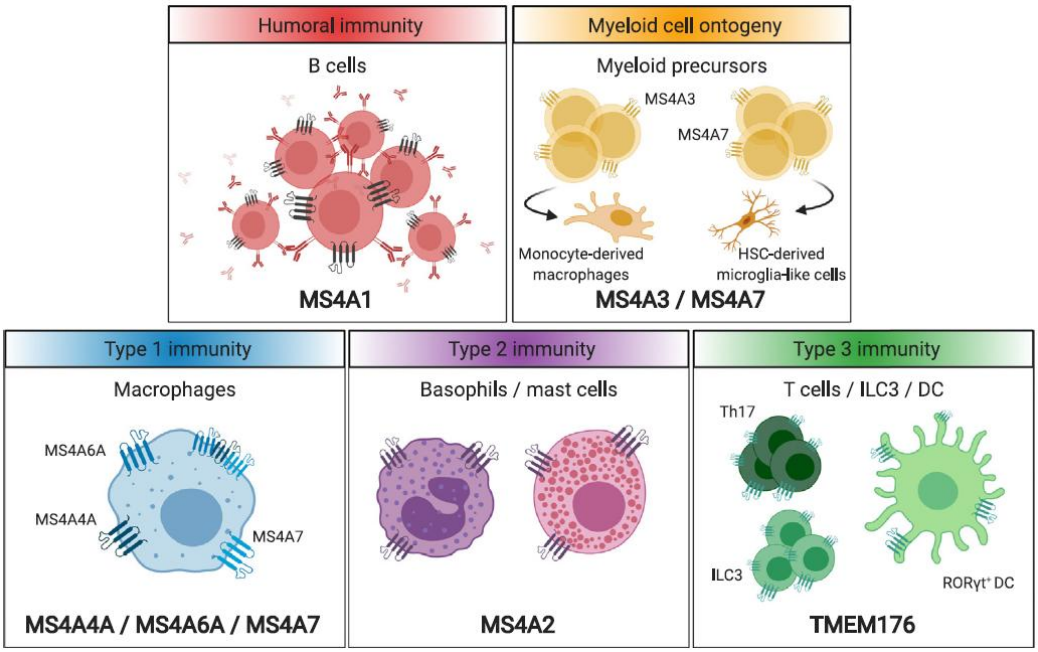

Figure 5. Expression pattern of membrane-spanning 4A (MS4A) proteins in different leukocyte subsets (32).

2.3 MS4A proteins functions

The biological functions of many MS4A family members remain poorly defined. Among the family, MS4A1 and MS4A2 are the most extensively studied and best understood in terms of their regulatory functions. Current evidence indicates that MS4A proteins may function as ion channels, modulators of immune receptors, or both (**Figure 6**).

2.3.1 MS4A proteins as ion channel

Recent evidence from the literature supports the hypothesis that members of the MS4A protein family may function as ion channels or channel regulators. MS4A1 (CD20), the most studied member, has been shown to form homo-tetramers that closely resemble the structure of the ion channel Orai1, suggesting a potential channel-like function. Transfection of MS4A1 into various cell lines leads to enhanced Ca^{2+} conductance, and its interaction with the B cell receptor (BCR) enhances BCR-induced cytoplasmic Ca^{2+} mobilization, indicating a role in calcium signaling (39,40). Similarly, MS4A12 expression in transfected cells significantly increases calcium influx, reinforcing the idea that certain MS4A members contribute directly to Ca^{2+} regulation(41) . MS4A2 (FcεRIβ), a component of the high-affinity IgE receptor complex in mast cells, has been proposed as a pore-forming subunit, as truncated forms impair antigen-induced Ca^{2+} signaling and downstream phosphorylation events (32). TMEM176B has been identified as a non-selective monovalent cation channel activated by extracellular acidification in *Xenopus* oocytes, suggesting a role in counterion conductance within acidifying compartments such as phagosomes. Its homolog, TMEM176A, exhibits similar acid-activated channel activity (42). MS4A4A, functionally related to MS4A2, has been shown to regulate Orai1-mediated calcium entry (43). Overall, these findings point to a broader role for MS4A proteins in ion transport and particularly involving Ca^{2+}.

2.3.2 MS4A proteins as immunomodulator

The second reported function of MS4A proteins is their ability to modulate the activity of other immunoreceptors. As said before, they share a four-pass transmembrane topology similar to that of tetraspanins, which are known to cluster into lipid rafts upon cell activation to form specialized microdomains where they physically associate with other membrane receptors and modulate downstream signaling. This functional analogy is supported by early evidence showing that CD20 (MS4A1) colocalizes with the B cell receptor (BCR) in lipid rafts

of human B cell lines and it can associate with MHC class I and II, CD53, CD81, CD82, CD40, although the precise functional relevance of these interactions remains to be fully elucidated (29,32). Another well-characterized family member, MS4A2, forms a tetrameric complex with FcεRIα and FcRγ in mast cells and basophils, where it plays a crucial role in IgE-mediated activation. Unlike in rodents, where MS4A2 is essential for FcεRI surface expression, in humans the receptor can also form $\alpha\gamma_2$ trimers in other immune cells such as monocytes and dendritic cells. MS4A2 is notably the only MS4A protein known to possess a canonical ITAM motif, contributing to the initiation of Syk-dependent signaling cascades upon antigen stimulation (29). Murine Ms4a6d, the homolog of human MS4A6A, interacts with the complement receptor Vsig4 in tissue-resident macrophages, functioning as a membrane adaptor that recruits JAK2 and activates the STAT3/A20 axis, ultimately dampening NF-κB activity and inflammatory gene transcription (44). MS4A4A has been shown to localize with KIT in the early endosome of the LAD-2 human mast cell line after stem cell factor (SCF) exposure, supporting its trafficking to the plasma membrane, recruitment to caveolin-1-enriched lipid rafts and endocytosis (36). Moreover, in human macrophages it interacts with itself MS4A6A, MS4A7, Dectin-1 and TREM2 (35,45). Collectively, these findings point to a conserved immunomodulatory function across MS4A proteins, operating through diverse receptor interactions.

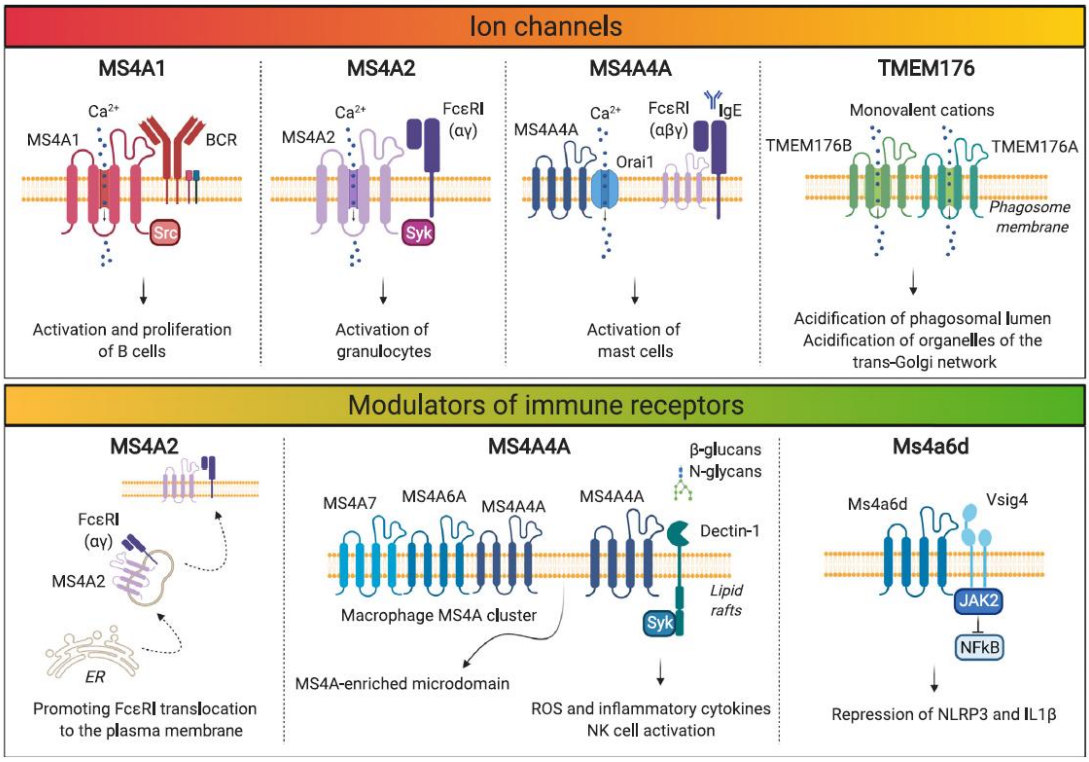

Figure 6. Multifaceted functions of hematopoietic cell-restricted membrane-spanning 4A (MS4A) proteins (32).

3. MS4A4A

MS4A4A exhibits a highly restricted expression pattern within the human immune system, being primarily expressed by macrophages (34,35). Its expression is considerably lower in a small subset of dendritic cells, monocytes and mast cells and is absent from granulocytes, NK cells, T cells, B cells, and hematopoietic progenitor populations (34,35).

At the tissue level, MS4A4A, along with its close homologs MS4A6A and MS4A7, is highly expressed in macrophage-rich organs, including the lung, liver, spleen, colon and placenta, as well as within central nervous system (CNS) microglia (34,35). Also in vivo, combined staining confirmed that MS4A4A expression was restricted to the CD163+ macrophages (35). These results indicate that MS4A4A expression is restricted to tissue resident macrophages.

Its expression progressively increased, both at the mRNA and protein level, during MCSF-dependent human monocyte differentiation to macrophages in contrast to other MS4A proteins. It is upregulated by immunomodulatory signals such as IL-4 and glucocorticoids (e.g., dexamethasone) (34,35,46). These findings suggest MS4A4A as a molecular marker of differentiated macrophages, particularly of alternatively activated macrophages.

Functionally, MS4A4A seems to affect the polarization of macrophages toward an M2-like pehnotype, which is typically associated with anti-inflammatory functions, tissue repair and tumor progression. Experimental silencing of MS4A4A using siRNA impairs the expression of key M2-associated genes, such as *Arg1*, *Fizz1*, *Mgl2*, and *Tgfb1*, while overexpression of MS4A4A leads to a significant increase in the expression of these markers (47). Some studies have show that *Arg1* is tightly regulated by MS4A4A, whereas other classical M2 markers - such as *Ym1*, *Mrc1*, *Marco*, and *Jmjd3* - remain largely unaffected, suggesting a gene-specific regulatory mechanism (48). In tumor-associated macrophages (TAMs), MS4A4A overexpression enhances the secretion of immunosuppressive cytokines IL-10 and TGF-β1, promoting an immunosuppressive microenvironment favourable to tumor progression (49). The hypothesis is that MS4A4A exerts these effects via activation of the JAK/STAT (notably STAT3 and STAT6) and PI3K/AKT/mTOR pathways. These signaling cascades are well-established mediators of M2 polarization, and pharmacologic inhibition of the PI3Kγ isoform can reverse MS4A4A-induced M2 skewing, highlighting a potential therapeutic target (47).

Beyond its expression and functional role in polarization, MS4A4A forms part of a protein interaction network within macrophage membrane microdomains – as mentioned before. It

was shown to physically interact with itself (homodimerization) and with other macrophage-enriched MS4A family members, namely MS4A6A and MS4A7, suggesting the formation of homo- and hetero-oligomeric complexes in the plasma membrane (35). These complexes likely contribute to the organization of specialized membrane domains, particularly lipid rafts, which are crucial for signal transduction. MS4A4A also interacts with several functionally important membrane proteins. One of its confirmed partners is Dectin-1, a pattern recognition receptor (PRR) that recognizes β-glucans from fungal cell walls. Upon fungal challenge with ligands such as zymosan, MS4A4A and Dectin-1 co-localize within lipid rafts, facilitating the activation of the Syk kinase pathway. This interaction is essential for the downstream production of reactive oxygen species (ROS) and pro-inflammatory cytokines (e.g., IL-6, TNF). Disruption of lipid rafts or genetic ablation of *Ms4a4a* in conditional knockout mice results in impaired Syk phosphorylation and reduced cytokine production, without affecting phagocytosis itself, indicating a specific role for MS4A4A in signal transduction rather than cargo internalization(35).

Another protein partners of MS4A4A is TREM2, a lipid-sensing receptor expressed on myeloid cells, with which MS4A4A co-localizes in caveolin-1-positive lipid rafts, suggesting potential cooperation in lipid-mediated signaling processes (45).

Together, these findings highlight MS4A4A as a multifunctional protein that actively contributes to macrophage functional polarization, immune regulation, and responsiveness to environmental cues via interactions with key receptors and signaling molecules. Its selective expression and mechanistic involvement in macrophage biology make it a promising target for therapeutic strategies aimed at modulating macrophage behaviour in diseases such as cancer, chronic inflammation, and autoimmune disorders.

4. MS4A4A in pathology

4.1 MS4A4A in Rheumatoid Arthritis

Rheumatoid arthritis (RA) is the most common chronic inflammatory autoimmune disease affecting joints. It is characterized by synovial hyperplasia and immune cell infiltration, leading to cartilage and bone damage. A wide range of therapeutic options is available to treat RA, including conventional synthetic disease-modifying anti-rheumatic drugs (csDMARDs) (e.g., methotrexate) and biologic targeted agents (bDMARDs) (e.g., TNF and IL-6 inhibitors) (50). However, many patients still require corticosteroids, despite their adverse effects and limited long-term use such as osteoporosis, infections or cardiovascular events, and resistance (51). MS4A4A is highly expressed in $CD163^{+}$ macrophages found in the synovial tissue of early-stage RA patients and its expression is further upregulated in response to the corticosteroids Dexamethasone (Dex) (35). Moreover, MS4A4A expression has been observed in other autoimmune conditions (cutaneous systemic sclerosis, polyangiitis and Kawasaki disease), indicating a broader relevance in immune-mediated diseases (52). Therapeutic antibodies targeting related MS4A family members, MS4A1/CD20 (targeted by rituximab), have already revolutionized RA treatment, and ongoing research may position MS4A4A as a promising biomarker or therapeutic target in RA (53).

4.2 MS4A4A in Alzheimer's disease

Alzheimer’s disease (AD), the most common neurodegenerative disorder, is strongly influenced by genetic factors, as highlighted by genome-wide association studies (GWAS) that have identified over 70 risk loci (33). Many of these loci contain genes highly expressed in microglia, the brain's resident immune cells. One such gene is TREM2, which encodes a transmembrane receptor involved in microglial activation, survival and phagocytosis. TREM2 also exists in a soluble form (sTREM2) in the cerebrospinal fluid (CSF) and it is produced via proteolytic cleavage or alternative splicing (54). Elevated sTREM2 levels in the cerebrospinal fluid are linked with reduced AD risk and delayed disease onset.

A key regulator of sTREM2 levels is the MS4A locus. Common variants in this region are associated with both AD risk and modulation of sTREM2 concentrations. The most significant genetic signal, located near MS4A4A (rs1582763), correlates with increased CSF sTREM2, reduced AD risk and delayed onset. In contrast, a coding variant in MS4A4A (rs6591561) is linked to decreased sTREM2 levels, increased AD risk and earlier onset. In

human macrophages, antibody-mediated targeting of MS4A4A reduced sTREM2 levels, whereas targeting MS4A6A did not affect sTREM2 despite its expression being correlated with higher sTREM2 in AD patients (45).

Rosner et al. revealed that MS4A4A and MS4A6A form a complex that stabilizes MS4A6A and enables it to inhibit TREM2 signaling by interacting with DAP12/TYROBP, a co-receptor essential for TREM2 localization and activity on the membrane of microglia. This mechanism suggests that MS4A4A and MS4A6A act as cooperative negative regulators of TREM2-mediated microglial functions (55). These findings point to a novel pathway involving multiple AD risk genes and highlight MS4A4A and MS4A6A as potential therapeutic targets to restore microglial activity and mitigate disease progression.

4.3 MS4A4A in cancer

Cancer is a complex disease driven by genetic mutations and the acquisition of key traits that allow normal cells to become malignant, leading to uncontrolled growth and tissue dysfunction. A critical component of cancer biology is the tumor microenvironment (TME), which consists of a complex network of immune and non-immune cells, soluble factors, extracellular matrix components (ECMs) and signaling molecules. Among the immune cells in the TME, Tumor-Associated Macrophages (TAMs) are predominantly associated with pro-tumor functions, especially when polarized toward an immunosuppressive (M2-like) phenotype. These M2-like TAMs contribute to tumor progression by promoting angiogenesis, ECM remodelling, immunosuppression, and facilitating tumor invasion and metastasis (56).

As mentioned before, MS4A4A has been identified as part of the transcriptional signature of M2-like macrophages and is specifically expressed by TAMs in several human tumors, including colon and lung adenocarcinomas and melanoma. In these tumors, MS4A4A expression is notably restricted to $CD163^{+}$ macrophages, a well-established M2 marker. Mechanistically MS4A4A localizes to lipid rafts in the macrophage membrane where it interacts with the C-type lectin receptor Dectin-1. Engagement of Dectin-1 by these glycan-rich tumor cells leads to the activation of Syk signaling in macrophages, promoting the production of key NK cell-activating cytokines such as IL-15, IL-18 and INAM. In Ms4a4a-deficient macrophages, this response is impaired, resulting in reduced activation of NK cells and decreased production of IFN-γ and cytotoxic activity, ultimately compromising their ability to eliminate metastatic tumor cells (35). Therefore, MS4A4A is essential for the cross-talk between macrophages and NK cells in mediating anti-metastatic immunity.

Additionally, MS4A4A has been functionally linked to TREM2, another receptor expressed on TAMs. Single-cell RNA sequencing data in murine sarcoma models revealed that the murine homolog of MS4A4A, Ms4a4c, is selectively expressed in a cluster of sarcoma-associated macrophages. This population was significantly diminished in Trem2-deficient mice, suggesting that TREM2 may regulate MS4A4A expression and that the TREM2/MS4A4A axis contributes to a tumor-promoting macrophage phenotype (57).

From a therapeutic standpoint, targeting MS4A4A has shown considerable potential. In vivo inhibition of MS4A4A, using monoclonal antibodies or genetic approaches, remodelled the TME by decreasing the infiltration of immunosuppressive M2 TAMs and exhausted T cells while increasing the presence of cytotoxic $CD8^+$ T cells (47).

Altogether, MS4A4A plays a pivotal role in establishing an immunosuppressive tumor microenvironment by supporting M2 macrophage polarization, impairing NK cell-mediated immunity and limiting T cell infiltration and activity. Its expression is associated with poor clinical outcomes in cancer patients, positioning MS4A4A as a biomarker of pro-tumor TAMs and as a promising therapeutic target for enhancing anti-tumor immunity across various cancer types.

AIM OF THE THESIS

Given the emerging importance of MS4A4A in immune response, this project aims to achieve a deeper mechanistic understanding of how this protein regulates key aspects of macrophage biology.

The main purpose of this study is to characterize the biological function of the MS4A4A protein in macrophages to clarify its role in macrophage plasticity and activation. To address this objective, the study integrates molecular, cellular and biochemical approaches and it is structured around the following main tasks:

1. Characterization of the structure and subcellular localization of MS4A4A.
2. Identification of MS4A4A partners and influence on their functions.
3. Functional characterization of MS4A4A in macrophage activation in inflammatory conditions.

MATHERIALS AND METHODS

1. Mice

Ms4a4a$^{flox/flox}$ mice have been crossed with *ubc*$^{cre/wt}$ mice (Jackson Laboratories cat. N° 007001), and the mates *ms4a4a*$^{flox/flox}$/*ubi*$^{cre/wt}$ were treated with tamoxifen before the crossing to generate Ms4a4a *Full Knock Out.* Mice genotype was identified using the following primer: F01, CCC CTT CTT CAG TGT ACA TAG GAT (5'-3'); R02, GGA TAG CTA GAG CAG AGA AAT ACC; F03, TCT ATG TAC CCT ATG CTG GCT T. All animals were housed in temperature-controlled facilities under a 12-hour light/dark cycle, with ad libitum access to food and water. Experimental procedures were conducted using sex- and age-matched mice between 8 and 12 weeks of age. Euthanasia was performed via inhalation of carbon dioxide (CO_2), in accordance with institutional ethical guidelines. All animal procedures were reviewed and approved by the Institutional Ethical Committee of the Humanitas Clinical and Research Center.

2. Human monocyte-derived macrophages

Human monocytes were isolated from buffy coats or fresh blood from healthy donors or using the StraightFrom™ Buffy Coat CD14 MicroBead Kit (Miltenyi, 130-114-976) accordingly to the manufacturer's instructions. Monocytes were plated in 6-well plate (2 million/well) s with 100 ng/ml rhM-CSF (Miltenyi, 130-096-492) for 7 days in RPMI 1640 (Euroclone, ECB9006), 10% endotoxin-free Fetal Bovine Serum (Euroclone, ECS0186L), 1% L-Glutamine (Euroclone, ECB3000D), 1% penicillin/streptomycin (Euroclone, ECB3001D) for macrophage differentiation.

3. MS4A4A silencing by siRNA in human macrophages

Human macrophages were plated in multiwell-6 (2 x 10^6/well) or multiwell-12 (1 x 10^6/well) and MS4A4A expression was silenced using DharmaFECT 3 Transfection Reagent (Horizon, T-2003), following the manufacturer's instructions. The MS4A4A-targeting siRNA was obtained using the TriFECTa® RNAi Kit (hs.Ri.MS4A4A.13), and a non-targeting scrambled siRNA was used as a control. Silencing experiments were carried out for 24, 48, and 72 hours using the following siRNA concentrations: 10, 25, 50 mM. The efficiency of gene silencing was evaluated by flow cytometry, Western blotting, and quantitative PCR

(qPCR) and 50mM had the highest performance. After silencing, cells were washed with PBS and stimulated.

4. BMDM isolation and cell culture

Bone marrow was isolated from mice and incubated overnight at 37 °C in IMDM complete medium (Euroclone, ECB2072L) containing 10% endotoxin-free Fetal Bovine Serum (Euroclone, ECS0186L), 1% L-Glutamine (Euroclone, ECB3000D), 1% penicillin/streptomycin (Euroclone, ECB3001D), 1% Na-pyruvate (Euroclone, ECM0542D), 1% Hepes (Avantor, 25-060-CI), 1% MEM Non essential aminoacid (Euroclone, ECB3054D): Non adherent cells were then cultured in 10 cm plates (Corning, 430591) in IMDM complete supplemented with 50 µg/ml rmM-CSF (Miltenyi, 130-101-704). The medium was changed after 3 days, and BMDMs were harvested by detaching them on day 6 with PBS 1X + 10 mM EDTA pH=8 and plated in 6-well plates (1,2 x 10^6/well) 12-well plates (5 x 10^5/well), 24-well plates (2 x 10^5/well).
Stimuli used to treat BMDM are reported in Table 1.

Table 1. Stimuli used for BMDM treatment.

Stimulus	Working concentration	Company, cat. n°
LPS from E.coli O55:B5	100 ng/ml	L4005
PAM3CSK4	100 ng/ml	Invivogen, tlrl-pms
Poly(I:C) HMW	50 µg/ml	Invivogen, tlrl-pic
Zymosan	100 µg/ml	Invivogen, tlrl-zyn
ODN 1668 (CpG)	1 µM	Invivogen, tlrl-1668
R848	1 µg/ml	Invivogen, tlrl-r848
Dexamethasone (Dex)	1 µM	Merck, D1159
GolgiPlug Protein (Brefeldin A)	1:1000	BD Bioscience, 555029
H-89 dihydrochloride dydrate	40 µM	Merck, B1427
Actinomicyn D	10 µg/ml	Gibco, 11805017
Nocodazole	10 µg/ml	Sigma, SML1665
Agg-Ivig	500 µg/ml	PrIVIgen

Aggregated Intravenous Immunoglobulin G (Agg- IVIg) were obtained by stirring a 5 mg/mL IVIg (PrIVIgen) solution in sodium citrate buffer (10 mM sodium citrate, 5% sucrose, pH 6.0) at room temperature (RT) for 20 h. OD600 was checked with the spectrophotometer using

the non-aggregated IVIG as blank. A “good” aggregated preparation should have an OD600 > 0,500.

5. RNA extraction, transcription and Real-Time PCR

Total RNA was purified using ReliaPrep™ RNA Cell Miniprep System (Promega, Z6012) according to the manufacturer’s instructions.

Reverse transcription was performed on 500 ng RNA using High-Capacity cDNA Reverse Transcription Kits (ThermoFisher, 1107283). Control reactions without the addition of the reverse transcription enzyme were performed.

Quantitative PCR was performed following the recommended protocols for TaqMan probe Fast Advanced Master Mix (Applied Biosystems, 4444557) or for Syber Green Master Mix (Applied Biosystems**,** 4309155**)** on 384-well plate using RealTime QuantStudio 5 (Applied Biosystems) with the following thermal profiles: 2 min at 50 °C; 20 sec at 95°C; 40 cycles, 1 sec at 95 °C, 20 sec at 60°C (for Taqman); min at 95 °C; 40 cycles, 15 sec at 95 °C, 1 min at 60 °C (for Syber). Taqman probes used are reported in **Supplementary Table 1** and primer sequences in **Supplementary Table 2**. Data were analysed using the $2^{-\Delta\Delta Ct}$ method and normalized on the housekeeping gene. The half-lives of the mRNAs were calculated by nonlinear least-square regression using GraphPad Prism 10 as described previously (58). Briefly, the mean Ct values for each time point was normalized to the mean Ct value of t = 0, to get the normalized Ct value. Relative abundance for each time point was then calculated as 2 to the power of normalized Ct value. mRNA decay rate was determined for the relative abundances using non-linear regression curve fitting in GraphPad Prism.

6. Enzyme-Linked Immunosorbent Assay (ELISA)

Culture medium from BMDM and human macrophages treated with different stimulation for 2, 8 and 24 h, were assayed for IL-6, TNFα, IL-10, IFNβ (human and mouse Duoset ELISA kit from Bio-Techne) following the manufacturer’s instructions. The optical density (O.D.) of each well were analysed at 450 nm by SpectraMax i3x software.

7. Western Blot

BMDMs were cultured as previously described. After stimulation, cells were washed with PBS 1X and then lysated with Cell Lysis Buffer 1X (Cell Signaling, 9803) + Protease/Phosphatase Inhibitor Cocktail (Cell Signaling, 5872) following the manufacturer’s

instructions. Proteins were quantified using BCA Protein Assay Kits (ThermoScientific, A55865). Equal amounts of cell extracts were running on Bolt™ Bis-Tris Plus Mini Gels (Invitrogen, NW04120BOX) according to the manufacturer's instructions. Gels were transferred to a nitrocellulose membrane using Trans-Blot Turbo RTA Mini 0.2 µm Nitrocellulose Transfer Kit (Biorad, 1704270). After incubation with blocking solution containing 5% (w/v) non-fat milk in cold PBS 1X, membranes were incubated with the specific primary antibodies overnight at 4°C and then with the appropriate secondary antibody conjugated with peroxidase for 1 h at RT. Immunoreactivity was detected with a chemiluminescence assay detection system according to the manufacturer's instructions (Immobilon Western, Millipore, WBKLS). For semiquantitative analyses, the densities of the protein bands were measured by densitometric scanning of the membrane with ChemiDoc MP Imaging System (Biorad) and a computer program (Image Lab™ Software, Bio-Rad). The primary antibodies used in western blotting are listed in **Supplementary Table 3**.

8. Co-immunoprecipitation

Immunoprecipitation was performed using Pierce Co-Immunoprecipitation (Co-IP) Kit (ThermoScientific, 26149) and cells were lysated using the lysis buffer of the kit. 500 ug of total protein lysate was immunoprecipitated according to the manufacturer's instructions following by Western Blot.

WT and Ms4a4a KO BMDMs were treated or not with Dex 1 µM for 18h. Immunoprecipitation of MS4A4A for proteomic analysis was performed using Pierce MS-Compatible Magnetic IP Kit (ThermoScientific, 90409) and cells were lysated using the lysis buffer of the kit. 150 ug of total protein lysate was immunoprecipitated for MS4A4A according to the manufacturer's instructions.

9. Flow Cytometry

Flow cytometry was performed using BD FACS Symphony A5 SE. Cells were incubated for 30 min at 4°C with directly conjugated anti-mouse antibodies and their appropriate isotype controls (FITC anti-mouse F4/80, Biolegend, 157310; PeVio770 anti-human/mouse CD282 (TLR2) , Miltenyi, 130-132-112). Live/dead cell discrimination was performed staining with the Zombie Aqua Fixable Viability Kit (Biolegend, 423101). To block Fc receptors, a purified anti-mouse CD16/CD32 (BD Bioscience, 553142) was used. For intracellular staining, cells were permeabilized and fixed using the FoxP3/Transcription Factor Staining Buffer Set

(Invitrogen, 00-5523-00). Data were analysed with FACS Diva (BD) and Flow Jo (Treestar) software.

10. Calcium flux assay

Calcium flux was analysed using the Fluo-4 NW Calcium Assay Kit (Invitrogen, F36206) through two different approaches: flow cytometry and microplate reader. For the flow cytometry-based assay, BMDMs were detached, resuspended in the assay buffer provided with the kit, and incubated with Fluo-4 dye according to the manufacturer's instructions in 96-well U-bottom plates (3×10^5 cells/well). Following incubation, cells were transferred to FACS tubes. Prior to flow cytometric analysis, 100 µM β-ionone (Merck, I12603) or 10 µM ionomycin (Invitrogen, I24222) was added to the cell suspension. Samples were then analyzed using flow cytometry. For the microplate reader-based assay, BMDMs were seeded in black 96-well plates at a density of 3×10^5 cells per well, following the manufacturer's protocol for adherent cells. Fluorescence was recorded for 30 seconds to establish a baseline, followed by the addition of ionomycin, and subsequent fluorescence measurements were taken every 30 seconds for a total duration of 3 minutes.

11. Confocal microscopy

BMDMs were plated on gelatin-coated 14 mm diameter glass coverslips in 24 multiwell plate. At the end of the treatment, cells were fixed for 15 minutes with 4% paraformaldehyde and then, kept in Ca^{2+}/Mg^{2+} PBS 1X at 4°C. Immunofluorescence staining was performed starting with cells permeabilized with 0.05% Triton X-100 in Ca^{2+}/Mg^{2+} PBS 1X for 5 minutes at room temperature (RT). Nonspecific ligands were blocked with 2% Bovine Serum Albumin (Merck, A7030) + 5% goat serum (Merck, S26-100M) in Ca^{2+}/Mg^{2+} PBS 1X for 30 minute at RT. Cells were then incubated with the following primary antibodies/isotypes: rat anti-mouse Ms4a4a, mouse anti-mouse IL10 (Invitrogen – ARC9102), rat anti-mouse IL-10 (R&D, MAB417), rabbit anti-mouse Rab11 (Cell Signaling, 5589S), mouse anti-mouse Rab7 (Cell Signaling, 95746S), rat IgG1kappa (Invitrogen, 14-4301-82), mouse IgG1kappa (Invitrogen, 14-4714-85), rabbit IgG1kappa (Abcam, ab172730). After 2 hours of incubation at RT, cells were washed with Ca^{2+}/Mg^{2+} PBS 1X + 0,05% Tween-20 and incubated with the following secondary antibodies for 2 hours at RT: Goat anti-rat IgG Alexa Fluor 647 (Invitrogen, A21247), Goat anti-mouse Alexa Fluor 488 (Invitrogen, A21236), Goat anti-rabbit Alexa Fluor 488 (Invitrogen, A11008). After another step washing cells with Ca^{2+}/Mg^{2+} PBS 1X +

0,05% Tween-20, nuclei were counterstained with DAPI (Thermo Scientific, 62248). Filamentous actin (F-actin) was stained incubating cells with Alexa Fluor 555-conjugated Phalloidin (Invitrogen, A34055) for 30 minutes at RT. Coverslips were mounted in Fluormount-G (Invitrogen, 00-4958-02) prior to imaging and kept in dark at RT for 24 hours. Then, samples were kept in the dark at 4°C until confocal acquisition. Quantitative analysis of immunofluorescence staining was performed on images acquired at 10X magnification using a Leica Stellaris 8 DLS confocal microscope. Image analysis was conducted using Fiji (ImageJ). For each marker, thresholding was standardized by applying the threshold determined from the isotype control across all corresponding experimental samples to ensure consistency. Following thresholding, the integrated density (sum of pixel values within the defined area) was calculated to assess signal intensity. Colocalization value has been assessed by the plugin Coloc 2 of Fiji, focusing on the single cell. It has been choosed the Bisection Threshold regression and it has been considered the Pearson's R value above threshold.

12. Sample Preparation for LC-MS/MS analysis

Murine bone marrow-derived macrophage immunoprecipitated stored at –80 °C were thawed on ice and processed as follows: samples were resuspended in 30 µL of 0.2% Rapigest™ SF (Waters Corp., Milford, MA, USA) prepared in 0.1 M ammonium bicarbonate (NH_4HCO_3) and incubated at 95 °C for 20 minutes at 400 rpm. Protein concentration was measured using the Invitrogen™ Qubit™ Protein Assay Kit (Thermo Fisher Scientific, Rockford, USA) following the manufacturer's protocol.

Proteins were subjected to enzymatic digestion using a Trypsin/Lys-C mix (Promega, Madison, WI, USA) at an enzyme-to-substrate ratio of 1:25. Digestion was performed overnight at 37 °C with shaking at 400 rpm. The reaction was stopped by adding trifluoroacetic acid (Sigma-Aldrich Inc., St. Louis, MO, USA) to a final concentration of 0.5%, and the pH was verified to be approximately 2. Samples were then incubated at 37 °C for 45 minutes, followed by centrifugation at 13,000 rpm for 10 minutes to pellet any insoluble material. Peptides were desalted using PepClean C18 spin columns (G-Biosciences Inc., St. Louis, MO, USA) according to the manufacturer's instructions. Eluates were transferred to conical glass vials, mixed with 20 µL of 0.1% formic acid (Sigma-Aldrich Inc., St Louis, MO, USA), and lyophilized for at least 30 min. This step was repeated twice, lyophilizing until complete solvent evaporation. Samples were then reconstituted in 0.1% formic acid and diluted to a final concentration of 0.1 µg/µL prior to nLC-hrMS/MS analyses.

13. Liquid Chromatography and Mass Spectrometry

Peptide mixtures were analyzed using an Eksigent nanoLC-Ultra® 2D System (Eksigent, part of AB SCIEX, Dublin, CA, USA) coupled to a cHiPLC-nanoflex system operating in trap-elute mode. For each experimental condition, two technical replicates were injected, each containing 0.8 µg of peptides loaded onto the cHiPLC trap column (200 µm × 500 µm ChromXP C18-CL, 3 µm, 120 Å). Peptide trapping was carried out with an isocratic flow of 0.1% formic acid in water at 3 µL/min for 10 minutes. Subsequently, peptides were eluted onto the analytical nano cHiPLC column (75 µm × 15 cm ChromXP C18-CL, 3 µm, 120 Å) using a 100-minute gradient at a flow rate of 300 nL/min. For the elution gradient, Solvent A (H_2O + 0.1% FA) and Solvent B (ACN 100% + 0.1% FA) at different concentrations were employed as follows: from 5% B to 10% B in 3 min.; from 10% B to 40% B in 62 min.; from 40% B to 95% B in 10 min.; from 95% B to 5% B in 2 min., maintaining this concentration for the next 13 min. (column equilibration). Mass spectrometric analysis was performed on an Orbitrap Exploris 120 (Thermo Fisher Scientific, Waltham, MA, USA) equipped with an EASY-Spray ion source. The EASY-Spray emitter (7 µm ID, 20 µm × 50 cm Transfer Line) was operated at 1.6 kV, with the ion transfer capillary maintained at 220 °C. Data were acquired in data-dependent acquisition (DDA) mode. Precursor ions were scanned in the m/z range of 375–1,500 at a resolution of 60,000 (FWHM at m/z 200). Fragmentation spectra were recorded at a resolution of 15,000 (FWHM at m/z 200) using higher-energy collisional dissociation (HCD) with a normalized collision energy of 30%. Dynamic exclusion was enabled for 20 seconds to minimize repeated selection of identical precursor ions. The isolation window was set to 2 m/z, and the first mass was fixed at 120 m/z. Control of MS and chromatographic conditions was performed through Xcalibur (Thermo Fisher Scientific, Waltham, MA, USA) and Eksigent Run Manager Software (AB SCIEX, Dublin, CA, USA).

14. Data Analysis for LC-MS/MS

Raw spectra files obtained from nLC-hrMS/MS analyses were processed with Proteome Discoverer 2.5 (Thermo Scientific, Waltham, MA, USA) to retrieve protein identification. In detail, a Processing Workflow for protein identification and quantification features detection was built with the following nodes: (1) Spectrum Files RC, (2) Spectrum Selector, (3) Minora Feature Detector, (4) Precursor Detector, (5) Sequest HT and (6) Percolator. In detail, Mus musculus proteome (www.uniprot.org, retrieved in April 2024) was set as protein database

and “Trypsin” was set as digestion enzyme. Precursor Mass tolerance was set at 10 ppm, while Frgament Mass Tolerance was set at 0.05 Da. No dynamic modifications were searched. Protein FDR was set as “strict” (1%).

For Consensus step, the following workflows was applied: (1) MSF Files, (2) PSM Grouper, (3) Peptide Validator, (4) Peptide and Protein Filter, (5) Protein Annotation, (6) Protein Scorer, (7) Protein FDR Validator and (8) Protein Grouping. The data matrix resulting from this analysis, comprehending the Peptide Spectral Matches (PSMs) values for each protein, was exported in Excel file to be further processed.

The resulting matrix, containing Label Free Quantification (LFQ) Intensity and Peptide Spectral Matches (PSMs) values for each protein, was exported in Excel file for further elaboration. After quality evaluation of MS/MS runs, for WT_NT condition 8 protein lists were retained (generated from 4 different biological replicates analyzed in two technical replicates); for KO_NT condition, 8 protein lists were retained (obtained by analyzing 4 different biological replicates); for WT_DEX, 4 lists were retained (2 biological replicates), and for KO_DEX 4 lists were considered (2 biological replicates).

Ms4a4a candidate specific interactors were selected applying two different orthogonal criteria:

1) The first method employed frequency of identification in confronts *WT_NT vs KO_NT* and *WT_DEX vs KO_DEX*: in the first comparison, selected candidates must have had at least frequency of identification ≥ 3 out of 8 in WT_NT, while no identifications in KO_NT; in the second case, proteins must have had frequency of identification ≥ 2 out of 4 in WT_DEX, and no identifications in KO_DEX.
2) The second method was based on LFQ Intensity values, concerning the confronts *WT_NT vs KO_NT* and *WT_DEX vs KO_DEX*: in the two comparisons proteins were considered as potential interactors only if they were quantified in WT conditions in at least 66% of produced lists, and never quantified in KO.

The selected proteins (divided according the condition) were uploaded in STRING database (https://string-db.org/) to retrieve a Protein-Protein Interaction (PPI) Network and to evaluate functional enrichment by means of Reactome present in STRING. For functional enrichment, FDR (False Discovery Rate) was set as minor or equal to 0.05, signal ≥ 0.01 and strength ≥ 0.01. PPI Networks for NT and DEX were exported in .jpg format, while enrichment results were exported in .svg format.

15. Bulk RNA-seq

RNA-sequencing (RNA-seq) libraries were prepared using SMART-Seq® mRNA LP kit (Takara Bio) following the manufacturer's protocol. RNA-seq libraries were sequenced on an Illumina Nextseq 2000 platform, generating 76bp single-end reads with an average depth of ~30 million reads per sample. FASTQ files were generated from raw BCL data using Illumina bcl-convert (version 3.8.2). RNA-seq data processing was performed using the nf-core/rnaseq pipeline (version 3.10.1), a Nextflow-based workflow for standardized RNA-seq analysis. The pipeline included quality control (FastQC), adapter trimming (fastp), alignment to the Mus Musculus genome (Ensembl release GRCm38) using HISAT2, and transcript quantification with Salmon. Gene-level count matrices were imported and analysed in R environment (version 4.3.3) using the edgeR package (version 4.0.16). Genes with low expression levels were filtered out, retaining only those genes with counts per million (CPM) greater than 1 in at least one experimental condition. Library size normalization was performed using the TMM (Trimmed Mean of M-values) method. A design matrix was constructed based on experimental conditions, and dispersion estimates were obtained from *estimateDisp* function using edgeR's empirical Bayes approach. The likelihood negative binomial model was fit using *glmQLFit*, and differential expression testing was conducted with *glmQLFTest*. Genes were defined as differentially expressed if they exhibited an absolute $\log_2$ fold-change ≥ 2 and FDR < 0.01, corrected using the Benjamini–Hochberg method.

A direct contrast between stimulus-treated WT and stimulus-treated KO samples at each timepoint was performed to identify genotype-specific responses to treatment. In parallel, differential expression analysis was conducted comparing stimulus-treated vs vehicle samples separately in WT and KO genotypes across timepoints. To assess differences in transcriptional response between genotypes, we examined the overlap of significantly up- and down-regulated genes between the two contrasts (stimulus-treated WT vs vehicle WT and stimulus-treated KO vs vehicle KO) at each timepoint. We then computed the difference in $\log_2$ fold-changes (ΔlogFC) between the WT and KO contrasts for each gene and calculated a z-score based on the distribution of ΔlogFC values. Two-tailed p-values were derived from the z-scores, and multiple testing correction was applied using the Benjamini–Hochberg method. Genes were considered significantly divergent in response between genotypes if they had an adjusted ΔlogFC < 0.001 and were also significantly differentially expressed (FDR < 0.01) in at least one of the two genotype-specific contrasts. To ensure

robustness, genes with unusually high variability among replicates in the same condition were excluded based on variability outlier detection.

16. Ingenuity Pathway Analysis (IPA) and Comparative Pathway Analysis

Differentially expressed genes (DEGs) identified from stimulus-treated versus vehicle samples within each genotype (WT, KO) and timepoint were used as input for IPA Core Analyses (Qiagen Inc.). DEGs were defined based on an absolute $\log_2$ fold change ≥ 2 and a false discovery rate (FDR) < 0.01. IPA Core Analysis was performed independently for each genotype and timepoint. Each analysis yielded a list of enriched canonical pathways, along with associated z-scores (reflecting predicted activation or inhibition) and Benjamini–Hochberg corrected p-values (expressed as $-\log_{10}(p)$). To compare IPA results between genotypes, canonical pathway outputs from WT and KO were imported into R and processed per timepoint. Only pathways meeting nominal significance ($-\log_{10}(p) > 1.3$, corresponding to FDR < 0.05) in at least one genotype were retained. For each pathway, the difference in activation between genotypes was quantified by calculating the delta z-score (ΔZ), defined as:

$$\Delta Z = ZWT - ZKO$$

To account for differences in activation magnitude, a Relative ΔZ-score was also calculated for each pathway as:

$$Relative\ \Delta Z = \frac{|\Delta Z|}{max(|ZWT|, |ZKO|)}$$

This metric normalizes the absolute difference in activation by the strongest signal observed, highlighting pathways with both strong activation (in at least one genotype) and divergent regulation between genotypes. Pathways were considered significantly divergent between WT and KO if they met both of the following criteria: (i) an absolute z-score ≥ 2 in at least one genotype; and (ii) a Relative ΔZ within the top 10% (≥ 90th percentile) of all pathways at that timepoint.

17. Statistics

In each figure is described how statistics was performed. All data are presented as mean ± SEM. A statistical level of significance of $p<0.05$. analysis was performed using GraphPad Prism software, version 10.

RESULTS

1. Characterization of the structure and subcellular localization of MS4A4A

1.1 Tertiary structure prediction and intrinsic disorder analysis of MS4A4A

The MS4A family of proteins, including MS4A4A, shares structural similarities with tetraspanins, a group of membrane proteins known to regulate cellular signaling by influencing the structure and localization of their interaction partners. Work in the past several years has yielded important advances in tetraspanin structural biology revealing how tetraspanins function at the molecular level. The MS4A proteins share structural topology with CD20 (MS4A1) and FcεRIβ (MS4A2). However, this is based on sequence analysis and not structural determination. To date, only CD20 has been structurally characterized through crystallography (59).

Therefore, investigating the structure of MS4A4A could uncover similar functional mechanisms, helping to clarify its role in cellular signaling and potentially linking its structure to specific biological outcomes.

The predicted intrinsic disorder profile of the MS4A4A protein was generated using the IUPred and ANCHOR algorithms (**Figure 7A**). The black line corresponds to IUPred predictions, indicating the likelihood of disorder at each residue (Disorder Probability index, DPI), while the red line from ANCHOR highlights potential disordered binding regions - segments that are likely disordered but may become structured upon interacting with a partner. The MS4A4A protein exhibits moderate disorder at its N-terminus (between residues 1 and 62) and high disorder at its C-terminus (between residues 208 and 239), while the central region appears largely ordered. The difference between the IUPred and ANCHOR profiles suggests for the highly disordered region loc at the N terminus a higher propensity to fold upon binding with respect to the one located at the C terminus

The predicted 3D structure and membrane topology of the MS4A4A protein were obtained by combining three different systems: AlphaFold2, IUPred, and ANCHOR (**Figure 7B**). The structure is characterized by four transmembrane alpha-helices that traverse the lipid bilayer, as indicated by the two dashed lines representing the membrane boundaries. Due to the protein's topological nature, both the N- and C-termini fall on the same side of the membrane, although it is not possible to determine a priori whether these termini are internal

or external to the cellular compartment. N-terminus showed moderate intrinsic disorder the C-terminus higher disorder. The flexible terminal regions may facilitate interactions with other proteins or allow dynamic responses to changes in the cellular environment.

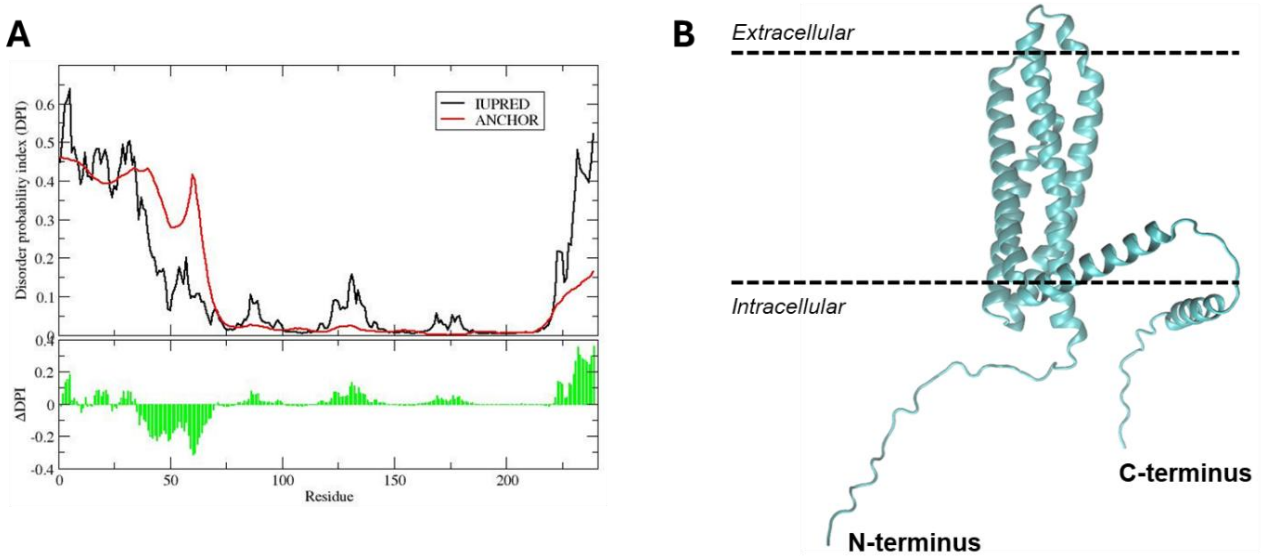

Figure 7. Intrinsic Disorder Profile and Predicted 3D Structure of MS4A4A Protein. (A) IUPRED (black) and ANCHOR (red) profiles of disorder, i.e., disorder probability index (DPI, ranging from 0 to 1), are reported as function of the protein sequence. The difference between the two curves (DDPI) is reported in green. (B) MS4A4A structure predicted by AlphaFold. The location of membrane polar surfaces is schematically represented with dashed lines.

To investigate potential interaction surfaces of MS4A4A with other molecules PESTO (Protein Ensemble Surface and Topology Organizer), a computational tool for mapping interaction interfaces on protein surfaces to predict binding interfaces on the protein's structure was used. Two distinct interaction profiles were identified: one favouring lipid interactions and the other favouring protein interactions. In the lipid interaction model, high-probability binding regions (highlighted in red) were predominantly located along the region of the protein that, as suggested by similarity with other molecules of the same family, corresponds to transmembrane helices. In contrast, the transmembrane tetra helical domain appears inherently inclined to interact directly with other transmembrane proteins. The protein interaction model revealed red-highlighted regions primarily on the intracellular domain (**Figure 8**).

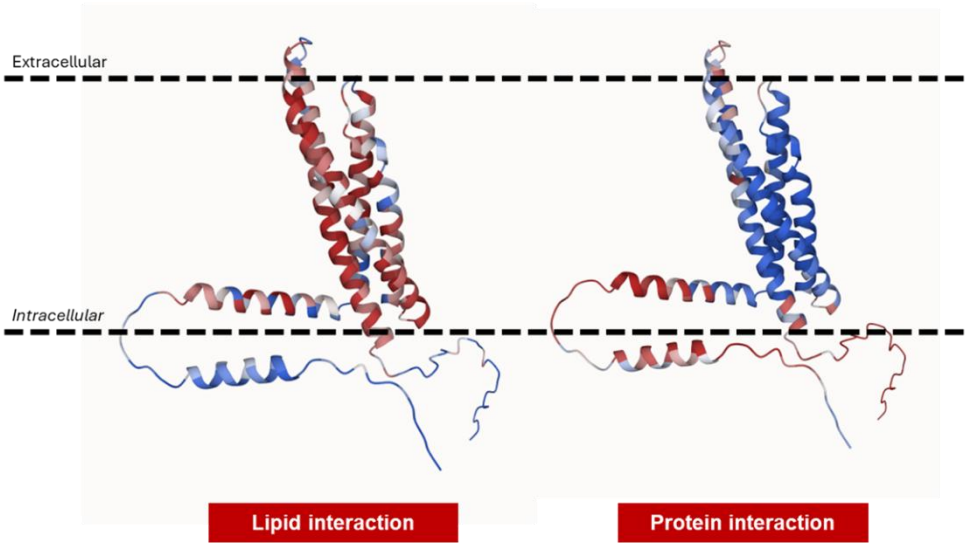

Figure 8. Predicted binding interface on MS4A4A structure for lipids and for polypeptide chains. The colour coding goes from red to blue, i.e., respectively from highest to lowest propensity for each class of molecules.

1.2 Identification and Characterization of Ligand-Binding Pockets in MS4A4A

Based on previous findings and existing knowledge about the tetraspanin-like MS4A protein family, MS4A proteins are believed to function through interactions with other molecular partners. To date, no MS4A protein has been classified as druggable. However, in this study, we aimed to explore the druggability of MS4A4A.

The potential of MS4A4A to bind ligands or interact with small molecules is supported by binding site predictions conducted using PrankWeb, a structure-based web server designed to identify and visualize ligand-binding pockets on proteins. Two potential pockets were identified by AlphaFold-predicted structure: Pocket 1 (score: 0.12/1) and Pocket 2 (score: 0.046/1), both located near the intracellular side (**Figure 9A**). Pocket 1 (black) lies at the interface of the transmembrane helices and the cytoplasmic domain, forming a small cavity that could take part in intracellular protein interactions or regulatory signaling. Pocket 2 (red) is slightly more surface-exposed suggesting potential involvement in protein-protein interactions or ligand engagement at the membrane interface. However, both pockets were predicted with relatively low confidence scores, prompting further structural analysis.
To improve the reliability of pocket identification, the same PrankWeb analysis was repeated using an MS4A4A model generated by the homology modelling service SWISS-MODEL (**Figure 9B**), with the aim of focussing on the structured conserved region of the protein and

to exclude disordered termini and a potentially biased prediction of their spatial arrangement. This approach revealed five distinct binding pockets, as illustrated in the figure:

- Pocket 1 (black) is situated along the intracellular transmembrane interface. It has the highest probability score (0.963) and is the most extensive pocket identified, suggesting strong potential for functional interaction.
- Pocket 2 (red) is also located on the intracellular side, with a high confidence score (0.819).
- Pocket 3 (yellow) is positioned near the extracellular region, particularly within the extracellular loop, forming a more enclosed cavity.
- Pocket 4 (orange) is located closer to the extracellular face. Pocket 5 (blue) appears within the intracellular compartment.
- Pocket 5 (blue) appears within the intracellular compartment.

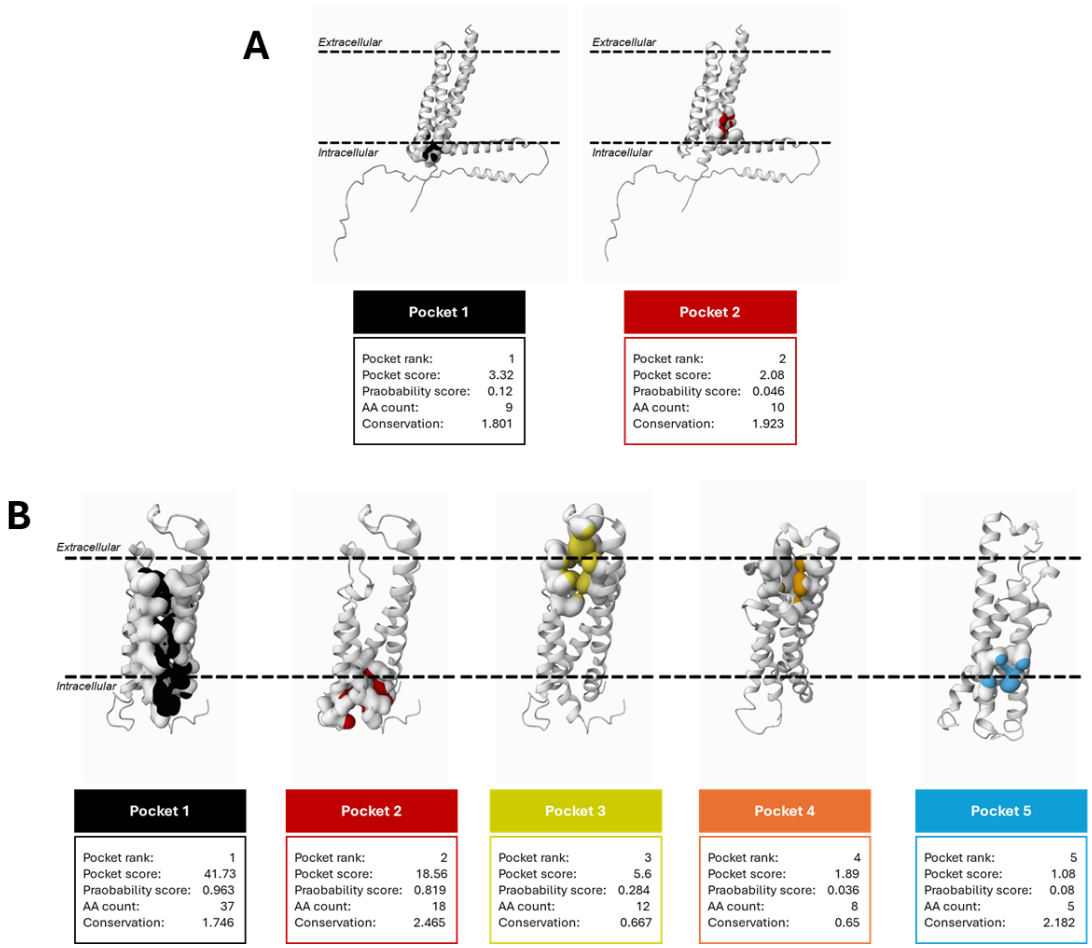

Figure 9. PrankWeb based prediction of the potential ligand binding regions of MS4A4A structure modelled using AlphaFold (A) and SwissModel (B). For each putative binding site the following parameters are reported: i) Pocket score: solvent accessibility based index of druggability (0-100); ii) Probability score: the knowledge based probability of a pocket to be real (0-1); iii) AA count: number of residues constituting the

pocket; iv) Conservation: degree of evolutive conservation of the pocket among the experimental structures of complexed (0-4).

Based on this result, subsequent analyses focused exclusively on Pocket 2. A virtual screening of commercially available ligands was performed against Pocket 2 with the aim of identifying a selection of candidate compounds that could potentially be tested in experimental assays (**Supplementary Table 4**).

As previously reported, the MS4A4A protein is upregulated in response to the glucocorticoid dexamethasone (34,35). Among the compounds screened, Pocket 2 of MS4A4A exhibited high binding affinity for dexamethasone (Dex) metasulfobenzoate. Docking simulations revealed that the dexamethasone molecule inserts deeply into the binding cavity forming favourable interactions within Pocket 2. In contrast, the metasulfobenzoate group remains exposed outside the binding site. This suggests that metasulfobenzoate group does not contribute directly to receptor binding (**Figure 10**).

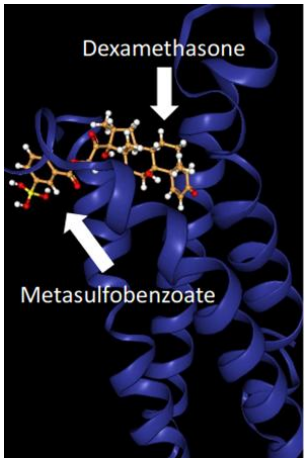

Figure 10. Docking simulation between MS4A4A and dexamethasone metasulfobenzoate.

To extend the analysis and to understand if the possible docking observed is reliable, docking was also performed for other molecules of the same family of dexamethasone metasulfobenzoate, such as dexamethasone, cortisol, estradiol benzoate and cholesterol. As expected, all of these molecules demonstrated binding to the glucocorticoid receptor 1 (GR1). Interestingly, among all compounds tested with MS4A4A, Dex- metasulfobenzoate showed the strongest binding affinity, supporting previous observations. However, this may not indicate specific recognition of Dex- metasulfobenzoate se by MS4A4A, but rather a broader affinity for a class of structurally similar steroidal compounds. While these findings imply that MS4A4A can accommodate such molecules from a chemical-physical

perspective, docking simulations alone do not provide definitive proof of transport or functional interaction (**Table 2**). The result highlights the potentiality of MS4A4A to recruit steroidal ligands in the cavity exposed to the cytosol as well as the ability of accommodating them in the inner hydrophobic core created by transmembrane helices.

Table 2. Knowledge based scores of different ligands docked against MS4A4A and GR1.

Ligand	Docking score MS4A4A	Docking score GR1
Dexamethasone metasulfobenzoate	-157	-228
Dexamethasone	-142	-217
Estradiol benzoate	-134	-211
Cortisol	-131	-168
Cholesterol	-120	-129

1.3 Structural and Functional Supports for MS4A4A as an Ion Channel

Members of the MS4A protein family have been proposed to function either as ion channels or as regulators of ion conductance. Data on CD20 (MS4A1) shows that its expression correlates with increased calcium flux, though its exact mechanism remains unresolved. Moreover, MS4A4A has been implicated in the regulation of Orai1-mediated Ca^{2+} entry in mast cells and is also expressed in a subset of olfactory sensory neurons, where it binds specific ligands and promotes influx of extracellular calcium (36,60). However, it remains unclear whether MS4A4A functions as a calcium-permeable channel itself or instead acts as a ligand-binding co-receptor in association with some receptors.

To investigate the potential functional role of MS4A4A as ion channel, a series of molecular dynamics simulations were performed (using GROMACS 2023.3 AMBER99SB-ILDN force field) with the protein embedded in a Dipalmitoylphosphatidylcholine (DPPC) lipid bilayer, solvated with water (**Figure 11**). Results showed that molecules of water can enter the channel formed by the four transmembrane helices. However, it remains unclear whether this process corresponds to a real transmembrane passage from one side of the membrane to the other. Nonetheless, the presence of water within the channel suggests that the channel formed by the transmembrane helices of the protein can support the passage of small polar or charged species, such as calcium ions.

To further examine this hypothesis, a second simulation was conducted under the same conditions but with the addition of Ca^{2+} ions in the aqueous phase. In this case, the Ca^{2+}

ions did not enter the channel but remained associated with the surface of the lipid bilayer, indicating. A third simulation was designed, in which a single Ca^{2+} ion was manually placed at the center of the MS4A4A transmembrane cavity. The ion remains stably coordinated within the cavity, with minimal displacement over time. This finding suggests that the central region of MS4A4A may act as an ion-binding site (**Figure 11**).

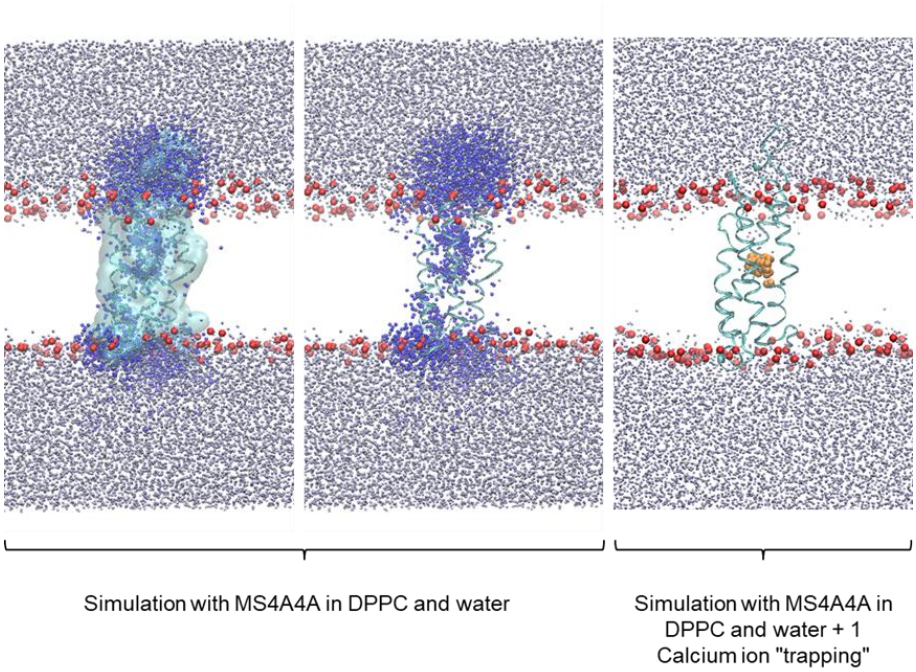

Figure 11. Molecular dynamics simulations of MS4A4A structure. Molecular dynamics simulations of MS4A4A in a model membrane have been performed to monitor its ability to act as a channel for water molecules (left) as well as for calcium divalent ion (right). The simulations revealed that the system can transport water molecules (violet spheres) across the membrane and that calcium (orange spheres) can penetrate the inner core of MS4A4A but lacking the ability to cross the membrane.

Together these data indicate that MS4A4A can accommodate water molecules within its transmembrane domain and potentially serve as a transient host for divalent cations such as Ca^{2+}. Moreover, the observed stability of Ca^{2+} within the channel supports a potential biological relevance that merits further investigation through experimental and computational experiments.

You et al. demonstrated that MS4A4A knockdown in THP-1 cells leads to elevated baseline intracellular calcium levels and enhanced calcium release following ionomycin stimulation, suggesting a regulatory role for MS4A4A in calcium homeostasis (61). However, if MS4A4A directly forms a calcium-permeable channel or modulates other calcium channel remains unclear. To further elucidate the role of MS4A4A in calcium flux, experiments comparing WT

and MS4A4A KO bone marrow-derived macrophages (BMDMs) were done evaluating calcium flux both at baseline and in response to stimulation.

We performed a calcium assay using the fluorescent probe Fluo-4, detecting fluorescence with a plate reader. Basal calcium flux levels were measured in WT and KO BMDMs for 30 minutes. Then, ionomycin, a calcium ionophore that facilitates transmembrane calcium transport, was added. As expected, this stimulus induced an increase in calcium flux. EDTA was subsequently added to block calcium influx, serving as a control to confirm that the system was functioning properly (**Figure 12A**). To compare calcium flux between WT and KO macrophages, we calculated the area under the curve (AUC). Ionomycin induced a significant increase in calcium flux compared to the vehicle control in both WT and KO BMDMs. We observed no difference in basal calcium levels between WT and KO macrophages, nor in the ionomycin-induced calcium flux between the two genotypes (**Figure 12A–B**). However, some variability was noted in the data, as indicated by the standard deviation.

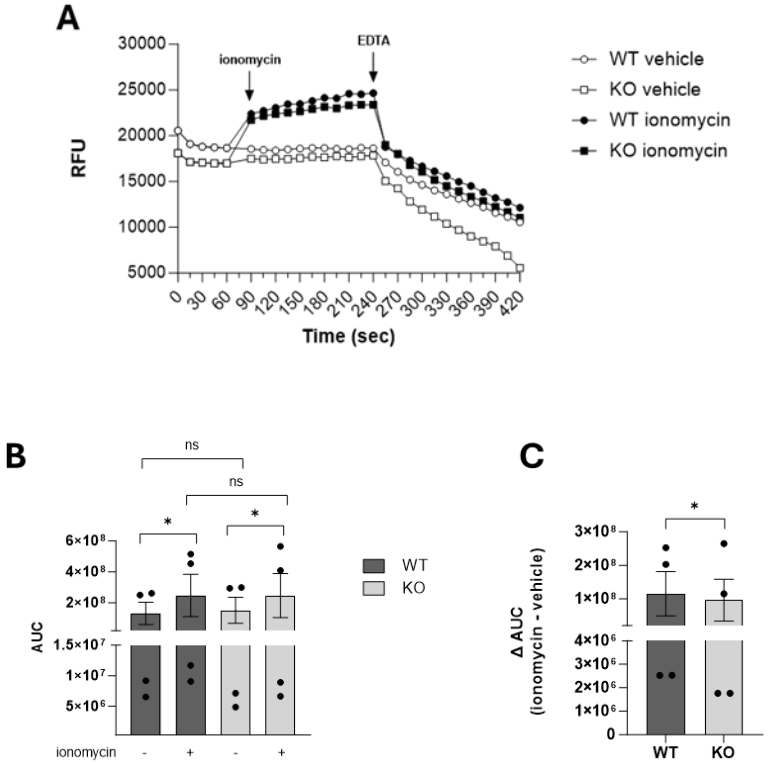

Figure 12. MS4A4A does not affect basal or ionomycin-induced calcium flux. Calcium fluxes were evaluated in WT and MS4A4A KO BMDMs by plate reader system in macrophages treated and not with ionomycin 10 μM. (A) Measurements are given in relative fluorescent units (RFU); one experiment representative of n=4. (B) The area under the curve (AUC) from 90 to 240 seconds, corresponding to the period following ionomycin addition and subsequent EDTA treatment, is shown (n=4). (C) Data are represented as difference between AUC(ionomycin) and AUC(vehicle) (n=4). Statistical analysis was performed using Paired t-test; p≤0.05 was considered significant.

To verify these results, we repeated the calcium flux assay using Fluo-4 and flow cytometry. This technique confirmed our initial findings: MS4A4A does not affect resting calcium concentrations, and ionomycin induced a robust increase in intracellular calcium levels in BMDMs, regardless of MS4A4A expression, contrary to the findings reported by You et al. (**Figure 13A–B**).

To investigate whether MS4A4A regulates calcium influx mediated by olfactory receptors, we stimulated macrophages with β-ionone, a volatile compound known to activate olfactory receptors. This approach was based on previous evidence that olfactory receptor agonists can elicit an MS4A-dependent influx of extracellular calcium (60). In our experiments, β-ionone induced a significant calcium response in WT macrophages. In contrast, KO macrophages exhibited only a non-significant trend toward increased calcium levels compared to negative control. When directly comparing the β-ionone-induced calcium flux between WT and KO macrophages, no statistically significant difference was observed, although there was a trend toward reduced calcium influx in the absence of MS4A4A (**Figure 13C**).

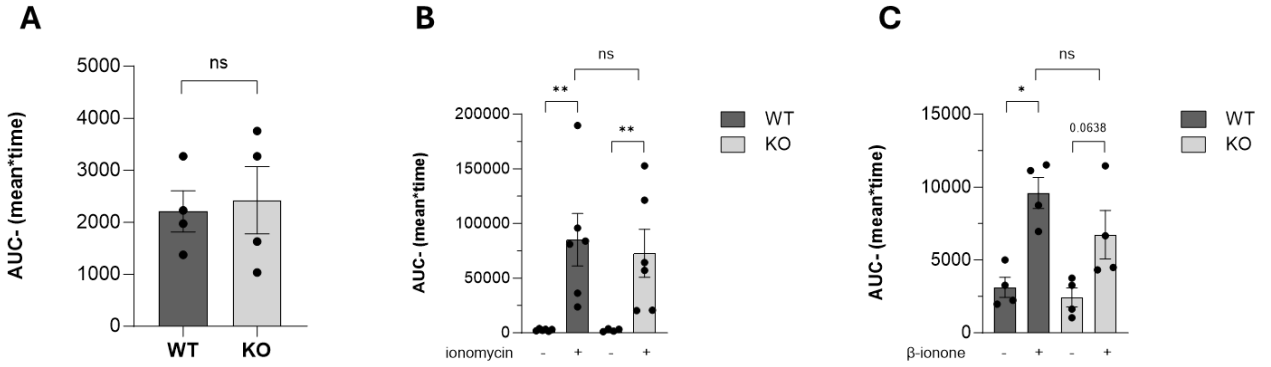

Figure 13. MS4A4A does not affect basal or ionomycin-induced calcium flux but may enhance β-ionone-induced calcium signaling. Calcium fluxes were evaluated in WT and MS4A4A KO BMDMs by FACS in the following conditions: (A) basal level; (B) after stimulation with Ionomycin 10 μM; (C) after stimulation with β-ionone 100 μM. Data are represented as Mean ± SEM and each symborepresentts a different biological replicate (n=4-6). Statistical analysis was performed using Paired t-test compared to non-treated cells; p≤0.05 was considered significant.

1.4 MS4A4A localization in macrophage

The MS4A protein family includes several members known to localize in lipid raft microdomains under specific stimuli. Previous studies have shown that some MS4A proteins co-localize with detergent-resistant membrane (DRM) fractions upon cell activation. Our preliminary data suggest that, unlike other MS4A members, MS4A4A does not associate with lipid rafts in resting macrophages. However, following dexamethasone (Dex) treatment, MS4A4A shows significant co-localization with lipid rafts, with a Pearson correlation coefficient increasing to 0.7 (unpublished data). We also demonstrated that MS4A4A co-localizes with Dectin-1 in lipid rafts after stimulation with depleted Zymosan (35). These findings suggest that the activation of macrophages can modify the intracellular localization of MS4A4A.

Deming et al., MS4A4A is mainly expressed on the plasma membrane of human macrophages but also shows intracellular distribution (45). In human mast cells, MS4A4A was found to co-localize with early and recycling endosomes (Rab5 and Rab11) but not with late endosomes (Rab7), pointing to a possible role in protein trafficking (62).

To better characterize MS4A4A localization in macrophages, particularly under resting and activated conditions, we performed co-localization experiments using specific intracellular markers:

- Phalloidin, a marker for filamentous actin (F-actin), highlights the cytoskeleton and helps identify membrane-associated structures.
- Rab11, a marker of recycling endosomes, indicates protein trafficking toward the plasma membrane.
- Rab7, a marker of late endosomes, reflects protein sorting toward lysosomes.

In resting macrophages MS4A4A showed a partial co-localization with phalloidin, Rab11, and Rab7 with Pearson correlation coefficients around 0.6 (**Figure 14**). This supports the idea that MS4A4A is not only locates in the plasma membrane, but it is also partially localized in the cytoplasm, likely within endosomal compartments.

After LPS stimulation, MS4A4A localization remained largely unchanged: co-localization with phalloidin persisted, while a slight increase in Pearson coefficients was observed with Rab11 and Rab7.

This analysis confirmed that in resting macrophages MS4A4A is partially associated with the actin cytoskeleton and intracellular compartments (endosome). Notably, LPS stimulation did not induce major changes in its distribution.

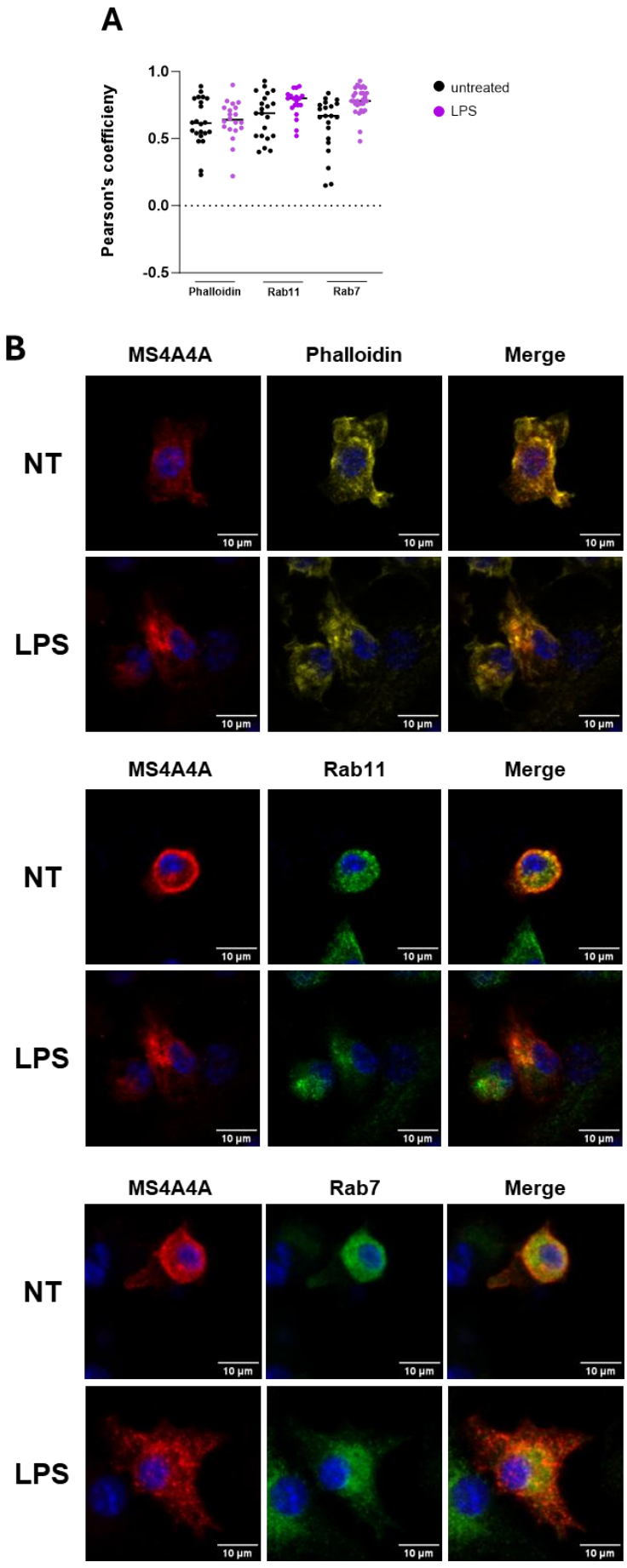
A
Pearson's coefficieny
1.0
0.5
0.0
-0.5
Phalloidin
Rab11
Rab7
untreated
LPS
B
MS4A4A
Phalloidin
Merge
NT
LPS
MS4A4A
Rab11
Merge
NT
LPS
MS4A4A
Rab7
Merge
NT
LPS
10 µm

Figure 14. MS4A4A partially co-localizes with phalloidin, Rab11 and Rab7 in resting and LPS-treated macrophages. Co-localization analysis of MS4A4A with phalloidin, Rab11 and Rab7 in resting and LPS-treated BMDM for 24 h. (A) shows images referring to one experiment representative of 3 analysed. (B) Data are shown as mean ± SEM of the colocalization rate in 20÷30 cells analysed in the experiments showed in panel A.

2. Identification of MS4A4A interacting partners

To explore the potential function of MS4A4A in macrophages, in the past the laboratory used a yeast split-ubiquitin screen to identify potential interacting proteins. Among these MS4A4A itself was identified, together with MS4A6A and CLEC7A (Dectin-1). The interaction between MS4A4A and these partners was further confirmed using FLIM-FRET analysis and super-resolution STED (35). Conversely, FLIM-FRET experiments did not confirm MS4A4A interaction with the tetraspanins CD63 and CD9. Another interestingly partner identified was Fc epsilon receptor 1 subunit gamma (FCER1G) that will be further investigates in chapter "*Role of MS4A4A in modulating dexamethasone response in rheumatoid arthritis*" (**Figure 15**).

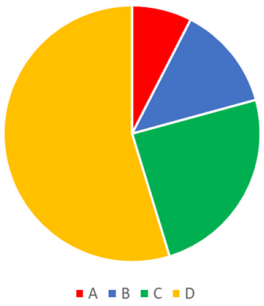

PBS	Gene Name	Protein
A	CD63 var 1	CD63 antigen var 1
	CD9	CD9 antigen
	MS4A4A	**Membrane-spanning 4-domains subfamily A member 4A**
	mitochondrion	
B	ATP6AP2	Renin receptor
	CLEC7A	**C-type lectin domain family 7 member A**
	FCER1G	**High affinity immunoglobulin epsilon receptor subunit gamma**
	LEPROT	Leptin receptor gene-related protein
	MS4A6A	**Membrane-spanning 4-domains subfamily A member 6A**
	SSR3	Translocon-associated protein subunit gamma
	mitochondrion	
C	ATP5G3	ATP synthase F(0) complex subunit C3, mitochondrial
	C18orf32	
	CERS2	Ceramide synthase 2
	CNIH	Protein cornichon homolog
	GLIPR1	Glioma pathogenesis-related protein 1
	GPR34	Probable G-protein coupled receptor 34
	LOC100128731	
	MFSD1	Major facilitator superfamily domain-containing protein 1
	OSTC	Oligosaccharyltransferase complex subunit OSTC
	TMEM49	Vacuole membrane protein 1 (VPM1)
D	ARL6IP5	PRA1 family protein 3
	CD63 var 5	CD63 antigen var 5
	FAM18B	Golgi apparatus membrane protein TVP23 homolog B
	FCGRT	IgG receptor FcRn large subunit p51
	FTL	Ferritin light chain
	HLA-DMA	HLA class II histocompatibility antigen, DM alpha chain
	IER3IP1	Immediate early response 3-interacting protein 1
	JKAMP	JNK1/MAPK8-associated membrane protein
	OCIAD1	OCIA domain-containing protein 1
	SAT1	Diamine acetyltransferase 1
	SLC25A3	Phosphate carrier protein, mitochondrial
	TM9SF3	Transmembrane 9 superfamily member 3
	VKORC1	Vitamin K epoxide reductase complex subunit 1

Figure 15. Identification of potential partners for MS4A4A by yeast split-ubiquitin. MS4A4A interactors has been identified by DUAL membrane Plus screening technology based on the split-ubiquitin system. Homo sapiens - MS4A4A (aa 1-239) has been used as reference bait fragment. For each interaction, a Predicted Biological Score (PBS) is computed to assess interaction reliability. Several thresholds have been arbitrarily defined to rank the results in 4 categories from A (the highest confidence rank) to D: A) Very high; B) High; C) Good; D) Moderate (including possible false positive).

Yeast split-ubiquitin assays may not accurately reflect interactions in physiological contexts due to the high likelihood of false positives. Among all the methodologies available for investigating protein-protein interactions, immunoprecipitation coupled with mass spectrometry (IP-MS) provides the advantage of capturing interactions within a biologically relevant cellular context. Using an in-house generated anti-MS4A4A antibody, we employed IP-MS to further explore MS4A4A interactomes in collaboration with the group of Dr. Dario Di Silvestre (ITB-CNR, Milan). BMDMs from WT and MS4A4A KO mice were either left untreated or treated with Dex. Following treatment, cell lysates were prepared and MS4A4A was immunoprecipitated and subjected to mass spectrometric analysis (**Table 3**).

As expected - and serving as a quality control - MS4A4A was detected in both resting and Dex-treated WT macrophages and not in KO samples, confirming the specificity of the immunoprecipitation. All proteins identified were exclusively detected in WT cells, further supporting the specificity of the interactions captured.

RESTING MACROPHAGES			
Description	**Gene Name**	**F(WT)**	**F(KO)**
Membrane-spanning 4-domains, subfamily A, member 4A	Ms4a4a	8	0
Large ribosomal subunit protein uL1	Rpl10a	4	0
Large ribosomal subunit protein uL5	Rpl11	4	0
NADH-ubiquinone oxidoreductase chain 5 (Fragment)	Mtnd5	4	0
[histone H4]-lysine(20) N-methyltransferase	Kmt5a	4	0
Pyrin and HIN domain-containing protein 1	Pyhin1	3	0
Dual specificity calcium/calmodulin-dependent 3',5'-cyclic nucleotide phosphodiesterase 1A	Pde1a	3	0
Toll-like receptor 2	Tlr2	3	0
Axonemal dynein light intermediate polypeptide 1	Dnali1	3	0
Bromodomain and WD repeat-containing protein 1	Brwd1	3	0
DEX-TREATED MACROPHAGES			
Description	**Gene Name**	**F(WT)**	**F(KO)**
Membrane-spanning 4-domains, subfamily A, member 4A	Ms4a4a	4	0
Keratin, type II cytoskeletal 79	Krt79	3	0
RING-type E3 ubiquitin transferase	Trim21	2	0
Actin-related protein 2/3 complex subunit 1B	Arpc1b	2	0
Keratin, type I cytoskeletal 10	Krt10	2	0
Large ribosomal subunit protein eL39	Rpl39	2	0
60S acidic ribosomal protein P0	Rplp0	2	0
Large ribosomal subunit protein El33	Rpl35a	2	0
Large ribosomal subunit protein eL27	Rpl27	2	0
Large ribosomal subunit protein eL6	Rpl6	2	0
Ribosomal protein L18	Rpl18	2	0
Sushi domain-containing protein 2	Susd2	2	0
40S ribosomal protein S15a (Fragment)	Rps15a	2	0
Sperm-associated antigen 17	Spag17	2	0
40S ribosomal protein S25	Rps25	2	0
Hist1h1b protein (Fragment)	H1f5	2	0
Alpha globin 1	Hba-a1	2	0

Table 3. Identification of potential partners for MS4A4A by Mass Spectrometry-based Immunoprecipitation Proteomics. List of potential interactors of Ms4a4a in resting macrophages and Dex-treated macrophages. For each protein, the value of peptide spectral matches (PSMs) in each sample analyzed is reported. Frequency in WT (F(WT)) and KO (F(KO)) conditions for ms4a4a express the number of times that a given protein is identified with at least one PSM in each replicate for that condition (n=2).

The profiles of interacting proteins showed significant differences between resting and Dex-treated BMDMs. This suggests that Dex treatment, known to upregulate MS4A4A expression and alter its subcellular localization, also modulates its protein partners. In both conditions ribosomal components and proteins involved in mRNA translation emerged as the only functionally enriched groups among the potential interactors (**Supplementary Figure 1**).

Interestingly, in resting macrophages Toll-like receptor 2 (TLR2) - a key transmembrane receptor involved in innate immune responses - was identified as putative partners. Consistent with this finding, surface expression of TLR2 was significantly reduced in MS4A4A KO BMDMs compared to WT, while total TLR2 protein levels remained unchanged (**Figure 16**). This data supports a possible role of MS4A4A in regulating the localization of TLR2 through direct or indirect interaction. To establish this interaction definitively, Co-immunoprecipitation experiments will be necessary in the future to establish and confirm definitively a physical interaction between MS4A4A and TLR2.

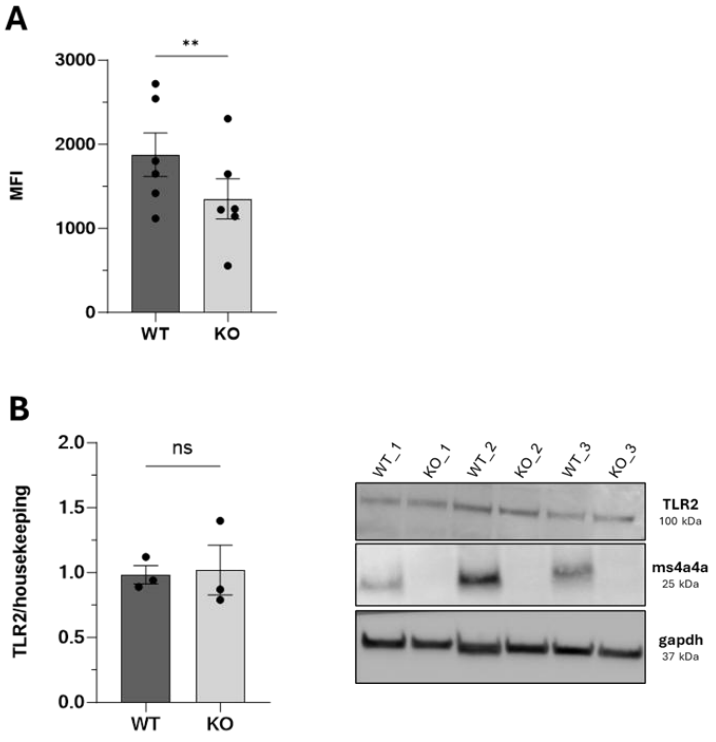

Figure 16. MS4A4A affect TLR2 surface expression but not total protein level. TLR2 protein expression was analysed in resting BMDMs WT and MS4A4A KO at membrane level by flow cytometry (n=5) (A); and by Western Blot (n=3) (B); total protein level of TLR2 was normalised on housekeeping protein levels. Data are represented as Mean ± SEM and each symbol represent a different biological replicate. Statistical analysis was performed using Paired t-test; p≤0.05 was considered significant.

Another protein identified as a potential partner of MS4A4A in resting macrophages is calcium/calmodulin-dependent 3',5'-cyclic nucleotide phosphodiesterase 1A (PDE1A). PDE1A plays a crucial role in modulating intracellular signaling and its enzymatic activity is regulated through binding to the calcium/calmodulin complex. These finding may be support the role of MS4A4A in modulating calcium flux.

3. Functional characterization of MS4A4A in inflammatory conditions

3.1 MS4A4A modulation upon LPS stimulation

MS4A4A has emerged as a key regulator of macrophage function, particularly through its role in activating the Syk-dependent signaling pathway downstream of Dectin-1 following depleted-zymosan stimulation. This leads to reduced production of TNF, IL-6, and reactive oxygen species (ROS) (35). As previously noted, IP-MS analysis identified TLR2 as a potential interaction partner of MS4A4A, and TLR2 membrane expression is impaired in MS4A4A KO BMDMs. These findings suggest that MS4A4A may play a broader role in modulating pattern recognition receptor (PRR) signaling networks. Additionally, MS4A4A has been implicated in the regulation of macrophage polarization, further underscoring its potential immunomodulatory role. Taken together, these observations provide us a compelling rationale for investigating the function of MS4A4A in the context of inflammatory responses.

It is well established that the anti-inflammatory glucocorticoid Dex induces MS4A4A expression at both the mRNA and protein levels (35). Interestingly, our results showed that MS4A4A expression is also induced by LPS stimulation, but only at 24 hours - not at 2 or 8 hours (**Figure 17A**). At the protein level, LPS treatment resulted in approximately a 4-fold increase in MS4A4A expression at 24 hours (**Figure 17B**). Immunofluorescence analysis further confirmed that the fluorescence intensity of the MS4A4A signal was elevated after treatment with both LPS and Dex (**Figure 18A-B**). Additionally, the number of BMDMs fully positive for MS4A4A increased following both LPS and Dex stimulation (**Figure 18C**).

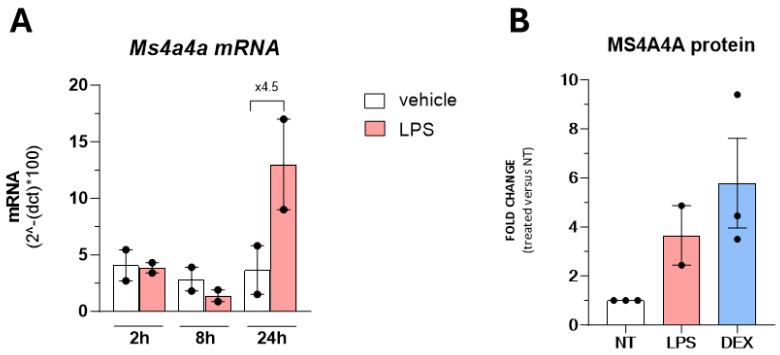

Figure 17. LPS induce up-regulation of MS4A4A at mRNA and protein level. (A) Ms4a4a qPCR on WT BMDM treated or not with LPS. (B) Western Blot on WT BMDM treated with or without LPS or DEX for 24h. TLR2 protein expression was analysed in resting BMDMs WT and MS4A4A KO at membrane level by flow

cytometry (n=5) (A); and by Western Blot (n=3) (B); total protein level of TLR2 was normalised on housekeeping protein levels. Data are represented as Mean ± SEM and each symbol represent a different biological replicate. Statistical analysis was performed using Paired t-test; p≤0.05 was considered significant.

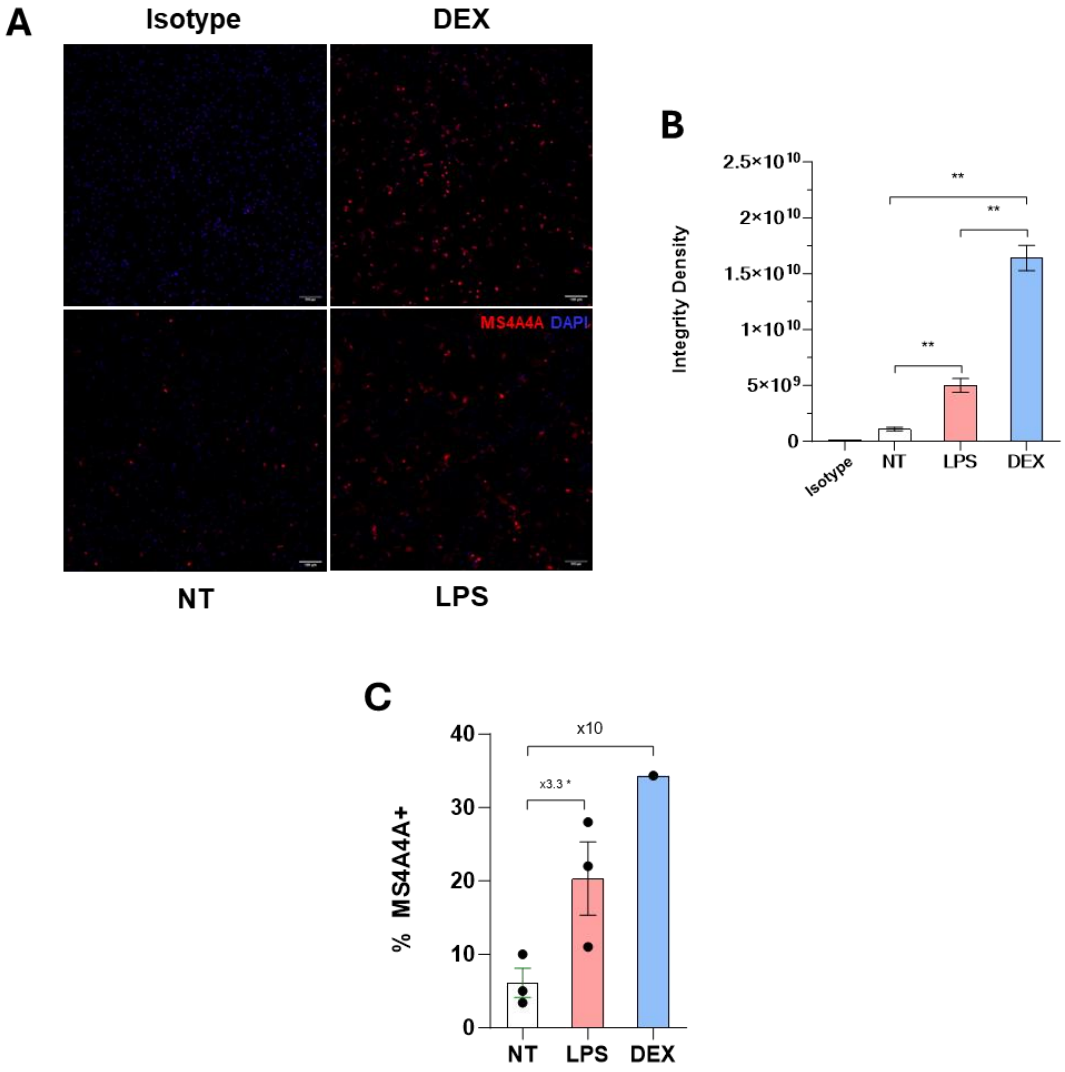

Figure 18. MS4A4A immunofluorescence after LPS and Dex treatment. MS4A4A immunofluorescence (IF) on WT BMDMs stimulated with LPS or DEX for 24h. (A) 10X IF images referring to one experiment representative of 3 analysed. (B) IL-10 IF quantification referred to panel A. Each symbol represents a field. (C) Number of MS4A4A positive BMDMs normalized on number of total cells. Data are represented as Mean ± SEM and each symbol represent a different biological replicate. Statistical analysis was performed using Mann-Withney test; p≤0.05 was considered significant.

This preliminary data suggests that LPS modulates MS4A4A expression, supporting the involvement of MS4A4A in the inflammatory response following LPS exposure.

To this end, we first compared the transcriptional profiling of WT and MS4A4A KO BMDMs by bulk RNA sequencing in resting conditions and then, following stimulation with

lipopolysaccharide (LPS), a TLR4 agonist widely used as an in vitro model of sepsis due to its ability to mimic macrophage-driven inflammatory responses. We further investigate the role or MS4A4A in LPS conditions comparing the cytokines profile of WT and KO macrophages.

3.2 Characterization of the impact of MS4A4A on macrophage basal phenotype

MS4A4A expression appears to be predominantly restricted to macrophages. Moreover, its expression progressively increased during M-CSF-driven differentiation of monocytes into macrophages, in contrast to other MS4A family members which did not exhibit a similar pattern (34,35). We observed that the % of F4/80 positive cells, corresponding to mature BMDMs, is comparable between WT and KO (**Figure 19A**). Notably, transcriptomic comparison between WT and MS4A4A KO BMDMs revealed a complete overlap in their basal gene expression profiles, suggesting that MS4A4A is not required for the establishment or maintenance of the resting macrophage transcriptional program (**Figure 19B**).

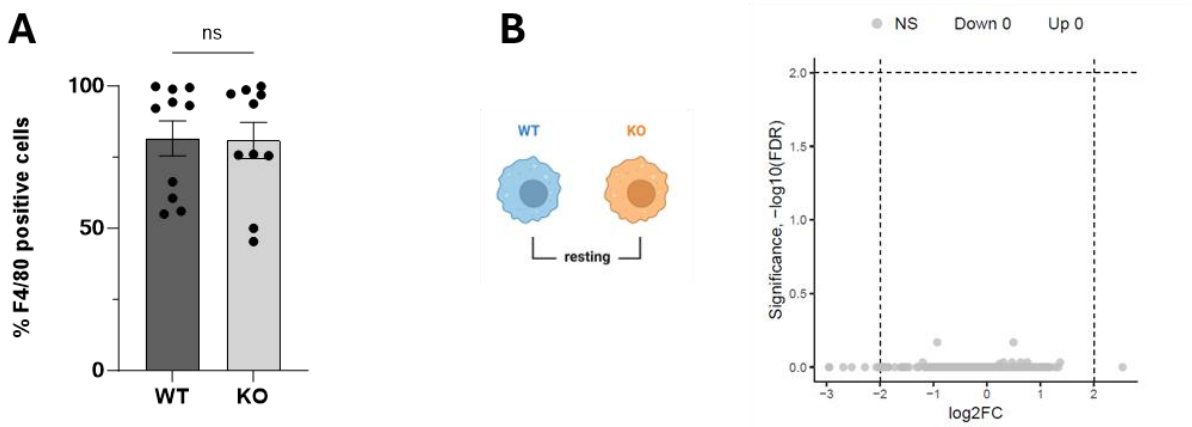

Figure 19. MS4A4A does not affect macrophage basal phenotype. (A) % F4/80 positive BMDMs by Flow cytometry (n=10). Statistical analysis was performed using Paired t-test; p≤0.05 was considered significant. (B) Volcano plots display log_2 fold-change on the x-axis and $-log_{10}$(FDR) on the y-axis for WT vs KO BMDMs in resting condition.

3.3 Transcriptional profile of MS4A4A KO macrophages after LPS stimulation

To investigate the transcriptional profiles of WT and KO following LPS stimulation, we first performed an unsupervised principal component analysis (PCA). The results revealed that sample segregation was primarily driven by treatment condition and time point (**Figure 20**).

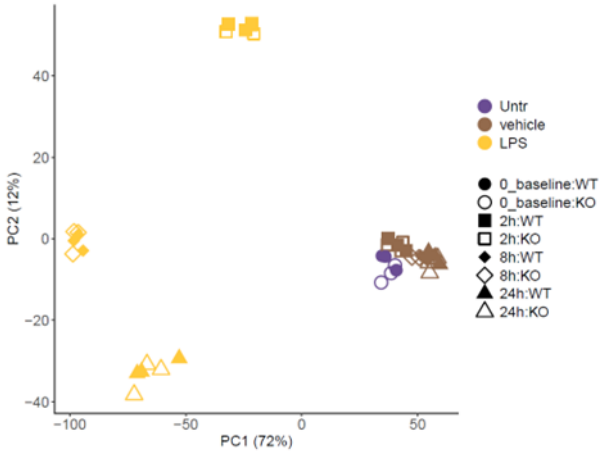

Figure 20. RNAseq samples cluster mainly by treatment and time point. PCA on all samples using the top 2000 most variable genes assesses samples similarities and visualizes the separation of experimental groups in a 2-Dimensional space.

To assess whether LPS stimulation induces differential gene expression between WT and KO BMDMs, we conducted a pairwise differential expression analysis comparing LPS-treated WT and KO samples at each time point. Across all time points analysed, no differentially expressed genes (DEGs) were identified between genotypes under LPS treatment (**Figure 21**).

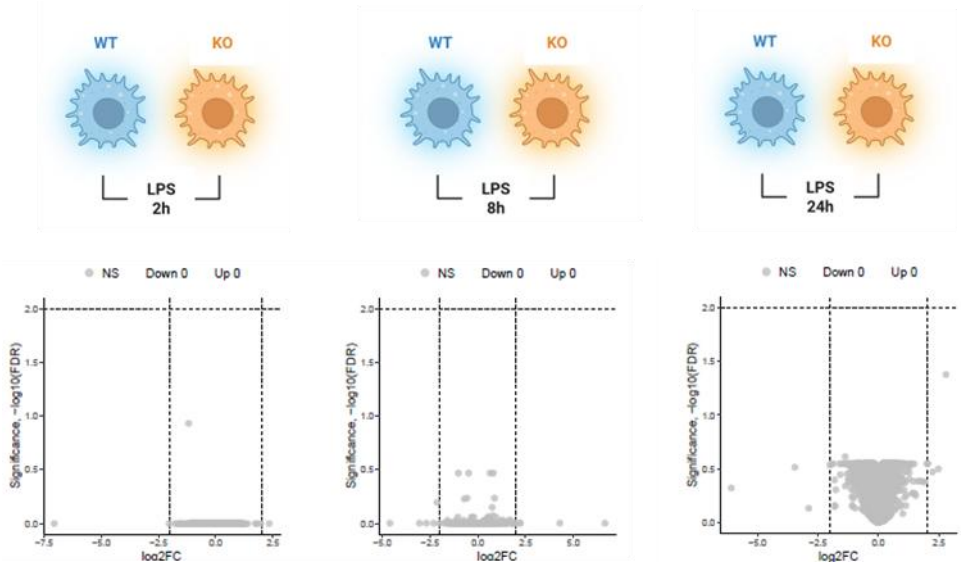

Figure 21. Differential expression genes (DEGs) between WT versus KO BMDMs. Volcano plots display log_2 fold-change on the x-axis and -log_{10}(FDR) on the y-axis for each contrast: LPS-treated vs vehicle both WT ad KO BMDMs at timepoint 2h, 8h and 24h.

Subsequently, we compared LPS-stimulated samples to their respective vehicle-treated controls within each genotype to evaluate the transcriptional response to LPS (**Figure 22A**).

LPS induced a robust transcriptional response, particularly at 8 hours post-stimulation, with a lesser effect observed at 24 and 2 hours in both genotypes (**Figure 22B-C**).

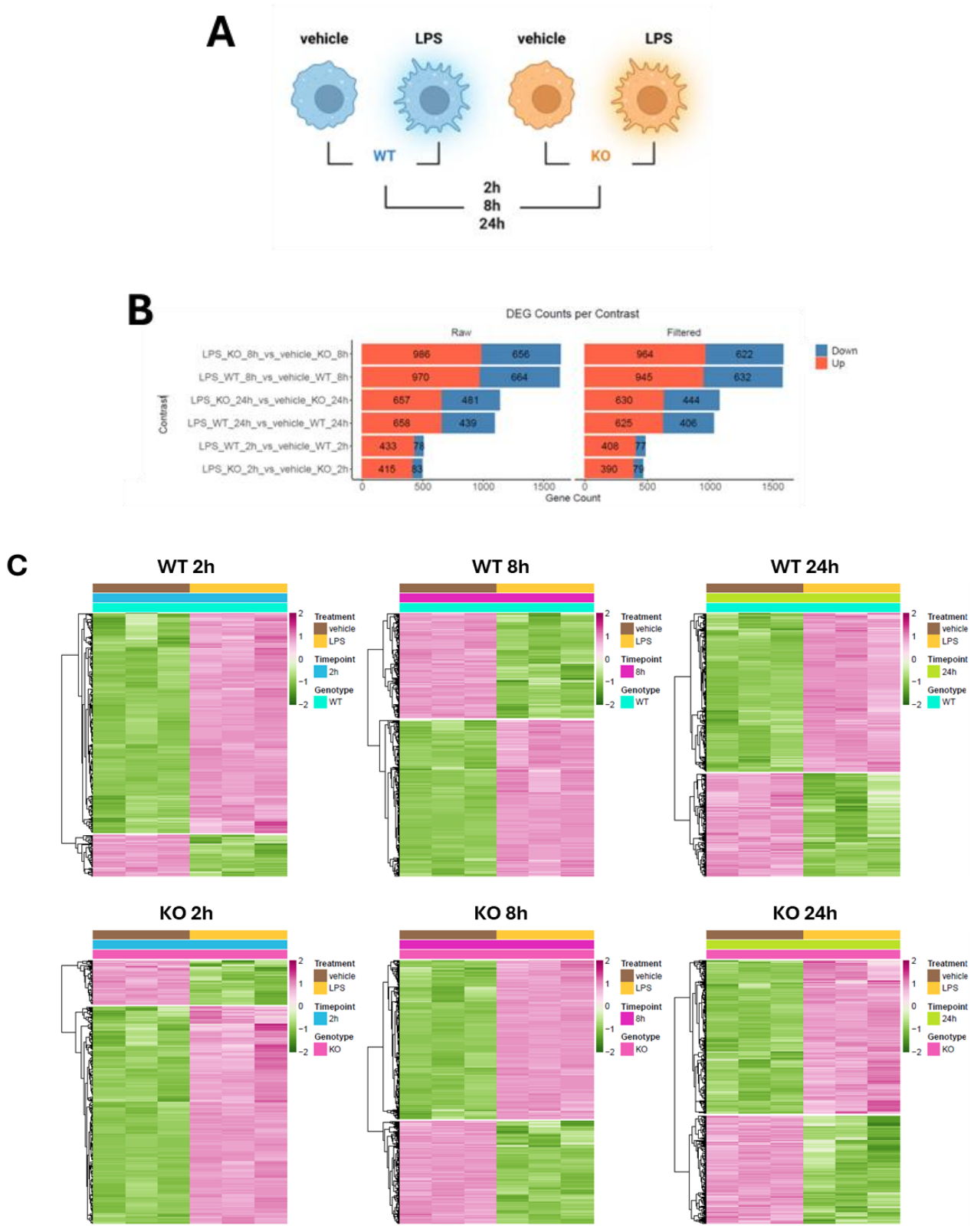

Figure 22. Differential expression genes (DEGs) between LPS versus vehicle. (A) Schedule of comparison analysis. (B) Barplot summarizing results of differential expression analysis: number of Up- and

Down-regulated genes per each of the 24 contrasts obtained by filtering genes having FDR < 0.01 and log2FC > 1. (C) Heatmap of DEGs; values are scaled by row and each column represent one replicate (three replicates for sample).

The fact that macrophages stimulated with LPS showed a pro-inflammatory phenotype was confirmed by performing a pathway enrichment analysis. It was conducted separately on the DEA WT and KO dataset and it revealed the activation of expected inflammatory pathways in response to LPS, similarly in both genotypes (**Figure 23**).

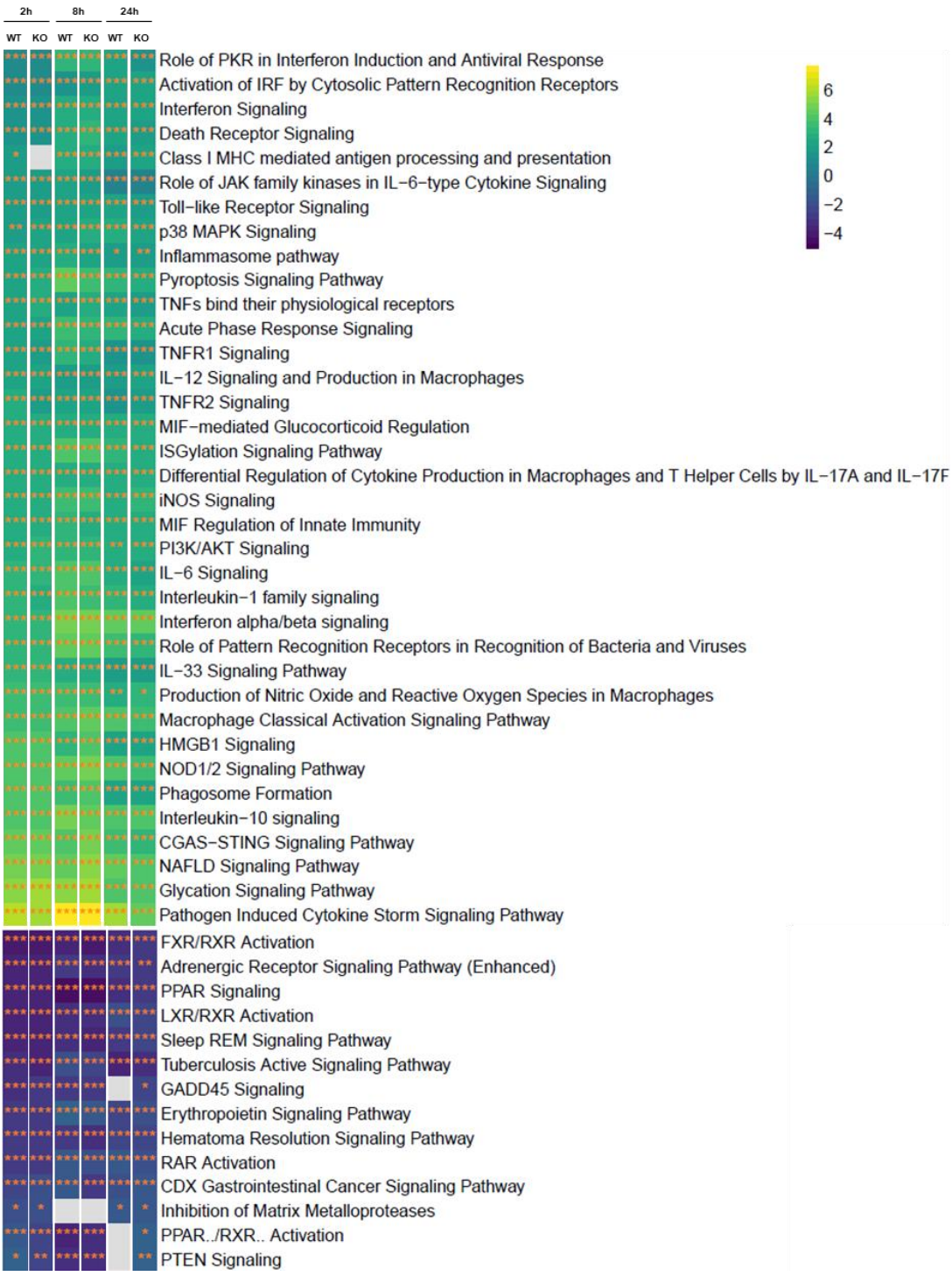

Figure 23. Pathway enrichment analysis on LPS-stimulated macrophages. Pathways enrichment analysis in WT and KO BMDMs. Rows report pathways significantly modulated (|z-score | ≥ 2) in at least one comparison. Colour intensity bar indicates the level of positive (in green) or negative (in blue) enrichment. The most up and down regulated pathway are reported, as representative on macrophage phenotype. Asterisks appear only when pathways are significantly enriched. Gray indicates no modulation.

This analysis confirms the expected activation of macrophages by LPS. However, our main aim was to identify any genotype-dependent differences in the transcriptional response to LPS.

To further explore this, we examined DEGs resulting from LPS stimulation (LPS vs. vehicle) for each genotype at all time points. The analysis of differentially expressed genes in WT and KO macrophages revealed a significant overlap, with only a limited number of genes regulated exclusively in one of the two genotypes (**Figure 24**).

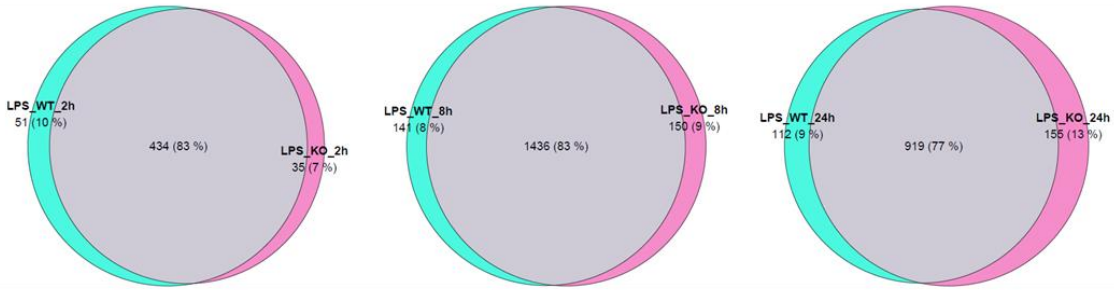

Figure 24. Gene intersections between WT and KO BMDMs. Venn-diagram of DEGs with a |logFC|≥2 in the two comparisons (green = LPS_WT vs vehicle_WT; pink= LPS_KO vs vehicle_KO).

To further assess differences in transcriptional response between genotypes, we examined the overlap of significantly regulated genes between the two contrasts (LPS-treated WT vs vehicle WT and LPS-treated KO vs vehicle KO) at each timepoint adding a new filter: we computed the difference in $\log_2$ fold-changes (ΔlogFC) between the WT and KO contrasts for each gene and calculated a z-score based on the distribution of ΔlogFC value. Genes were considered significantly divergent in response between genotypes if they had an adjusted ΔlogFC < 0.001. The list of the genes with ΔlogFC < 0.001 for each time point are considered differentially expressed between WT and KO and they are reported in **Supplementary Table 5.** However, the number of genes is very low compared with the total amount of gene regulated in each time point and they may reflect subtle differences in transcriptional regulation.

To assess whether, from a functional perspective, macrophages from KO mice differed from WT mice following LPS stimulation, for each pathway obtained from IPA analysis, the difference in activation between genotypes was quantified by calculating the delta z-score (ΔZ) defined as $\Delta Z = ZWT – ZKO$. To account for differences in the magnitude of activation, a Relative ΔZ-score was also calculated for each pathway as mentioned in Materials and Methods. Pathways considered significantly divergent between WT and KO applying this method are reported in **Figure 25-A-B-C**.

We identified a consistent set of pathways that were differentially modulated in WT and KO macrophages, some of which may have biological relevance in the context of macrophage biology and LPS activation. Additionally, we examined the activation of these pathways at multiple time points to determine whether the differences observed at one time point persisted at additional time points (**Figure 25D**).

Although the analysis highlights some pathways that are differentially modulated between WT and KO, we did not identify any robust or biologically relevant differences in the context of the inflammatory response at transcriptional level.

A


2h
WT KO
Acute Myeloid Leukemia Signaling
Caspase activation via Death Receptors in the presence of ligand
Estrogen−Dependent Breast Cancer Signaling
RIPK1−mediated regulated necrosis
BMP signaling pathway
Paxillin Signaling
PAK Signaling
Signaling by PDGF
NGF Signaling
Cardiac Hypertrophy Signaling
Post−translational protein phosphorylation
Virus Entry via Endocytic Pathways
Regulation of Insulin−like Growth Factor (IGF) transport and uptake by IGFBPs
D−myo−inositol−5−phosphate Metabolism
3−phosphoinositide Biosynthesis
Signaling by the B Cell Receptor (BCR)
VDR/RXR Activation
ABRA Signaling Pathway
Warburg Effect Signaling Pathway
6
4
2
0
−2
−4

B

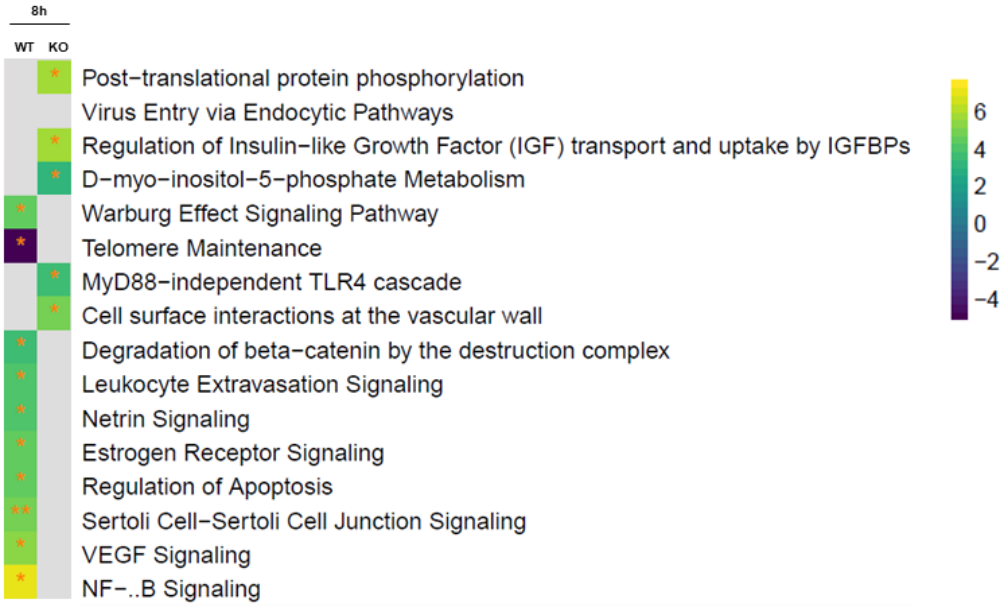
8h
WT KO
Post−translational protein phosphorylation
Virus Entry via Endocytic Pathways
Regulation of Insulin−like Growth Factor (IGF) transport and uptake by IGFBPs
D−myo−inositol−5−phosphate Metabolism
Warburg Effect Signaling Pathway
Telomere Maintenance
MyD88−independent TLR4 cascade
Cell surface interactions at the vascular wall
Degradation of beta−catenin by the destruction complex
Leukocyte Extravasation Signaling
Netrin Signaling
Estrogen Receptor Signaling
Regulation of Apoptosis
Sertoli Cell−Sertoli Cell Junction Signaling
VEGF Signaling
NF−..B Signaling
6
4
2
0
−2
−4

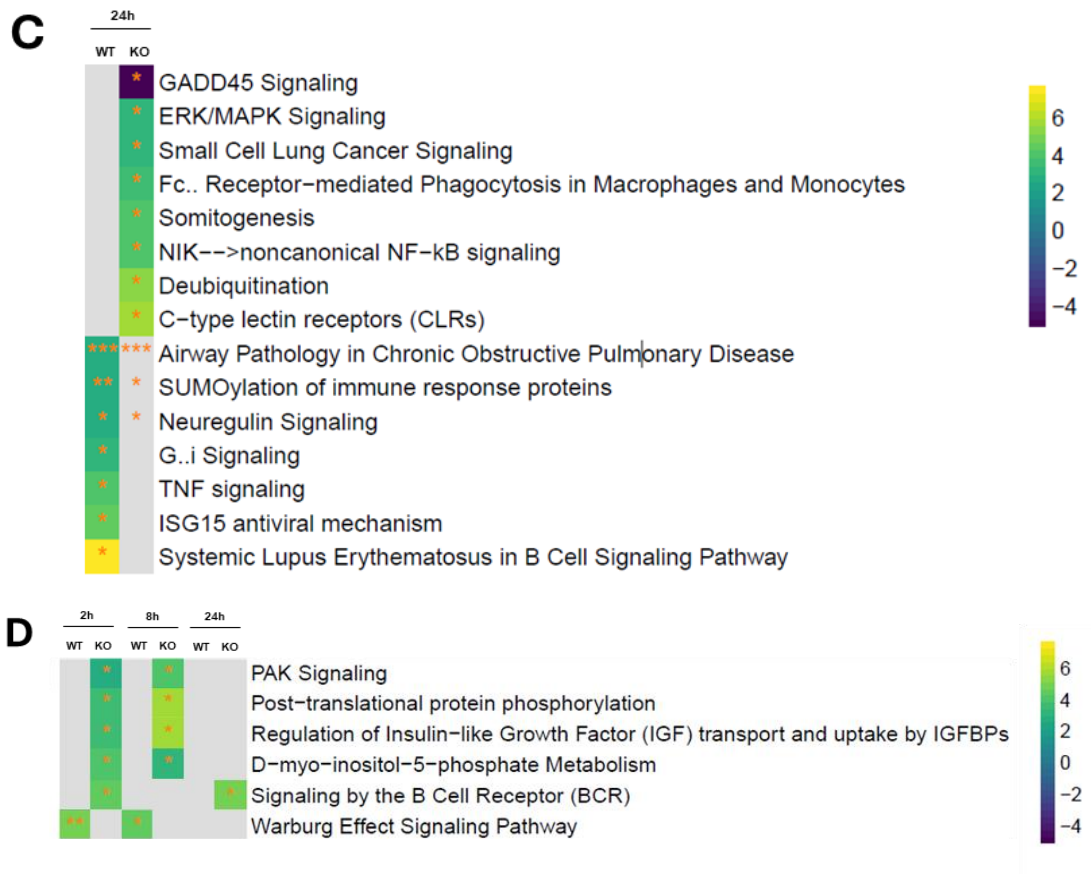

Figure 25. Pathway enrichment analysis comparison between WT and KO LPS-stimulated macrophages. Pathways enrichment analysis in WT and KO BMDMs. (A) Comparison at 2h. (B) Comparison at 8h. (C) Comparison at 24h. (D) Pathways differentially modulated In WT or KO macrophages maintained across time points. Rows report pathways significantly modulated (|z-score | ≥ 2) in at least one comparison. Colour intensity bar indicates the level of positive (in green) or negative (in blue) enrichment. Asterisks appear only when pathways are significantly enriched; gray indicates no modulation.

3.4 Functional role of MS4A4A in LPS-induced macrophages response

Given that the transcriptional analysis revealed only minimal differences between LPS-stimulated WT and KO macrophages and considering that MS4A4A is known to play a critical role in cytokine release during inflammatory responses mediated by Dectin-1, we hypothesized that MS4A4A might influence cytokine secretion upon LPS stimulation. To explore this possibility, we further investigated whether MS4A4A could modulate cytokine release in this specific inflammatory context.

As expected, LPS induced the secretion of pro inflammatory cytokines, such as IL-6 and TNF-α, however there is no difference in the secretion between WT and KO BMDMs at any time point across (**Figure 26 A-B**).

MS4A4A has been reported to influence macrophage polarization toward an M2-like state, which is typically associated with anti-inflammatory functions. Given MS4A4A's apparent role in promoting an anti-inflammatory phenotype, we hypothesized that it might contribute more to the resolution of inflammation rather than the initiation of inflammatory responses. To test this, we examined the production of IL-10, a key anti-inflammatory cytokine involved in inflammation resolution and known to be induced by LPS.

As expected, LPS stimulation induces IL-10 secretion in BMDMs, with detectable levels beginning at 2 hours post-stimulation. IL-10 production continues to increase peaking at 8 hours and remains stable up to 24 hours post-stimulation (**Figure 26C**). (KO BMDMs also produce IL-10 in response to LPS; however, the amount secreted is significantly reduced compared to WT macrophages. This reduction is already evident at 2 hours post-LPS stimulation and remains consistently lower at both 8 and 24 hours. To account for variability across independent experiments and to better quantify the extent of the IL-10 secretion defect in KO BMDMs, the fold change in IL-10 levels by normalizing KO values (pg/mL) to their corresponding WT values (pg/mL) was calculated (**Figure 26D**). The results revealed that IL-10 secretion in KO macrophages is approximately 50% lower than in WT at 2 hours, and about 40% lower at both 8 and 24 hours following LPS stimulation.

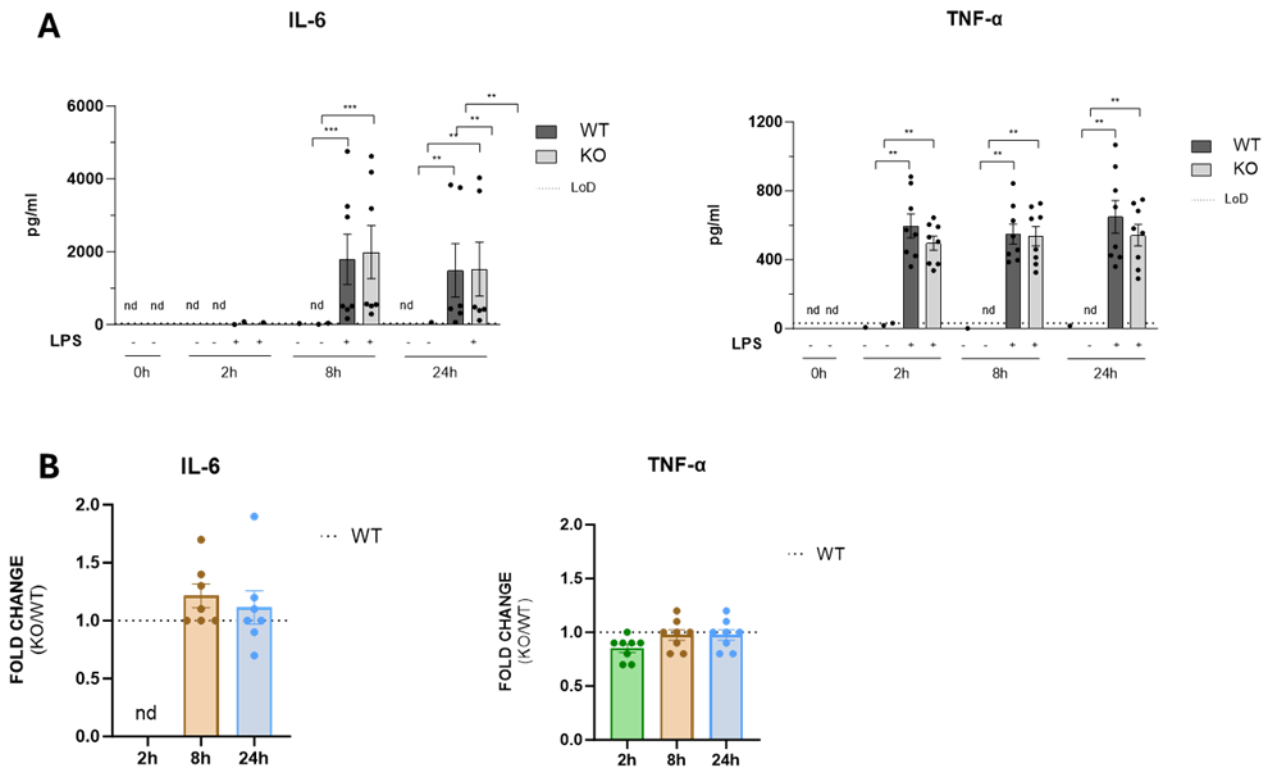

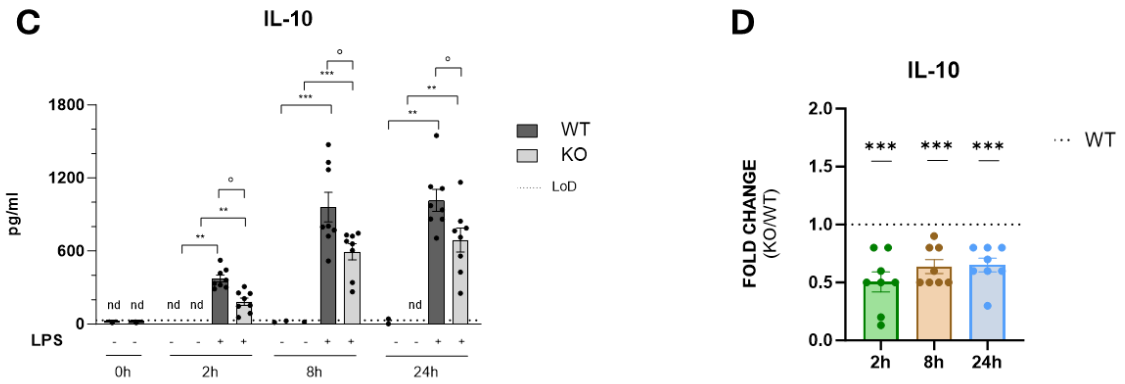

Figure 26. MS4A4A affect IL-10 but not IL-6 and TNF-α secretion after LPS stimulation. Cytokine productions were analysed by ELISA on WT and MS4A4A KO BMDMs treated or not with LPS 100ng/ml for, 2h, 8h and 24h. IL-6 and TNF-α secretion is showed: (A) in pg/ml; (B) as FOLD CHANGE (pg/ml KO versus pg/ml WT). IL-10 secretion is showed: (C) in pg/ml (D) as FOLD CHANGE (pg/ml KO versus pg/ml WT). Data are represented as Mean ± SEM and each symbol represent a different biological replicate (n=8); nd= not detectable. (A-C) statistical analysis was performed using Mann-Withney test LPS versus vehicle (*,**,***) or KO versus WT (°); (B-D) statistical analysis was performed using One sample t test KO versus WT; p≤0.05 was considered significant.

In our dose-response experiments, IL-10 secretion was initiated at 1 ng/mL LPS but showed a marked increase starting from 10 ng/mL, reaching peak levels at 1000 ng/mL LPS (**Figure 27**). Importantly, the impairment in IL-10 secretion in MS4A4A KO macrophages became apparent starting at 100 ng/mL LPS and it has still present at 1000 ng/mL LPS.

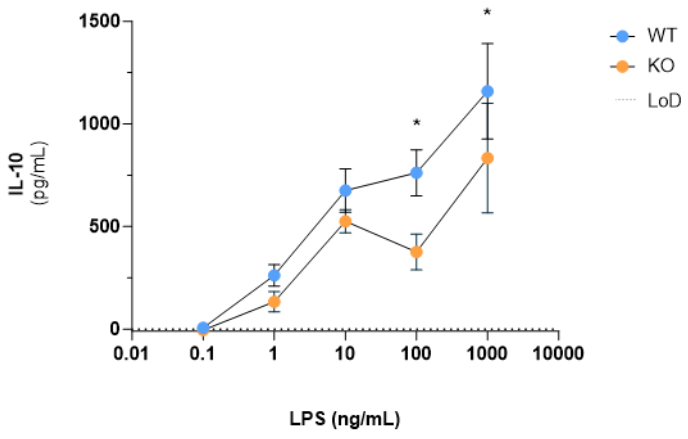

Figure 27. Dose-dependent IL-10 impairment in MS4A4A KO Macrophages. IL-10 cytokine release was analysed by ELISA on WT and MS4A4A KO BMDMs after LPS for 24h. LoD = ELISA Limit Of Detection. Data are represented as Mean ± SEM (n=3). (B) Statistical analysis was performed using One sample t test KO versus WT; p≤0.05 was considered significant.

IL-10 plays a crucial role in limiting immune responses acting in an autocrine and paracrine manner to suppress the expression of pro-inflammatory cytokines, MHC class II, and co-stimulatory molecules. For this reason, a controlled secretion for IL-10 is fundamental in order to prevent excessive inflammation (63). In addition to signaling through the MyD88-dependent pathway, TLR4 can also activate a TRIF-dependent pathway. This involves the adaptor protein TRIF (Toll/IL-1R domain-containing adaptor-inducing IFN-β), which leads to activation of the transcription factor IRF3 and subsequent production of type I interferons β (IFN-β). Although IFN-β is well-known for its antiviral roles, it also has anti-inflammatory properties. One of the key mechanisms underlying this effect is their ability to induce IL-10 production. Given the central role of IFN-β in inflammation, we investigated whether MS4A4A influences its secretion.

Upon stimulation with LPS, IFN-β is released as early as 2 hours post-treatment and remains relatively stable at later time points (8 and 24 h). KO macrophages showed a tendency to release lower level of IFN-β compared to WT cells (**Figure 28**).

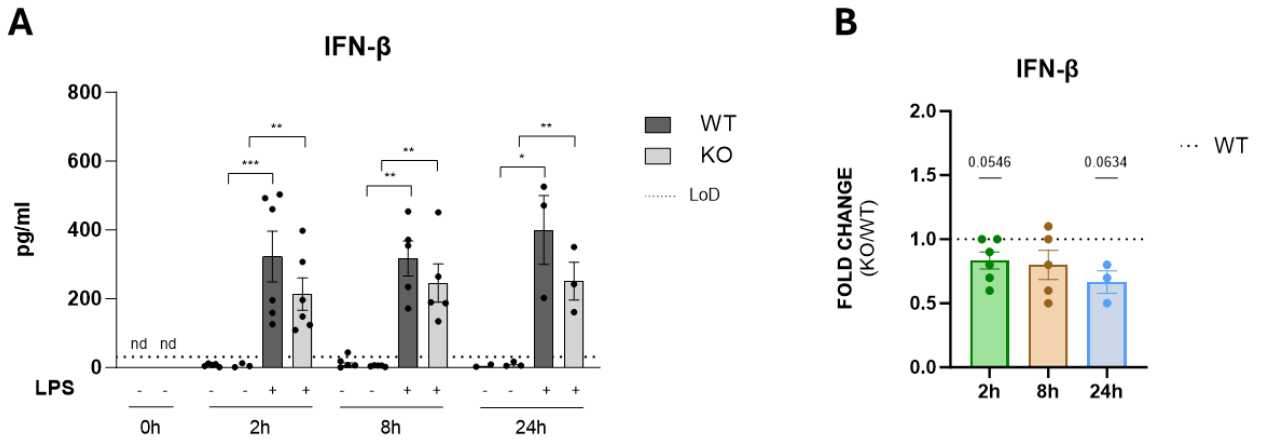

Figure 28. MS4A4A effect on IFN-β release. IFN-β production were analysed by ELISA on WT and MS4A4A KO BMDMs treated or not with LPS 100ng/ml for, 2h, 8h and 24h. (A) Data are represented in pg/ml. (B) Data are represented as FOLD CHANGE (pg/ml KO versus pg/ml WT) as Mean ± SEM. (A-B) each symbol represents a different biological replicate (n=3-6); nd= not detectable. (A) Statistical analysis was performed using Mann-Withney test LPS versus vehicle; (B) statistical analysis was performed using One sample t test KO versus WT; p≤0.05 was considered significant.

Macrophages produce both IL-10 and IFN-β after the activation of Toll-like receptors (TLRs). via MyD88 and TRIF-signalling pathway. The production of IL-10 in response to LPS requires both the MyD88- and TRIF-dependent pathways. In contrast, IFN-β production is driven mainly through the TRIF pathway alone. Based on this, we hypothesized that the impairment may result from a defect in TRIF-mediated signaling. To test this, we analysed

IL-10 production in response to a range of TLR agonists - some that activate both pathway (TLR4 and TLR3 agonists) and others that stimulate only MyD88 signaling (TLR2, TLR5, TLR7/8) (64).

All the TLR agonists tested were capable of inducing IL-10 secretion in macrophages, with detectable levels starting at 2 hours post-stimulation. In general, IL-10 secretion increased progressively over time, continuing through to 24 hours. However, the kinetics and the extent of IL-10 induction depend on the specific agonist. Both LPS and Zymosan induced rapid IL-10 secretion, reaching a plateau at 8 hours that was maintained at 24 hours. In contrast, other stimuli - R848, P3C4, PolyIC, CpG - produced a slower IL-10 release, with a peak at 24 hours post-stimulation (**Figure 29A**). Although all stimuli produced IL-10, they differed markedly in the extent of induction. Zymosan consistently induced the highest levels of IL-10 secretion across time points, followed by LPS and R848, which showed moderate but robust responses. In contrast, Pam3CSK4, PolyIC and CpG induced relatively lower IL-10 levels, although their kinetic is similar (**Figure 29B**). These data indicate that, while IL-10 induction is a common feature of TLR activation in macrophages, the intensity and the kinetics of the response are stimulus-dependent.

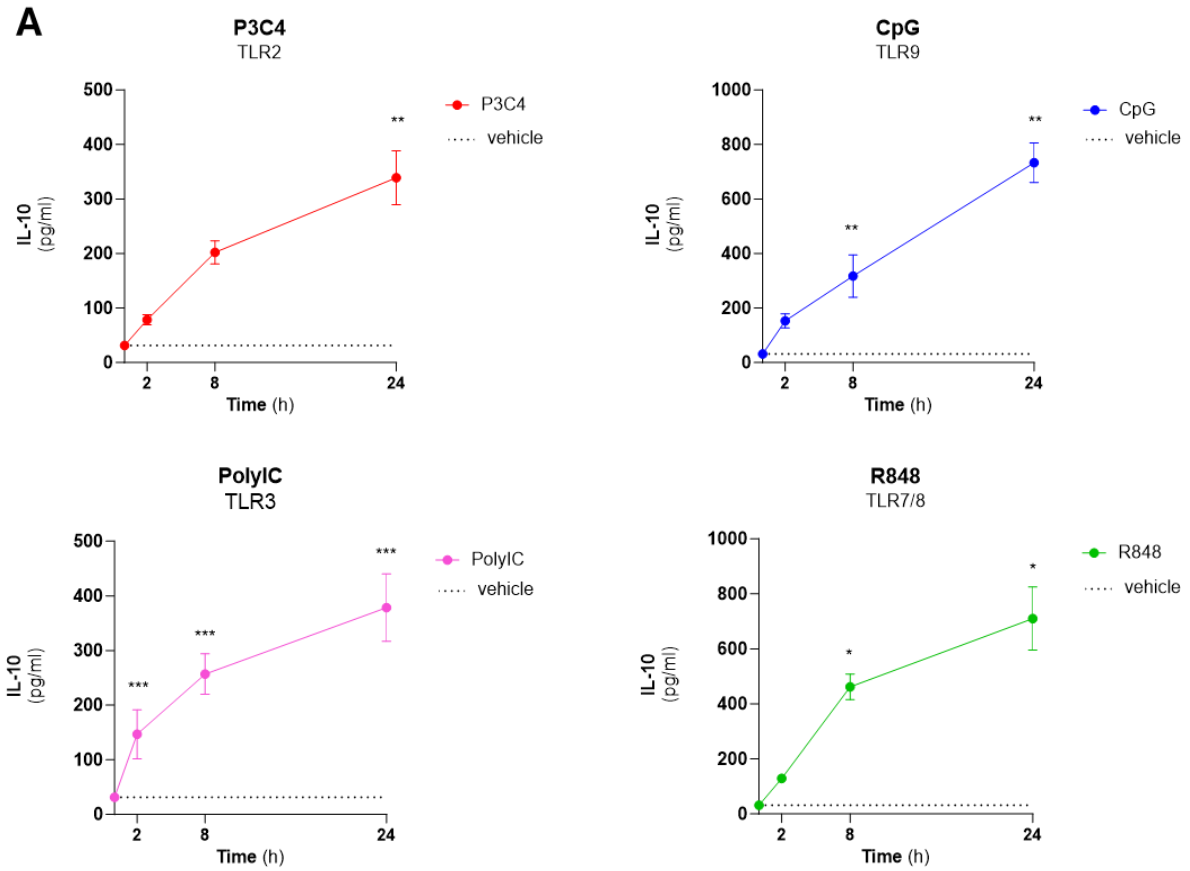

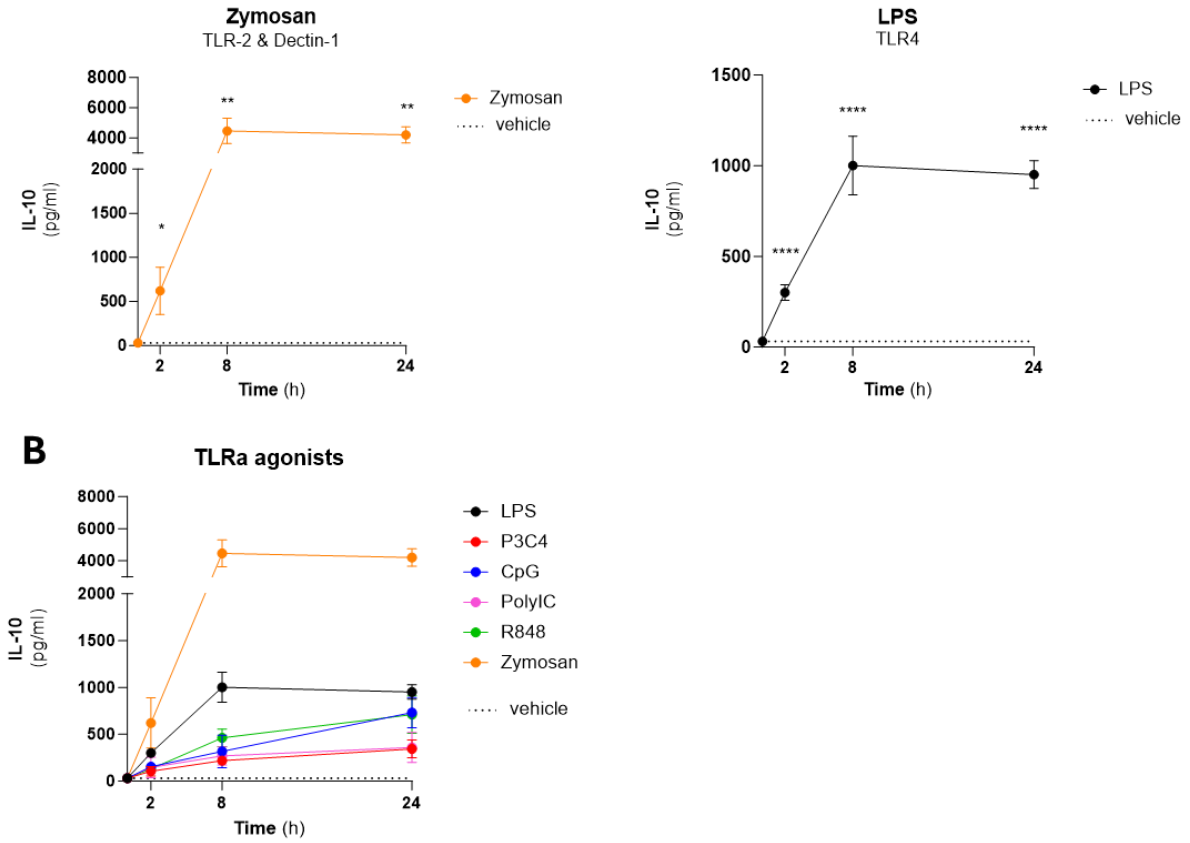

Figure 29. Kinetic and magnitude differences in TLR-induced IL-10 production. (A-B) IL-10 production was analysed by ELISA on WT BMDMs treated with different TLRs agonist for, 2h, 8h and 24h. Data are represented as Mean ± SEM (n=4-6). (A) Statistical analysis was performed using Mann-Withney test stimulated versus vehicle; p≤0.05 was considered significant.

Then, quantitative analysis revealed that KO BMDMs released IL-10 at levels generally comparable to WT cells across all conditions tested. Both genotypes exhibited similar kinetics of IL-10 secretion, with detectable levels appearing as early as 2 hours post-stimulation and continuing to rise through the 24-hour time point (**Figure 30A**). However, a consistent trend emerged in which KO macrophages secreted slightly lower levels of IL-10 compared to WT, depending on the stimulus and time point - except in response to PolyIC, where no clear reduction was observed (**Figure 30B**). We could exclude that IL-10 impairment was due to a defect in TRIF-signaling pathway. KO P3C4 showed reduced IL-10 induction in KO macrophages at 24 hours; CpG demonstrated a similar trend at 2 and 8 hours, with a significant reduction at 24 hours; and R848 and Zymosan elicited noticeably lower IL-10 levels in KO cells at the early 2-hour time point. While these differences were somewhat variable across stimuli and time points, the most consistent and robust impairment in IL-10 release was observed following LPS stimulation. Given this and that LPS is a well-established and widely used stimulus modelling inflammatory responses in

macrophages in vitro, subsequent investigations focused on characterizing the IL-10 impairment in KO macrophages specifically in response to LPS.

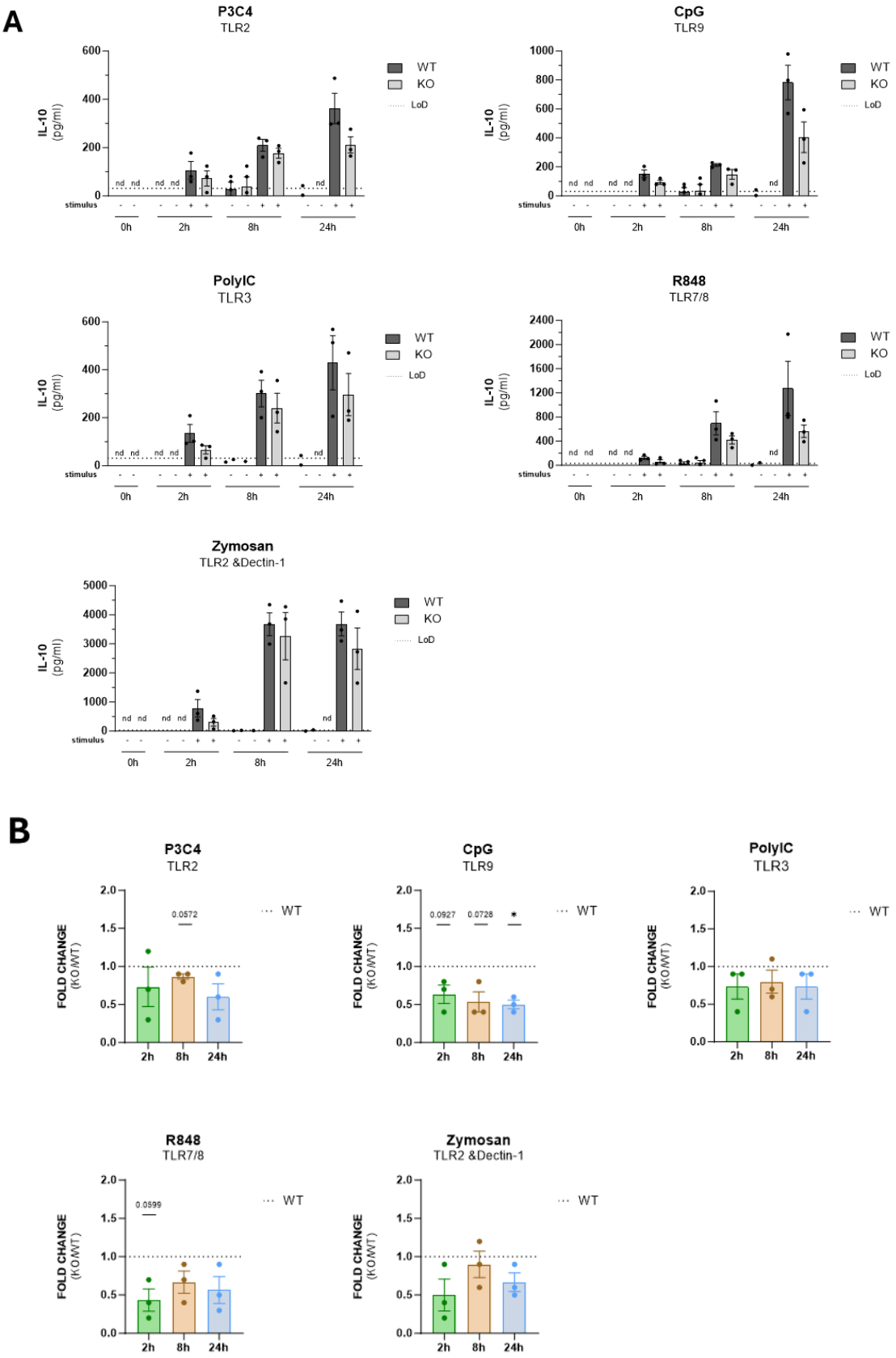

Figure 30. TLR-induced IL-10 production IN WT and MS4A4A KO macrophages. (A-B) IL-10 production was analysed by ELISA on WT and KO BMDMs treated with different TLRs agonist for 2h, 8h and 24h. (A) IL-10 release is represented in pg/ml. (B) IL-10 release is represented as FOLD CHANGE (pg/ml KO versus pg/ml WT). Data are represented as Mean ± SEM and each symbol represent a different biological replicate (n=3); nd= not detectable. (A) Statistical analysis was performed using Mann-Withney test; (B) Statistical analysis was performed using One sample t test; p≤0.05 was considered significant.

The observed impairment in IL-10 release in KO macrophages following LPS stimulation suggests a critical role of MS4A4A in the regulation of anti-inflammatory cytokine production. Since the impairment in IL-10 release was already evident at the early 2-hour time point following LPS stimulation, we initially hypothesized that MS4A4A might be involved in the transcriptional regulation of *Il10*. Previous studies have reported that Il10 mRNA levels remain relatively stable between 1 and 3 hours post-LPS stimulation (65). Our data showed *Il10* mRNA expression peaked at 2 hours, remained stable at 8 hours, and declined by 24 hours (**Figure 31A**). Importantly, no significant differences in *Il10* gene expression were observed WT and KO macrophages at any time point, indicating that MS4A4A is unlikely to regulate Il10 transcription. Furthermore, mRNA stability assays showed no differences in Il10 mRNA decay between WT and KO BMDMs, suggesting that MS4A4A does not influence Il10 mRNA stabilization either (**Figure 31B**). Together, these results indicate that the reduction in IL-10 secretion observed in KO macrophages is not due to altered transcription or mRNA stability, pointing instead to a potential role for MS4A4A in post-transcriptional regulation, such as protein production, processing or secretion.

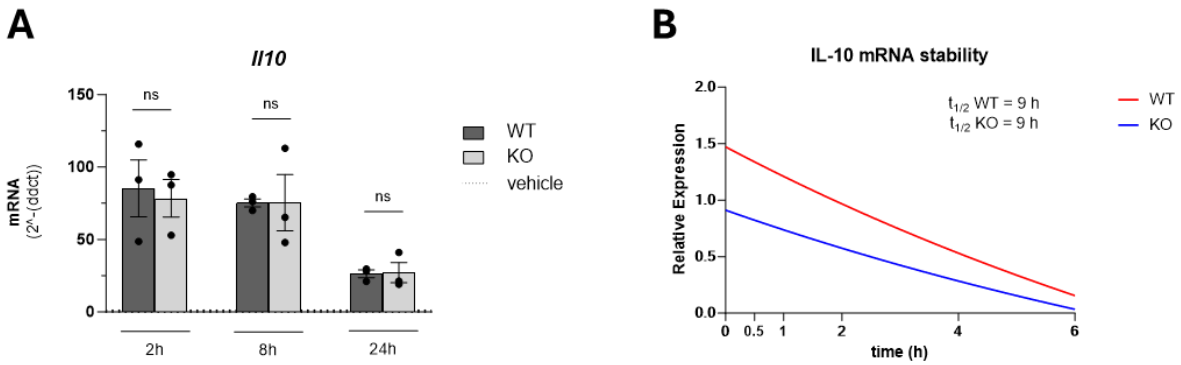

Figure 31. MS4A4A does not affect Il10 mRNA expression and stability. (A) Gene expression of IL10 in BMDMs WT and KO after treatment with vehicle and LPS 100 ng/ml for 2h, 8h and 24h. Data are represented as Mean ± SEM and each symbol represent a different biological replicate (n=3). Statistical analysis was performed using Mann-Withney test; p≤0.05 was considered significant. (B) Il10 mRNA decay in WT and KO MDMs after LPS + Actinomycin D treatment.

After being synthesized in the endoplasmic reticulum (ER), IL-10 is transported to the Golgi apparatus. At the trans-Golgi network (TGN), IL-10 can enter one of two distinct secretory pathways. In the first pathway, approximately 80% of IL-10 is packaged together with IL-6 and TNF-α into carriers that deliver their cargo to the recycling endosome. From there, the cytokines are sorted and transported to the cell surface for secretion. In the second pathway, IL-10 is packaged together with ApoE into Golgi-97-labeled tubules at the TGN. This route bypasses the recycling endosome and transports IL-10 directly to the cell surface. This pathway depends on protein kinase A (PKA) activity and an intact microtubule network (66). Our KO macrophages do not show impaired IL-6 or TNF-α secretion, suggesting that MS4A4A may specifically affect the PKA- and microtubule-dependent secretion route of IL-10 and ApoE. To test this, LPS-activated macrophages were treated with nocodazole, which disrupts microtubules or with the PKA inhibitor H89. After one hour of treatment, IL-10 levels in the culture medium were significantly reduced, indicating that both microtubule integrity and PKA activity are important for IL-10 secretion (**Figure 32A**). However, the extent of IL-10 reduction was similar in both WT and KO macrophages. This suggests that MS4A4A does not directly impair IL-10 release through the microtubule- or PKA-dependent pathway (**Figure 32B**).

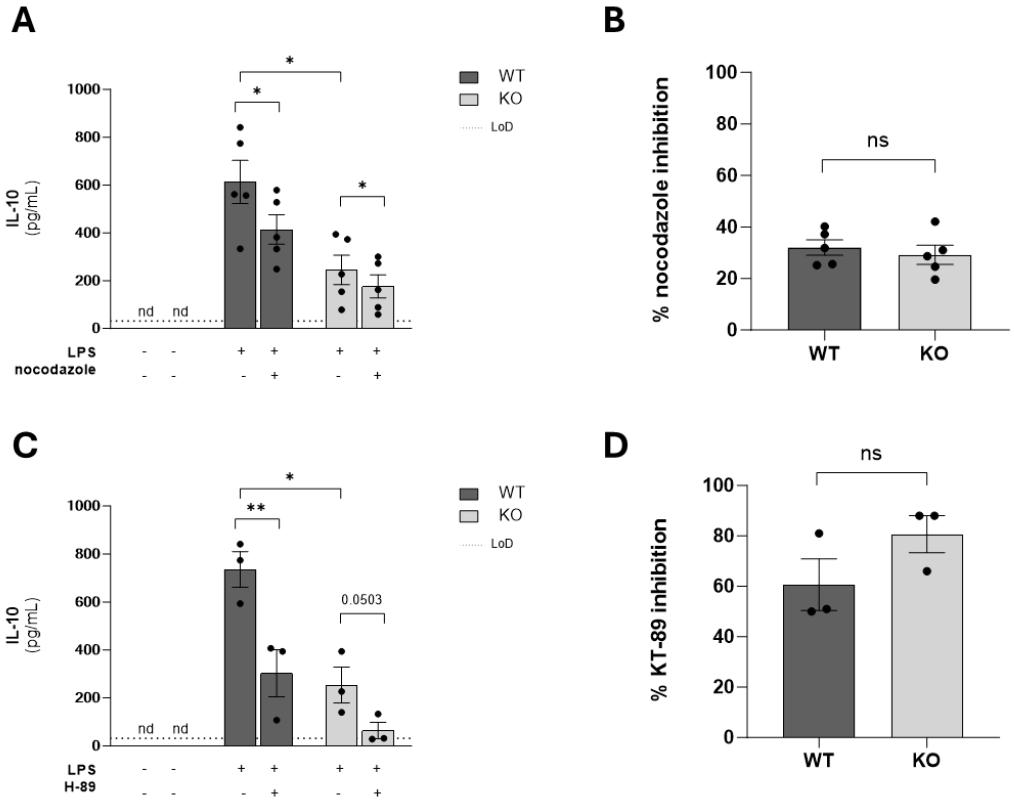

Figure 32. Impact of microtubule disruption and PKA inhibition on IL-10 Secretion. WT and KO BMDMs were stimulated with 100 ng/ml LPS for 2 h prior to treatment with nocodazole (10 µM) or the PKA inhibitor

H89 (40 μM) for the final 1 h. (A-B) Effect of nocodazole on IL-10 ELISA. (C-D) Effect of H89 on IL-10 ELISA. Data are represented as Mean ± SEM and each symbol represent a different biological replicate (n=3-5). Statistical analysis was performed using Mann-Withney test; p≤0.05 was considered significant.

To determine whether MS4A4A is involved in IL-10 production and secretion, BMDMs were stimulated with LPS for 2 or 8 hours, in the presence or absence of Brefeldin A, a protein transport inhibitor that blocks cytokine secretion. Intracellular IL-10 levels were then measured in cell lysates using ELISA (**Figure 33**).

When Brefeldin A was present, preventing IL-10 export and allowing its accumulation in the cytosol, KO macrophages tended to accumulate less IL-10 compared to WT macrophages at the 2-hour time point. Despite this difference was not statistically significant, increase in the experimental sample size may reveal a significant trend. At the 8-hour time point, the reduction in intracellular IL-10 levels in KO BMDMs was statistically significant compared to WT cells. Additionally, no significant difference was observed between the negative control (vehicle) and the LPS + Brefeldin A samples. These results suggest that MS4A4A may play a role in the production or early synthesis of IL-10.

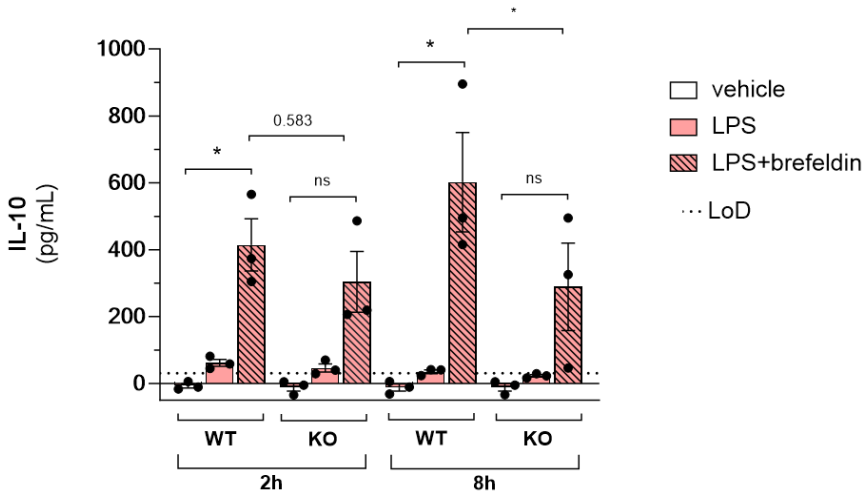

Figure 33. MS4A4A impairs IL-10 accumulation in LPS-stimulated macrophages. IL-10 ELISA on protein lysates from WT and KO BMDMs stimulated or not with LPS ± Brefeldin for 2h or 8h. Data are represented as Mean ± SEM and each symbol represent a different biological replicate (n=3). Statistical analysis was performed using unpaired t test; p≤0.05 was considered significant.

These findings were further supported by IL-10 immunofluorescence analysis. WT and KO BMDMs were treated with LPS with or without Brefeldin A and IL-10 staining was performed. Quantification of the IL-10 fluorescence signal showed that KO macrophages treated with LPS + Brefeldin A had similar IL-10 levels to LPS-treated KO BMDMs, but significantly lower

levels compared to WT cells treated with LPS + Brefeldin A (**Figure 34**). This supports the ELISA results and further indicates that MS4A4A may contribute to IL-10 biosynthesis.

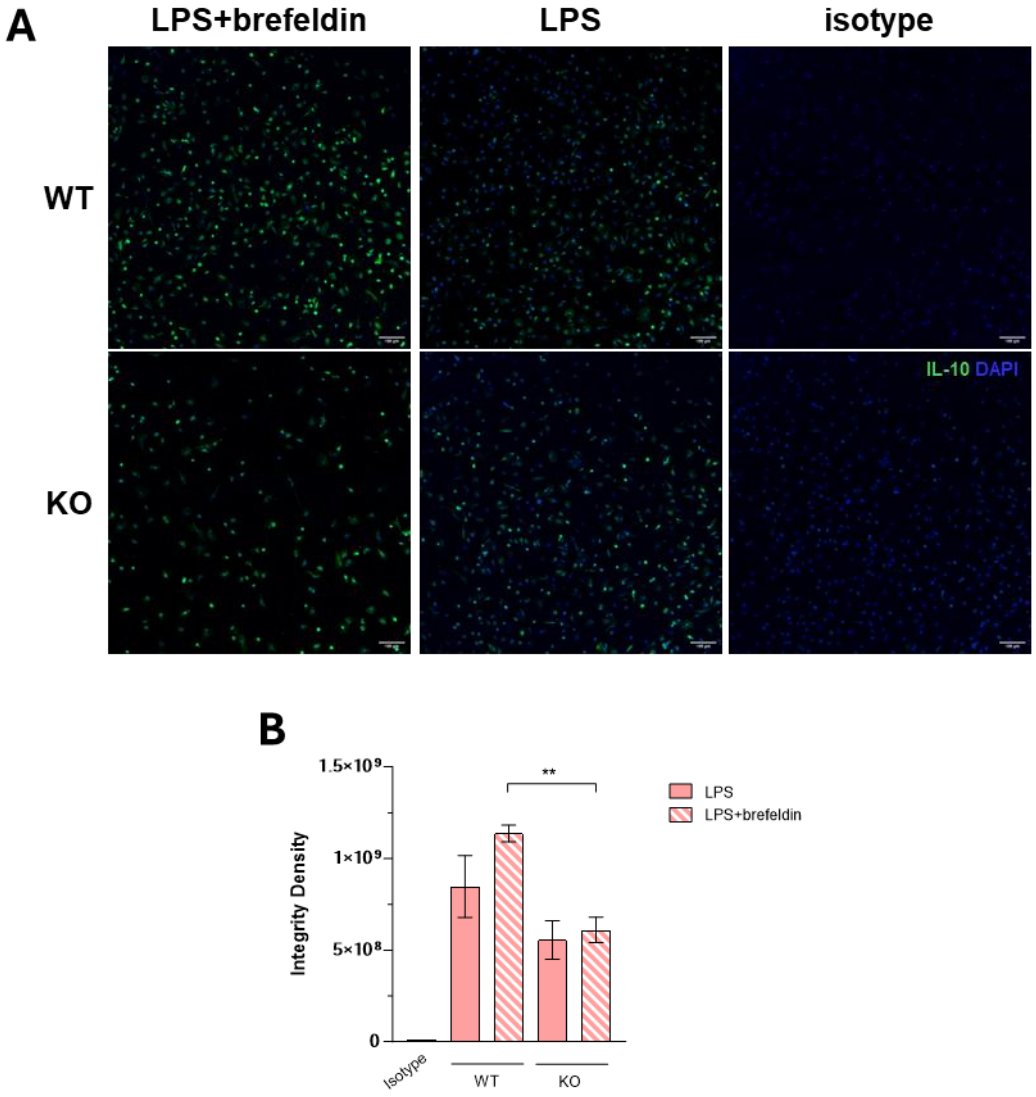

Figure 34. Reduced intracellular IL-10 in MS4A4A KO Macrophages by immunofluorescence. IL-10 immunofluorescence (IF) on WT and KO BMDMs stimulated with 100 ng/ml LPS ± Brefeldin A for 8h. (A) 10X IF images referring to one experiment representative of 2 analysed. (B) IL-10 IF quantification referred to panel A. Data are represented as Mean ± SEM. Statistical analysis was performed using Mann-Withney test; p≤0.05 was considered significant.

In general, macrophages do not store large amounts of cytokines in the cytosol and constitutive expression is rare since most cytokines are induced transcriptionally upon cell activation. However, *Tnfa* mRNA is constitutively expressed and controlled by mRNA stability and translation (66). It can be pre-formed and stored in recycling endosomes allowing rapid secretion. In contrast, in literature it is not reported that IL-10 is constitutively

expressed in BMDMs, but low-level expression may occur in select tissue-resident macrophage populations, such as those in the gut or lungs, where immune tolerance is critical (67).

Unexpectedly, our IF analysis revealed detectable IL-10 signal in resting BMDMs using two antibodies against IL-10 from different sources (**Figure 35A**). In both cases, the IL-10 staining was clearly above the respective isotype controls indicating specific signal (**Figure 35B**). The intracellular IL-10 levels in LPS-treated BMDMs were comparable to those in untreated cells, consistent with the expected secretion of IL-10 in the media upon activation. However, co-treatment with LPS and Brefeldin A resulted in an increased intracellular IL-10 signal, supporting the idea that IL-10 is produced and rapidly secreted upon stimulation, and that Brefeldin A blocks this secretion, leading to intracellular accumulation.

Our results suggest the existence of an intracellular IL-10 pool constitutively present in macrophages. For this reason, the impairment in IL-10 release observed in our KO cells could be due to differences in the amount of IL-10 stored constitutively in KO BMDMs.

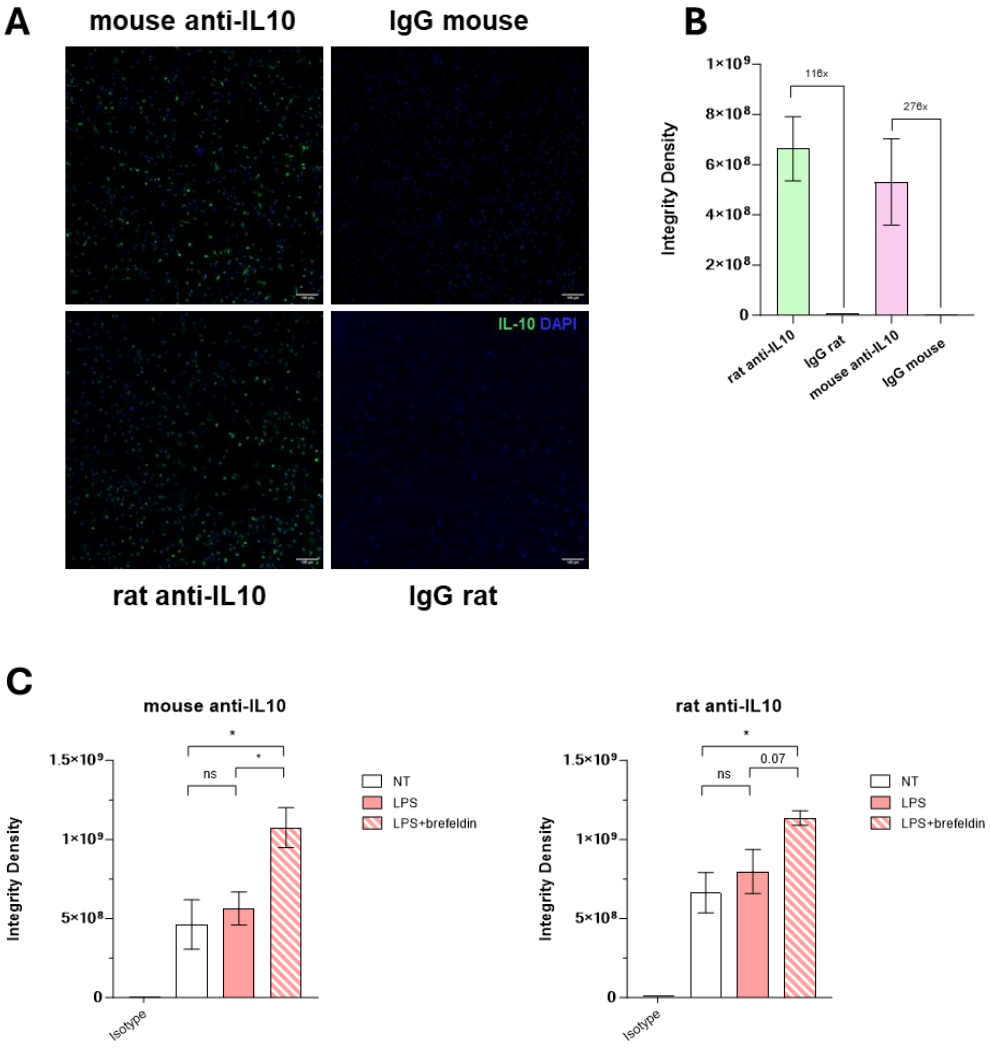

Figure 35. Identification of an IL-10 storage pool in resting macrophages by immunofluorescence. (A) IL-10 IF on untreated WT BMDMs. 10X IF images referring to one experiment representative of 2 analysed. (B) IL-10 IF quantification referred to panel A. (C) IL-10 IF quantification on WT BMDMs treated or not with LPS ± Brefeldin for 8h. (B-C) Data are represented as Mean ± SEM and quantification is representative of one experiment of 2 analysed. Statistical analysis was performed using Mann-Withney test; p≤0.05 was considered significant.

In order to confirm the relevance of the IL10 impairment in KO BMDMs, we set up a siRNA knockdown system for MS4A4A in human macrophages. Western blot analysis confirmed that MS4A4A silencing achieved approximately 60% reduction in protein levels compared to scrambled siRNA controls (**Figure 36**). Using this system, we measured IL-10 release upon LPS stimulation via ELISA. Consistent with our mouse data, silencing MS4A4A in human macrophages led to a marked impairment in IL-10 secretion, supporting a conserved and regulatory role for MS4A4A in modulating anti-inflammatory responses across species (**Figure 37**).

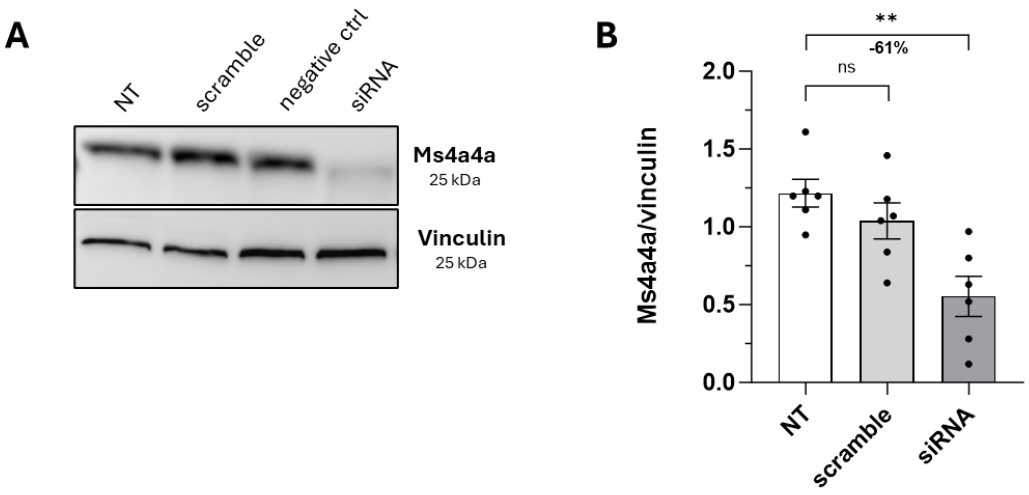

Figure 36. Validation of MS4A4A knockdown by siRNA in human macrophages. WB on total protein lysates for MS4A4A and vinculin. Panel (A) shows image referring to one experiment representative of 6 analysed. (B) Quantification of MS4A4A normalised on housekeeping (vinculin). Bars represent mean ± SEM and each symbol represent a different biological replicate (n=6). Statistical analysis was performed using two-tailed unpaired (Mann-Whitney) Student's t test; p≤0.05 was considered significant.

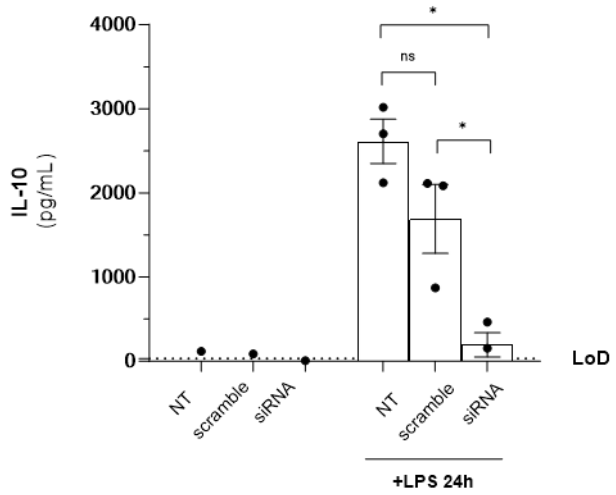

Figure 37. MS4A4A silencing impairs IL-10 release in LPS-stimulated human macrophages. IL-10 production was analysed by ELISA on human macrophages ± LPS. Bars represent mean ± SEM and each symbol represent a different biological replicate (n=3). LoD = ELISA Limit Of Detection. Statistical analysis was performed using two-tailed unpaired (Mann-Whitney) Student's t test; p≤0.05 was considered significant.

4. Role of MS4A4A in modulating dexamethasone response in rheumatoid arthritis

Rheumatoid Arthritis (RA) is a chronic autoimmune disease characterized by synovial inflammation, cartilage degradation and bone erosion. Despite the availability of various therapeutic options - including conventional synthetic Disease-Modifying Anti-Rheumatic Drugs (DMARDs) like methotrexate and biologic agents targeting proinflammatory cytokines or immune cell subsets - corticosteroids (CS) remain widely used to control active disease. However, their long-term use is limited by adverse effects.

MS4A4A has emerged as a molecule of interest due to its high expression in $CD163^{+}$ macrophages in the synovial tissue of RA patients. Moreover, its expression is upregulated by the corticosteroid Dexamethasone (Dex) (35). Recent transcriptomic analyses have identified MS4A4A as part of a peripheral blood leukocyte gene signature that distinguishes RA patients from healthy and undifferentiated arthritis patients (68).

As part of my doctoral research, I was involved in a study aimed to investigate the role of MS4A4A in RA pathogenesis and it effect on corticosteroids therapy.

We first consulted public transcription datasets and we observed that MS4A4A is the only MS4A protein whose expression is selectively induced in the synovial tissue of RA patients (69). Moreover, the induction of MS4A4A was not observed in other types of chronic inflammatory arthritis. In the clinical cohort of RA patient, we observed that MS4A4A expression and the MS4A4A+ cells are significantly higher in lympho- myeloid pathotypes compared with diffuse-myeloid and pauci-immune fibroid pathotypes (**Figure 38 A-B**). Three distinct synovial pathotypes are identified in RA patient based on immune cell composition: lympho-myeloid is rich in lymphocytes and myeloid cells; diffuse-myeloid features a prevalent but disorganized infiltration of myeloid cells, primarily macrophages; pauci-immune fibroid is characterized by a low immune cell count with a predominance of fibrotic or stromal cells. These pathotypes are linked to different disease severities: lympho-myeloid patients exhibit higher disease activity, followed by diffuse-myeloid and pauci-immune fibroid patients. MS4A4A expression positively correlated with the arthritis score (**Figure 38C**). RNA-seq analysis of synovial tissue from RA patients revealed a positive correlation between expression levels of MS4A4A and proinflammatory mediators, neutrophil chemoattractant, and genes promoting bone resorption and a negative correlation with gene preventing bone resorption.

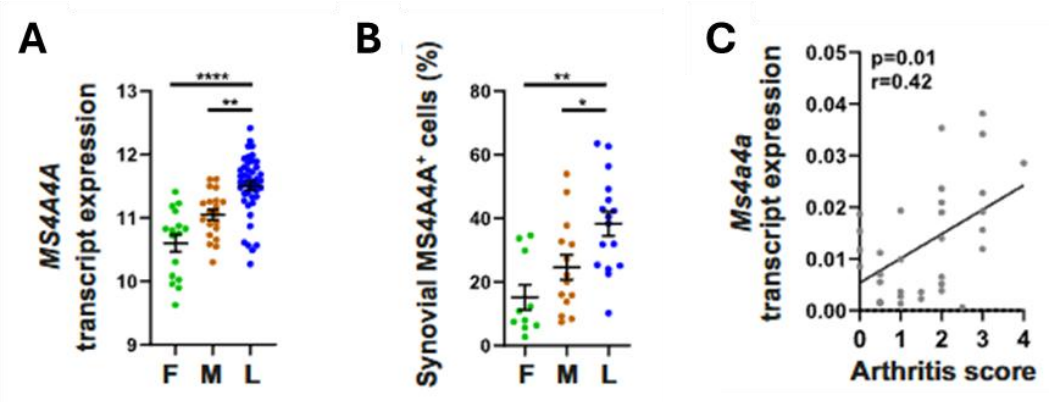

Figure 38. MS4A4A expression correlates with joint inflammation and RA progression. MS4A4A transcript expression in synovial tissues presenting an F, M, or L pathotype, assessed by RNA-sequencing. P-values were calculated using the Kruskal–Wallis test with Dunn's post test, **P < 0.01, ****P < 0.0001. (D) Percentage of MS4A4A+cells in synovial tissues presenting an F, M, or L pathotype, assessed by immunohistochemistry (IHC) and quantified by digital image analysis. P-values were calculated using the Kruskal–Wallis test with Dunn's post test, *P < 0.05, **P < 0.01. Correlation between Ms4a4a relative expression and arthritis score (/4) for each individual paw (n = 33, distributed across day 2, day 6, and day 12 timepoints). P-value and r coefficient were calculated according to the Spearman correlation test (69).

To better clarify the impact of MS4A4A in RA pathogenesis, we conducted in vivo experiments of serum-transfer induced arthritis (STIA) model on WT and MS4A4A KO mice. The KO mice did not show differences in STIA severity compared to WT. Then we investigated the potential role of MS4A4A on the therapeutic treatment. The synovial tissue of patients treated with csDMARDs alone was compared to that of patients treated with both csDMARDs and CS. CS treatment did not affect the overall macrophage infiltration in the synovium but significantly enhanced MS4A4A expression levels, suggesting a direct effect of CS on the modulation of MS4A4A expression in synovial macrophages. We investigated if MS4A4A was expressed the regulated by CS also in the murine a murine arthritic joint. As expected, MS4A4A is expressed and upregulated by CS (Dex) also in murine synovial macrophages (69).

In the in vivo STIA model the therapeutic activity of Dex was significantly enhanced in KO mice as demonstrated by the lower arthritis scores in the KO animals. Of note, MS4A4A deletion did not influence the efficacy of other therapeutic drug, like methotrexate and Intravenous Immunoglobulin G (IVIGg) (**Figure 39 A-B-C**). In line with this data, MTX and IVIg did not modulate MS4A4A expression by macrophages contrary to effects seen with Dex (**Figure 39D**). Consistent with the clinical scores, KO mice treated with Dex showed a significant reduction in the number of inflammatory cells compared to Dex-treated WT mice

Figure 39E-F). Take together, these findings demonstrated that MS4A4A limits the CS efficacy in a RA model.

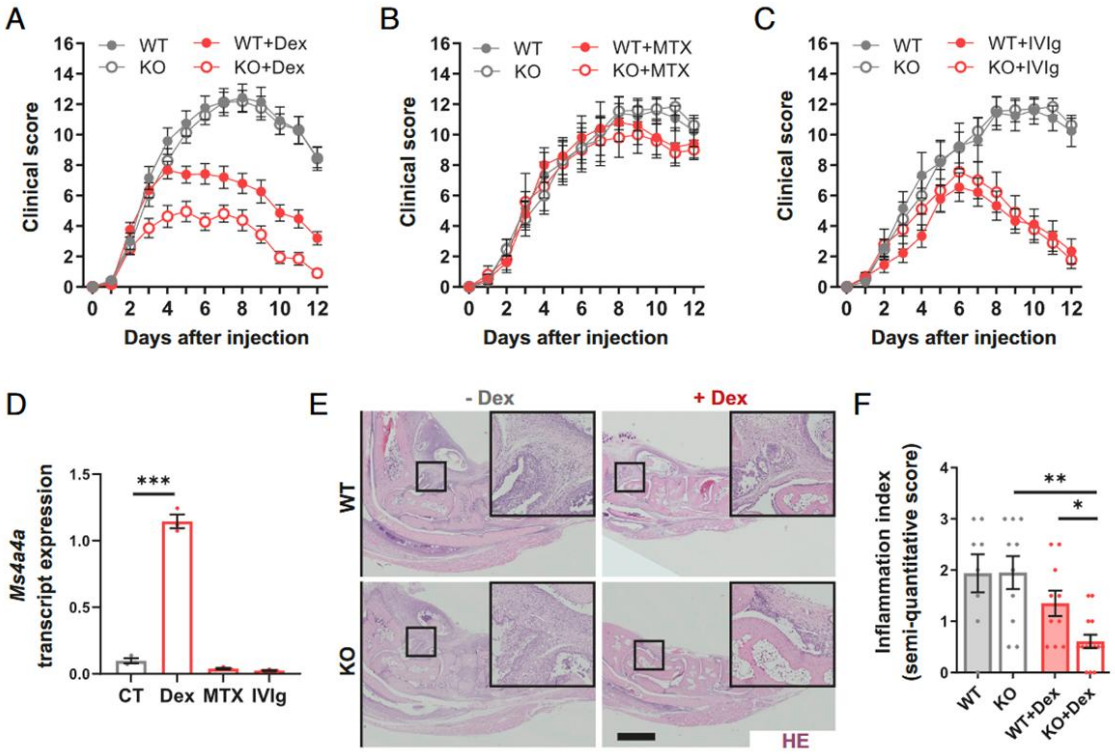

Figure 39. MS4A4A expression in macrophages limits the CS therapeutic activity in arthritis. (A) Clinical score assessing forepaws and hind paws inflammation after STIA induction in WT and KO mice, injected intraperitoneally daily from D2 with 10 µg Dex or its vehicle. N = 20 to 22 animals per group. Scores of the KO+Dex group are significantly lower compared WT+Dex from day 3 ($P < 0.01$, as assessed by the two-way ANOVA test followed by Tukey's multiple comparisons). (B) Clinical score after STIA induction in WT KO mice, injected intraperitoneally 25 µg MTX or with PBS every 2 d from D2. N = 5 to 12 animals per group. Scores of the WT+MTX and KO+MTX groups do not statistically differ from untreated corresponding animals (as assessed by the two-way ANOVA test followed by Tukey's multiple comparisons). (C) Clinical score after STIA induction in WT and KO mice treated with a single intraperitoneal injection at day 2 of 2 mg/kg IVIg or with PBS. N = 5 to 12 animals per group. WT+IVIg and KO+IVIg scores are similarly and significantly reduced compared to untreated WT and KO from day 8 ($P < 0.05$, as assessed by the two-way ANOVA test followed by Tukey's multiple comparisons). (D) Ms4a4a transcript expression in BMDM stimulated with IL-4 alone (CT) or in combination with 1 µM of Dex, 5 ng/mL of MTX or 80 µg of IVIg for 18 h. n = 3 per group. P- values were assessed using the Mann–Whitney test, ***$P < 0.001$ (69).

The part of this project I was most involved was focused on clarifying the molecular mechanisms responsible for the increased therapeutic response to Dex in KO mice. To better understand the role of MS4A4A in modulating Dex therapeutic effect, we analysed neutrophil infiltration in joint tissues since they contribute to the initiation and maintenance of joint inflammation. Our findings showed that KO mice exhibited significantly reduced

neutrophil accumulation in the joints after Dex stimulation, and an increased levels of circulating neutrophils in the blood compared to WT controls. Moreover, Dex-treated arthritic joints of KO mice displayed less cartilage and bone destruction (69). Taken together, these results indicated that MS4A4A is associated with synovial neutrophil infiltration and joint damage upon Dex treatment.

Fc gamma receptors (FcγRs) play a pivotal role in the development and progression of RA: altered levels of FcγRs in the immune cells (including macrophages) have been observed in RA patients. These receptors, expressed in various immune cells including macrophages, bind to the Fc portion of IgG antibodies. Through this interaction, they mediate key immune functions such as phagocytosis, cytokine secretion and antibody-dependent cellular cytotoxicity. RA is an autoimmune condition marked by persistent joint inflammation, largely driven by immune complexes formed between autoantibodies and self-antigens. FcγRs recognize and bind these complexes, triggering inflammatory responses that contribute to joint damage. In autoimmune conditions, cross-linking of FcγRs by immune complexes amplifies inflammation. Among the FcγRs, FcγRIII (*FCGR3A* gene) plays a key role in balancing immune responses, helping to prevent excessive inflammation and autoimmunity. Our RNA-sequencing analysis of the synovium of RA patients showed a positive correlation between the expression of *FCGR3A*, its γ signaling chain of FcγRI (FC*ER1G*) and MS4A4A (**Figure 40 A**). Moreover, FCGR3A expression has been associated with RA severity, such as MS4A4A, and treatment with Dex was found to upregulate FCGR3A expression in BMDMs without affecting other Fc receptors (**Figure 40 B-C**).

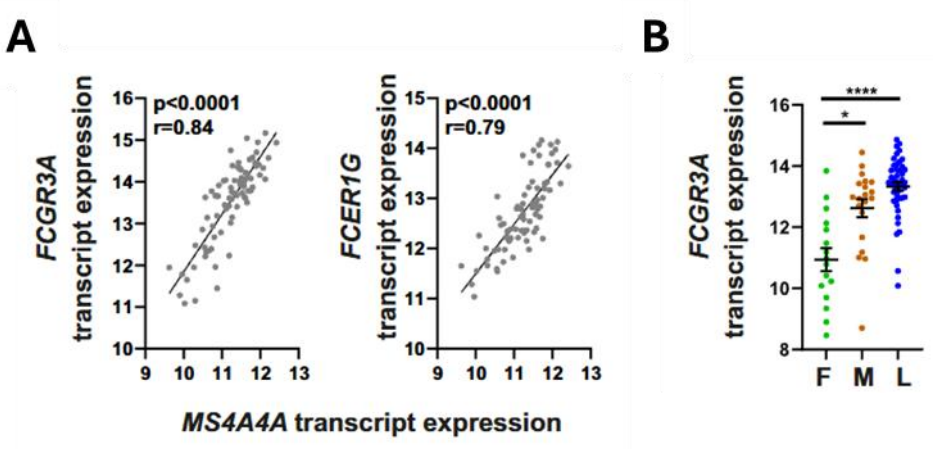

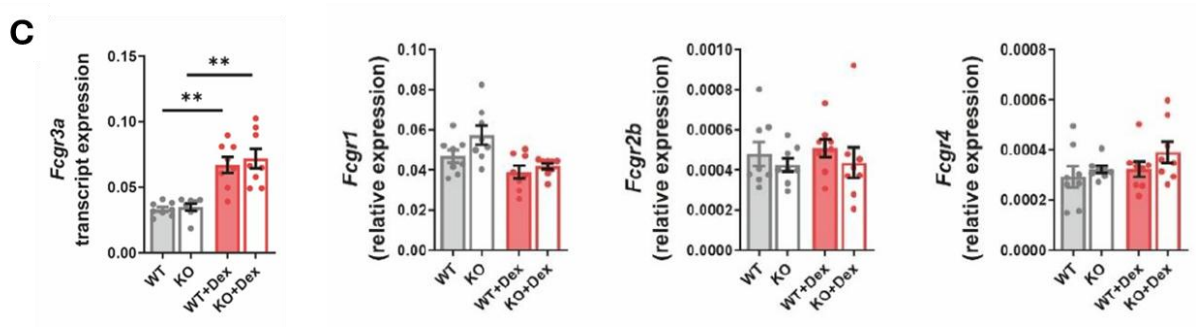

Figure 40. Dexamethasone affect specifically Fcg3a and Fcer1g expression. (A) Correlation between MS4A4A transcript expression and FCGR3A (Left panel) orFCER1G (Right panel). P-value and r coefficient were calculated according to the Spearman correlation test. (B) FCGR3A transcript expression in synovial tissues presenting a pauci-immunefibroid (F), diffuse-myeloid (M), or lympho-myeloid (L) pathotype, assessed by RNA-sequencing. P-values were calculated using the Kruskal–Wallis test with Dunn'sposttest, **P < 0.01, ***P < 0.001. (C) Fcgr3a, Fcgr1, Fcgr2b Fcgr4 and transcript expression in BMDM from WT and KO mice treated or not with 1 µM of Dex. Data are represented as Mean ± SEM and each symbol represent a different biological replicate. Statistical analysis was performed using the Mann‑Whitney test; p≤0.05 was considered significant (69).

As already reported, FCER1G, was identified as a possible interactor of MS4A4A through a yeast split-ubiquitin screening (**Figure 14**), supporting the hypothesis of a functional link between these molecules. This led us to further investigate if MS4A4A influences FcγRIII activity.

To investigate the role of MS4A4A in modulating the inflammatory response mediated by FcγRs, WT and KO BMDMs were stimulated with aggregated Intravenous Immunoglobulin G (Agg-IVIg) to activate Fc receptor signaling pathway via FcγRIII. KO macrophages showed a trend toward reduced secretion of TNFα and CXCL2, key proinflammatory cytokines involved in joint inflammation and neutrophil recruitment during the pathogenesis of RA. When macrophages were co-stimulated with Agg-IVIg and Dex, the secretion of these proinflammatory cytokines was further reduced, consistent with the known anti-inflammatory effects of glucocorticoids. Notably, the tendency of KO BMDMs to produce lower levels of TNFα and CXCL2 became statistically significant following Dex treatment (**Figure 41A**). Supporting this observation, a similar reduction in *Tnfα* and *Cxcl2* expression was detected in arthritic joints from the STIA model after Dex administration (**Figure 41B**). Furthermore, MS4A4A did not alter the anti-inflammatory response to Dex in macrophages stimulated with LPS, indicating that its modulatory effect is specific to FcγR-mediated pathways (**Figure 41A**).

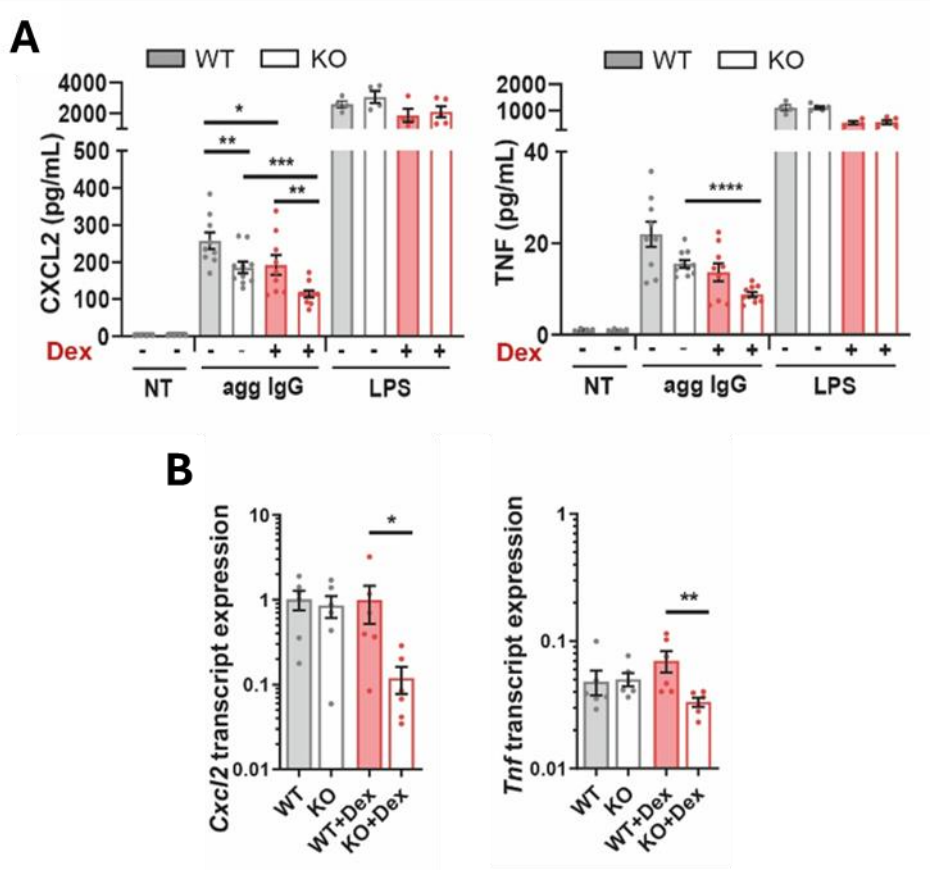

Figure 41. MS4A4A affect Dex effect on TNF-α and CXCL2 during Fcγ-mediated inflammatory response. (A) TNFα and CXCL2 cytokine production were analysed by ELISA on WT and MS4A4A KO BMDMs treated or not with 500 µg/mL of Agg-IVIG or 100 ng/mL LPS for 8h. 1 µM Dex was added 1 h before Agg-IVIg or LPS stimulation (n=4-10). (B) Tnfα and Cxcl2 transcript expression was assessed by RT-qPCR in the ankles of WT and KO mice treated with PBS or Dex at day 6 after STIA induction (n=6). Data are represented as Mean ± SEM and each symbol represents a different biological replicate. Statistical analysis was performed using the Kruskal–Wallis test with Dunn's post test; p≤0.05 was considered significant (69).

To confirm that the observed modulation of Dex responsiveness by MS4A4A is dependent on FcγR signaling rather than on Dex itself, we performed transcriptomic profiling of WT and KO BMDMs treated with Dex (**Figure 42A**). Principal component analysis (PCA) of transcriptomes revealed that samples separated mainly by treatment and by timepoint (**Figure 42B**). To understand if there are some transcriptional changes between WT and KO BMDMs upon exposure to Dex, we first focused our analysis comparing Dex-treated WT versus Dex-treated KO BMDMs for each time point: in all the comparison there are no differentially expressed genes (**Figure 42C**). Then, we performed a second analysis comparing Dex with vehicle counterparts both in WT and KO to highlight the functional effect of Dex stimulation. Dex treatment induced hundreds of DEGs - predominantly at 8- and 24-hours post-treatment - with similar numbers between WT and KO (**Figure 42D**). Although a

few genes were differentially expressed between WT and KO BMDMs, these were not biologically relevant **(Figure 42E)**. The analysis revealed genes modulated in a genotype-dependent way. However, the magnitude and number of these changes are limited, supporting the conclusion that MS4A4A deficiency does not substantially alter the transcriptional response to corticosteroid stimulation in macrophages.

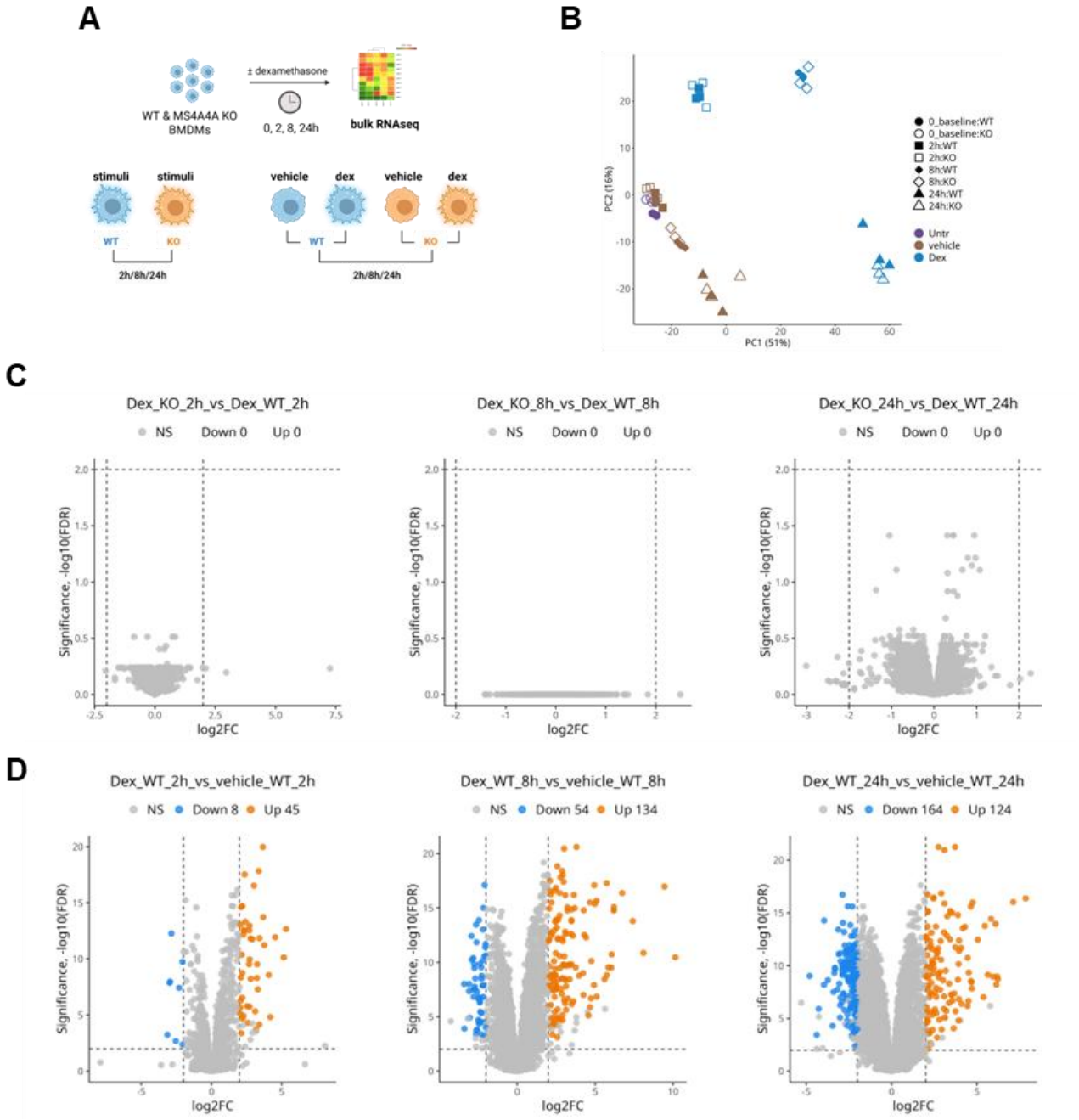

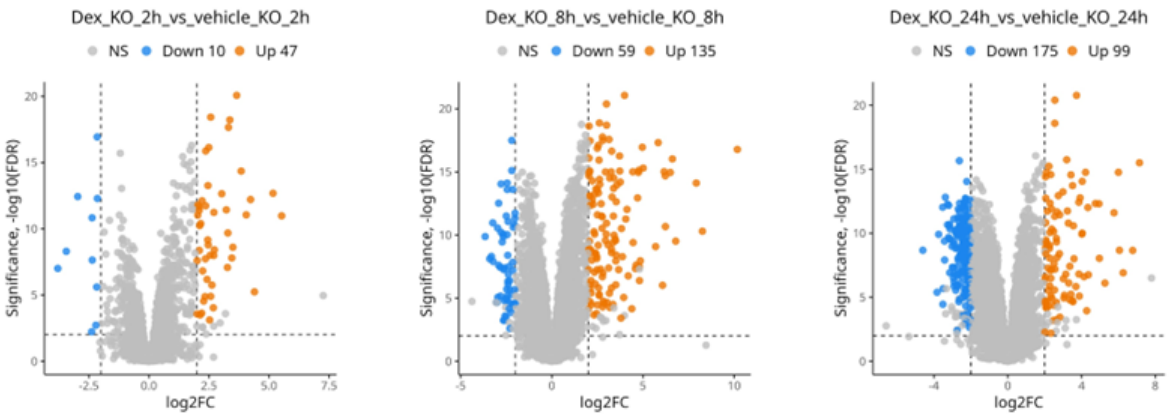

E

Gene Symbol	logFC WT	Regulation	logFC KO	Regulation	Δ logFC	intersection
Mrap	4,7	Up	3,1	Up	1,5	Dex_KO_24h|Dex_WT_24h
Tg	4,7	Up	3,0	Up	1,7	Dex_KO_24h|Dex_WT_24h
Rdh9	3,9	Up	1,9	NS	2,0	Dex_WT_24h
Egfr	3,7	Up	1,7	NS	2,0	Dex_WT_24h
Ttpa	2,9	Up	4,7	Up	-1,8	Dex_KO_8h|Dex_WT_8h
Dpep3	2,6	Up	1,3	NS	1,3	Dex_WT_8h
Ankrd29	2,4	Up	1,3	NS	1,1	Dex_WT_8h
Rsad2	-0,9	NS	-2,1	Down	1,1	Dex_KO_8h
Ptchd1	-4,0	Down	-2,7	Down	-1,2	Dex_KO_24h|Dex_WT_24h

Figure 42.Transcriptional profiling of WT and MS4A4A KO macrophages revealed no difference in response to Dex. (A) Experimental design of bulk RNAseq: WT and MS4A4A KO BMDMs were treated with/without Dex (1 μM) for 2, 8 and 24 h. This experimental design generated 14 different experimental conditions investigated by RNAseq in biological triplicates. Schedule of performed comparison analysis is reported. (B) PCA on all samples using the top 2000 most variable genes assesses samples similarities and visualizes the separation of experimental groups in a 2-Dimensional space. (C-D) Volcano plots display $\log_2$ fold-change on the x-axis and $-\log_{10}$(FDR) on the y-axis for each contrast: (C) Dex-treated WT vs Dex-treated KO BMDMs at timepoint 2h, 8h and 24h; (D) Dex-treated vs vehicle both WT ad KO BMDMs at timepoint 2h, 8h and 24h; significantly up- and down-regulated genes (FDR < 0.01, $|\log_2 FC| \geq 2$) are highlighted in orange and blue, respectively. (E) Differential expression of selected genes in WT and MS4A4A KO BMDMs. For each gene, the table reports the $\log_2$ fold-change (logFC) in WT and KO (Dex-treated vs vehicle), the corresponding direction of regulation (Up, Down or NS = Not Significant), and the ΔlogFC, defined as the difference in logFC between WT and KO. The final column ("intersection") indicates the specific contrast(s) in which the gene was identified as significantly modulated. For example, "Dex_WT_24h" indicates the gene was significantly differentially expressed in WT at 24h, while "Dex_KO_24h | Dex_WT_24h" indicates the gene was regulated in both genotypes at the 24h timepoint (69).

Together, these results suggested that MS4A4A can potentially regulates the FcγR function. This hypothesis was further supported by the identification of FCER1G as a potential interacting partner of MS4A4A. To validate this interaction, a co-immunoprecipitation (Co-

IP) assay was performed. However, despite successful immunoprecipitation of MS4A4A, no interaction with the γ-chain was detected in either resting or Agg-IVIg–stimulated macrophages (**Figure 43**).

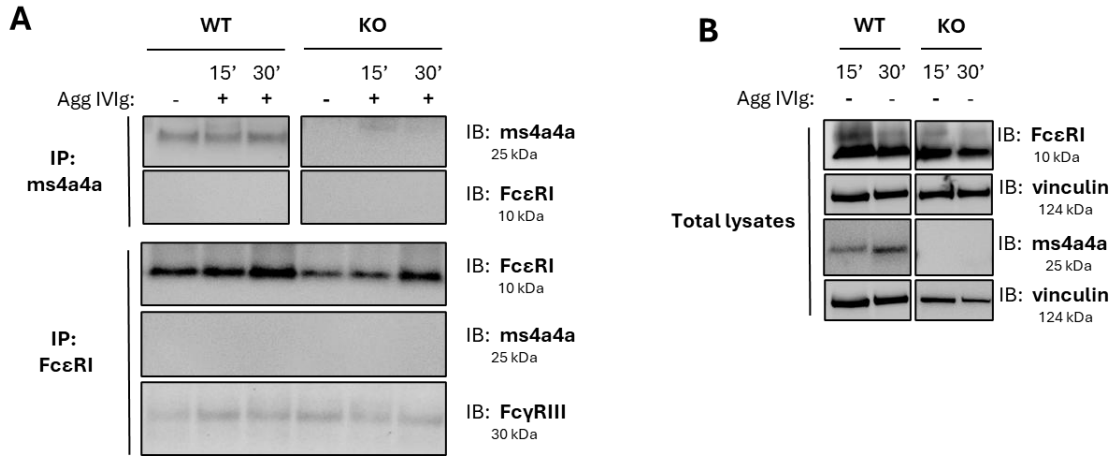

Figure 43. MS4A4A does not interact with γ-chain of FcγRs. WT and KO BMDMs were stimulated or not with Agg-IVIg 500 μg/ml for 15 and 15 minutes. Cells were lysed, γ-chain and ms4a4a were immunoprecipitated (IP). (A) IP samples and total protein samples were immunoblotted (IB) for γ-chain, ms4a4a, FcγRIII and vinculin (housekeeping protein). (B) WB on total protein lysates that were immunoprecipitated as positive control of the IP. Panels show images referring to one experiment representative of 3 analysed (n=3).

The functional defect observed in MS4A4A KO macrophages following FcγR activation by Agg-IVIg is not due to a direct interaction between MS4A4A and the γ-chain of the FcγR signaling complex. Nevertheless, MS4A4A appears to modulate the FcγR-dependent pathway. Our previous work demonstrated that MS4A4A is essential for effective Dectin-1 signaling, particularly in facilitating optimal Syk phosphorylation, which is necessary for cytokine release and reactive oxygen species (ROS) production (35). FcγRIII activation by immunoglobulin binding triggers intracellular signaling cascades that are primarily initiated through the activation of Src and Syk family tyrosine kinases following FcγR cross-linking. Syk, a key tyrosine kinase associated with FcγRIII, phosphorylates downstream targets and recruits adaptor proteins, thereby orchestrating various FcγR-mediated responses such as cytokine production.

Given this context, we investigated whether the reduced production of TNF-α and CXCL2 in MS4A4A KO BMDMs following FcγR activation could be attributed to impaired Syk phosphorylation. Notably, stimulation with Agg-IVIg induced Syk phosphorylation as early as 5 minutes post-stimulation, with increased phosphorylation levels peaking at 15 minutes and remaining stable up to 30 minutes. This phosphorylation pattern was observed in both WT

and KO macrophages, with no significant differences between the two genotypes (**Figure 44**).

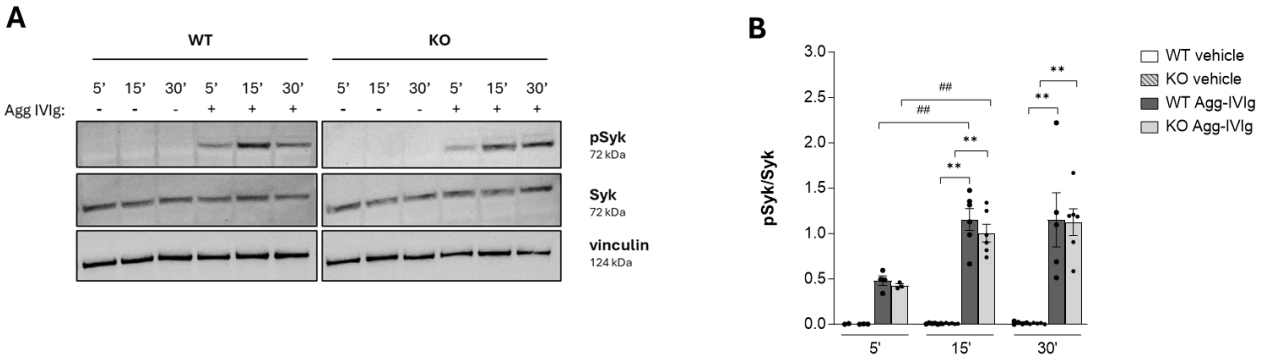

Figure 44. Agg-IVIg induces pSyk activation independent of MS4A4A regulation. WT and KO BMDMs were stimulated or not with Agg-IVIg 500 µg/ml for 5, 15 and 15 minutes. (A) WB on total protein lysates for pSyk, total Syk and vinculin. Panel shows image referring to one experiment representative of 3-6 analysed. (B) quantification of phosphorylated Syk corrected for total Syk. Bars represent mean ± SEM (n= 3-6). Data are represented as Mean ± SEM and each symbol represent a different biological replicate. Statistical analysis was performed using two-tailed unpaired (Mann-Whitney) Student's t test; p≤0.05 was considered significant; * versus vehicle; # versus 5 minutes.

DISCUSSION

MS4A4A has emerged as a molecule potentially involved in the regulation of macrophage plasticity and functions. Previous studies suggest that it can organize homo- and hetero-complexes, preferentially in lipid raft-associated microdomains, resembling the behaviour of tetraspanins and proposing it to act as an ion channel or as modulator of other immunoreceptors. Although MS4A4A has been implicated in various pathological conditions, its biological function remains poorly defined. Given its emerging importance in immune response, this project aims to characterize the role of MS4A4A in macrophage activation and function.

Starting from current knowledge that MS4A4A shares structural similarities with tetraspanins, the present project investigated the structural properties, potential interactions and functional implications of MS4A4A to clarify its function.

Consistent with the structural features observed in other MS4A family members, MS4A4A was found to adopt a four-pass transmembrane topology, with both the N- and C-termini located on the same side of the membrane. By integrating advanced machine learning and AI-based modelling approaches, we identified regions of intrinsic flexibility and disorder at both termini. These disordered regions suggested a regulatory role in protein-protein interaction or in modulating signaling pathway. This observation is consistent with previous findings in the MS4A and tetraspanins families, where disordered domains contribute to membrane organization and the formation of signaling complexes. Taken together, the structural analysis supports the hypothesis that MS4A4A does not act as receptor or ion channel, but rather as a scaffold protein, potentially organizing membrane microdomains or modulating the activity of associated proteins. This is in line with role of tetraspanins and MS4A proteins in organizing membrane microdomains and influencing signaling receptor localization.

Interestingly, a hydrophobic cavity within the transmembrane domain was identified to potentially interact with small molecule. A high-affinity binding site on the cytoplasmic-facing side of the protein was identified to have a high affinity for the drug dexamethasone metasulfobenzoate, known to upregulate MS4A4A expression (35). Despite promising docking results, these interactions likely reflect a general affinity for steroidal scaffolds rather than specific ligand recognition. No MS4A protein has been shown to bind small molecules or function as a druggable target. Therefore, while MS4A4A appears capable of accommodating steroidal ligands structurally, its classification as a druggable protein

remains hypothetical. Further experimental validation (e.g. ligand binding affinity assays and mutational analysis of the pocket) is required to clarify this potential.

A key question of this study was whether MS4A4A plays a direct role in calcium signaling, as previously proposed for related proteins like MS4A1 (CD20) and suggested by some studies on MS4A4A (45,70). Molecular dynamics simulations showed that the transmembrane MS4A4A portion can support the passage of small molecules or ion. However, these analyses are not sufficient to confirm the idea of MS4A4A as ion channel.

Results obtained by in vitro functional assay, showed that MS4A4A does not affect the homeostatic calcium concentration in macrophages, in contrast to previous studies on THP-1 cells. This discrepancy may reflect differences in cell type, culture conditions, or experimental approaches. However, the KO macrophages showed a tendency to induce lower amount of calcium upon β-ionone stimulation, supporting the possible involvement of MS4A4A in regulating the calcium flux mediated by the olfactory receptors.

Take together, these findings reinforce the idea that MS4A4A is best described as a membrane-associated scaffold or modulator rather than as a ligand-gated receptor or ion channel. To further validate and expand upon these findings, high-resolution structural studies - including cryo-electron microscopy - are essential for confirming the protein's topology and pocket geometry. Additionally, electrophysiological assays could help determine whether MS4A4A modulates ion flow under specific conditions, and ligand-binding assays combined with site-directed mutagenesis will be crucial for understanding the specificity and biological relevance of its interaction with steroidal compounds.

The second part of the project focused on functionally characterize MS4A4A during macrophage activation, taking advantage of the identification of new potential protein partners and experimental comparisons between WT and KO macrophages under inflammatory conditions. Until now, MS4A4A has been associated with an anti-inflammatory phenotype in macrophages since its expression is induced by anti-inflammatory stimuli (IL-4 and the corticosteroid) (35). Moreover, previous studies have reported that MS4A4A deficiency impairs the expression of M2-like markers in murine macrophages stimulated with anti-inflammatory cytokines (IL-4, IL-13), suggesting a role in the regulation of macrophage plasticity promoting an anti-inflammatory phenotype (47,48). Despite this, in the present study we investigated the role of MS4A4A under inflammatory conditions and demonstrated its involvement in the activation of immunoreceptors that mediate inflammatory responses in macrophages. Similar findings have been reported in the literature, where MS4A4A has

been shown to be dispensable for Dectin-1 receptor activation upon Zymosan stimulation (35). Additionally, MS4A4A has been described to cooperate with its family member MS4A6A to regulate and stabilize the DAP12–TREM2 complex, thereby modulating microglial function (55). In mast cells, MS4A4A promotes PLCγ1 signaling, store-operated calcium entry (SOCE) and degranulation through FcεRI, supporting its role in IgE-mediated mast cell activation (43). Altogether, these findings indicate that, although MS4A4A silencing impairs M2-like gene expression, its functional role has been described in pro-inflammatory contexts. The modulation of MS4A4A expression following LPS stimulation observed in our study further supports its involvement in the macrophage inflammatory response.

The RNA-seq analysis provide a comprehensive characterization of MS4A4A function from a transcriptomic profile. It demonstrated that MS4A4A is dispensable for the steady-state transcriptional program in macrophages as highlighted by the overlap in gene expression profiles between WT and KO macrophages in resting conditions. Nonetheless, few genes were differentially regulated exclusively in either WT or KO macrophages after LPS stimulation and pathway enrichment analysis identified a small number of signaling pathways that were differentially modulated between genotypes. In particular, the identification of differentially regulated pathways related to signaling activation between WT and KO LPS-stimulated macrophages supports the notion that MS4A4A may modulate the activation of signalling mediated by its immunoreceptors partner. Although we concluded that MS4A4A does not significantly impair the basal phenotype of macrophages and their transcriptional response to LPS, this analysis led us to hypothesize that MS4A4A could be involved in cytokines secretion, as suggested by differential regulation of pathways related to MyD88-independent and NF-κB signaling.

The functional characterization of cytokine release showed that MS4A4A does not affect pro-inflammatory cytokines (TNF-α, IL-6) after LPS stimulation, whereas it impairs the secretion of the anti-inflammatory cytokine IL-10. The MS4A4A effect in limiting IL-10 release was validated also in human macrophages where MS4A4A was silenced. Of note, the IL-10 defect is not limited to TLR4 activation, as demonstrated by stimulating KO macrophages with various TLR agonists. IL-10 production and release happen upon the activation of the inflammatory response via an inflammatory stimulus to enhance the production of IL-10 to counterbalance pro-inflammatory signals and promote resolution of inflammation. This finding showed that MS4A4A is required for release of IL-10 protein in macrophages in response to TLRs activation.

LPS-induced IL-10 production in macrophages requires activation of both the MyD88-independent (TRIF) and MyD88-dependent pathways. The MyD88-dependent pathway primarily induces the rapid production of cytokines, while the MyD88-independent (TRIF) pathway leads to type I IFN production and enhances IL-10 synthesis, contributing to the anti-inflammatory response (71). KO macrophages showed a trend to release lower amount of IFN-β compared to WT controls, suggesting a possible defect in TRIF-mediated signaling. However, the observation that IL-10 release is impaired upon activation with different TLR agonists that act via both MyD88-dependent (TLR-2, -5, -7/8) and MyD88-independent (TLR-3, -4) pathways, indicates that the defect in IL-10 production in KO macrophages is not a consequence of an impairment on these signaling cascades. This interpretation is further supported by RNA-seq analysis, which confirmed that the MyD88-Independent pathway is activated in KO macrophages. In addition, comparable levels of IL-10 mRNA expression and mRNA stability between WT and KO cells excluded that MS4A4A affect IL-10 at the transcriptional or post-transcriptional level.

IL-10 in an anti-inflammatory cytokine and, unlike other anti-inflammatory stimuli, it has not been reported to modulate MS4A4A expression (35). However, we speculate that the upregulation of MS4A4A upon LPS-stimulation at later time point (24h) could be affected by a mechanism mediated by IL-10 that is released in response to LPS. To evaluate this hypothesis IL-10 should be blocked using an anti-IL10 receptor antibody followed by LPS stimulation and MS4A4A expression should be analysed.

Our findings demonstrated that MS4A4A is not involved in the secretory pathway of IL-10. For the first time, MS4A4A was found to localize in cytosolic compartment as shown by its partial co-localization with actin and markers of early and late recycling endosomes. However, MS4A4A does not appear to regulate IL-10 release via the recycling endosome pathway. This is supported by the observation that the release of other cytokines known to use this pathway (TNF-α, IL-6) are not impaired in KO macrophages. Furthermore, no re-localization of MS4A4A was observed upon LPS stimulation. In addition, the PKA and microtubule-dependent secretory pathways are not affected by MS4A4A, as showed by the same inhibitory responses between WT and KO BMDMs.

Instead, our results support a role for MS4A4A in IL-10 biosynthesis or post-translational modification. KO BMDMs accumulated lower amount of IL-10 following Brefeldin A treatment, both by ELISA and immunofluorescence, suggesting impaired synthesis or availability of IL-10 in the cytosol.

One unexpected finding of this study is the existence of an intracellular pool of IL-10 in resting macrophages, challenging the current view that IL-10 is only produced upon activation and proposing a novel mechanism of IL-10 storage in macrophages. This finding raises the possibility that MS4A4A may contribute to the maintenance of the intracellular pool. We tried to validate the presence of the IL-10 storage pool by Western Blotting but none of the antibodies tested technically worked. In the literature IL-10 detection by Western blot is limited, with most studies reporting results only from tissue lysates. Given the potential significance of IL-10 storage in macrophage biology, further investigation will be necessary. To confirm our finding, flow cytometry can be used to confirmed intracellular IL-10 pool. In addition, to assess whether the observed impairment in IL-10 release in KO BMDMs is independent of de novo synthesis, IL-10 release can be quantified in the supernatant of macrophages treated with cycloheximide to block protein biosynthesis before LPS stimulation.
To support the existence of IL-10 storage pool is that the impairment in IL-10 release is observed at early time point – 2h LPS post stimulation – and MS4A4A does not affect Il10 at transcriptional level. The fulminant release of IL-10 from macrophages was previously described by Stoolman et al. that showed that mitochondrial electron transport chain (ETC) was required for fulminant induction of the IL-10 anti-inflammatory response to LPS (72).
In case the storage pool will be validate, it will be necessary to compare WT and KO IL-10 storage pool to clarify if the defect on IL-10 release is due to a role of MS4A4A in IL-10 de novo production and/or in the release of the IL-10 storage pool.

IL-10 is a master regulator of immunity playing and essential role in limiting or terminating inflammation. It helps to maintain the balance between pro-inflammatory and anti-inflammatory responses, ensuring efficient pathogen clearance while preventing collateral tissue damage. IL-10 deficiency can have both a beneficial and a detrimental outcome. In the early stage of infection, its deficiency may enhance innate and adaptive immune responses improving microbial clearance. If the deficiency persists, it leads to systemic, exaggerated inflammation and immune-mediated tissue damage and participates to the onset or aggravation of chronic inflammatory diseases and autoimmune pathologies (73). In macrophages, decreased IL-10 production impairs the transition from a pro-inflammatory state to a M2-like phenotype, a switch essential for resolving inflammation. This supports the hypothesis that MS4A4A plays a role in promoting M2 polarization, as previously suggested in the literature. Taken together, these findings suggest MS4A4A as a positive

regulator of IL-10 production influencing the inflammatory responses, resolution of inflammation and the immune tolerance.

In patients with sepsis and septic shock, IL-10 plays a dual role in modulating the immune response. During the early hyperinflammatory phase, IL-10 is rapidly upregulated helping to limit excessive inflammation and protect tissues from damage. However, excessive IL-10 production contributes to the development of immunosuppression, characterized by reduced antigen presentation, lymphocyte dysfunction and increased susceptibility to secondary infections. This immune paralysis is associated with poor outcomes and higher mortality. Elevated IL-10 levels are considered a negative prognostic marker in sepsis. Understanding the timing and regulation of IL-10 expression is therefore critical for restoring the immune balance. Several published datasets have identified MS4A4A as one of the most upregulated genes in septic patients, although without distinguish between sepsis and septic shock. Recently, a study investigating severity biomarkers in sepsis reported for the first time a positive correlation between MS4A4A expression and IL-10 levels in a cohort of septic patients (35,74). However, this evidence was observed in monocytes and not in macrophages. Sepsis could represent a relevant pathological context in which the relationship between MS4A4A and IL-10 may be further investigated. To date, no studies using murine models of sepsis have directly linked MS4A4A to the disease. A key missing element that would strengthen our finding is the use of an in vivo sepsis model to evaluate whether MS4A4A KO mice display altered IL-10 levels in response to infection, thereby validating the in vitro phenotype in a disease-relevant setting.

Among the TLRs that were identified to impair the IL-10 release in KO BMDMs there were the TLR-2 that we identified as a new potential MS4A4A partners TLRs belong the class of pattern recognition receptors (PRRs) that are responsible of the recognition of pathogens to start a robust immune response. The interaction between MS4A4A and TLR-2 was also functionally supported by the significant reduction of TLR-2 surface expression in MS4A4A KO macrophages. This suggests a role for MS4A4A in regulating TLR2 trafficking or membrane localization. When macrophages were activated with TLR-2 agonist, MS4A4A deficiency did not alter the production of pro-inflammatory cytokines, like TNF-α and IL-6 (data not shown). However, MS4A4A KO macrophages exhibited a trend to release lower amount of IL-10 at 24 hours post-stimulation compared to WT controls. These findings strongly support a functional connection between MS4A4A and TLR-2 although functional implications need further investigation. Taken together, the identification of the γ-chain and

TLR-2 as putative MS4A4A partners sustains the concept that MS4A4A play a broader role in regulating inflammatory responses in macrophages by modulating the membrane receptor localization and the functional activity of immunoreceptors fundamental in macrophages inflammatory response.

Another mechanism for recognition and clearance of nonself material is carried out by IgG antibodies, which provide specific recognition of antigens. Binding of antibodies to the surface of macrophages is mediated by the FcγRs. Another identified partner of MS4A4A was the γ- signalling chain of Fc gamma receptor (FcγR) encoded by FCER1G. It is a signal-transducing polypeptide initially described as a component of the high-affinity IgE receptor FcεR. Signaling events necessary for FcγR-mediated response are likely initiated by the activation of Src- and Syk-family tyrosine kinases after FcγR cross-linking. Syk is a multifunctional tyrosine kinase that associate with FcγRs and phosphorylates several substrates and recruits many adaptor molecules allowing FcγR signaling to initiate a complex variety of divergent cellular responses phagocytosis. The identification of the γ-signalling chain of FcγR as a putative MS4A4A partner is in line with previous observations from our group demonstrating that MS4A4A modulates Syk phosphorylation downstream of Dectin-1 activation, further supporting the role of MS4A4A in regulating immunoreceptor signaling pathways (35).

In rheumatoid arthritis (RA) altered level of FcγRs in the immune cells (including macrophages) have been observed, in particular FcγRIII (75,76). To evaluate the role of MS4A4A in RA pathogenesis and in corticosteroid therapy, MS4A4A was found to be highly expressed in $CD163^{+}$ macrophages within the inflamed synovium of RA patients which is associated with more aggressive disease and worse outcomes (35,69). $CD163^{+}$ macrophages are known to be involved in chronic inflammation and tissue remodelling. This suggested the involvement of MS4A4A in macrophage-mediated pathways of immune activation and tissue degradation supporting the hypothesis that MS4A4A could modulate the function of macrophages in RA. Importantly, MS4A4A expression correlated with higher disease severity, particularly in treatment-naïve and treatment-resistant RA patients (69). These associations reinforce the idea that MS4A4A contributes to disease progression and may have a role in shaping the inflammatory response in RA.

Corticosteroids (CS) play a crucial role in regulating inflammation and immune responses and they influence macrophage biology, often promoting a shift toward tissue repair phenotypes. MS4A4A is up regulated by CS, both in vitro and in vivo. We demonstrated that

CS treatment leads to an increase in MS4A4A expression within the synovial tissue of RA patients as well as in the joints of arthritic mice, supporting previous observations (34,35). The expression of MS4A4A positively correlates with transcript level of FcγRIII and the γ-chain of FcγRs. Moreover, Dex concomitantly enhances the expression of MS4A4A and FcγRIII, both in vitro and in the RA synovium, without affecting the expression of other FcγRs. Using a model of serum-transfer induced arthritis (STIA), we showed that MS4A4A deficiency alone did not alter disease onset or severity, while it significantly enhanced the therapeutic efficacy of Dex, leading to reduced neutrophil infiltration, lower pro-inflammatory cytokine production (TNFα, CXCL2) and decreased bone erosion (69). Importantly, these effects were specific to Dex, with no similar enhancement observed for methotrexate or IVIg. This suggests that MS4A4A plays a role in modulating corticosteroid sensitivity. These findings suggest that CS, by upregulating both MS4A4A and FcγRIII, might enhance the response to immune complexes, potentially diminishing their own anti-inflammatory effects. Research from our group and others indicates that MS4A4A modulates macrophage activation by influencing the function of other surface receptors rather than directly triggering intracellular signaling pathways. This supports the idea that MS4A4A may regulate immunoglobulin-mediated signaling through interactions with Fc receptors. Although the γ chain of the FcγRs was identified as a possible MS4A4A partner, Co-iP experiments did not confirm a direct interaction and MS4A4A does not affect FcγR-mediated signaling activation. Together, these results suggest that the modulatory role of MS4A4A on Dex efficiency appears to be independent on direct influence on FcγR signaling, and the precise mechanism remains to be defined.

Given the novelty and clinical relevance of these findings, several important directions for future research should be pursued. First, it is essential to clarify the molecular mechanisms by which MS4A4A influences the therapeutic effects of Dex. Understanding whether MS4A4A's role is intrinsic to macrophages or dependent on interactions with other immune cells will be crucial; in this regard, conditional knockout models targeting specific cell populations would be highly informative. Additionally, due to known differences between human and mouse pathophysiology, further complementary studies are needed to validate these results in human tissues. Overall, our findings not only contribute to a deeper understanding of macrophage function in RA but also suggest MS4A4A as a potential therapeutic target to amplify the action of CS. These results open the possibility of exploring pharmacological inhibition of MS4A4A as a strategy to improve CS efficacy, which could

allow for lower dosing and reduced side effects, two major challenges in the long-term management of inflammatory diseases.

In summary, this study significantly advances the current knowledge about MS4A4A providing a comprehensive functional characterization in macrophages. Unlike previous assumptions of MS4A4A as a classical receptor or ion channel, our data support its role as a regulator of immunoreceptor involved in their localization or immune signaling. Of note, we identified novel potential receptor that may be regulated by MS4A4A and demonstrated its role in optimizing IL-10 release upon TLRs activation, highlighting a previously unrecognized intracellular pool of IL-10 in resting macrophages. Furthermore, the study suggests a potential involvement of MS4A4A in protein synthesis, receptor stabilization supported by its localization in intracellular compartments and its interaction with ribosomal components. We also showed that MS4A4A participates in macrophage activation during both TLR- and FcγR-mediated inflammatory responses, although the mechanisms responsible remain to be fully defined. Finally, our findings suggest MS4A4A as a possible biomarker of joint inflammation in RA and a target to amplify the therapeutic activity of corticosteroids. This study provides a valuable contribution to the field, expanding the current state of knowledge on MS4A4A function in macrophage activation.

ACKNOWLEDGMENTS

I would like to thank all our collaborators whose contributions were essential to the successful execution of this study:

- For proteomics LC-MS/MS analysis: the group of Dr. Dario Di Silvestre (Clinical Proteomics Laboratory, Institute for Biomedical Technologies, ITB-CNR, Segrate, Milan, Italy).
- For the study of MS4A4A structure: the group of Prof. Luca Mollica (Department of Medical Biotechnologies and Translational Medicine, University of Milan; Segrate, Milan, Italy).
- For bioinformatic analysis: Dr. Anna Rita Putignano (IRCCS Humanitas Research Hospital; Rozzano, Milan, Italy) and her supervisor Prof. Federica Marchesi (Department of Medical Biotechnologies and Translational Medicine, University of Milan; Segrate, Milan, Italy).
- For confocal imaging acquisition: Dr. Tilo Schorn (Department of Medical Biotechnologies and Translational Medicine, University of Milan; Segrate, Milan, Italy).

REFERENCES

1. Shapouri-Moghaddam A, Mohammadian S, Vazini H, Taghadosi M, Esmaeili S, Mardani F, et al. Macrophage plasticity, polarization, and function in health and disease. J Cell Physiol. 2018 Sep;233(9):6425–40.

2. Zhao Y, Zou W, Du J, Zhao Y. The origins and homeostasis of monocytes and tissue-resident macrophages in physiological situation. J Cell Physiol. 2018 Oct 17;233(10):6425–39.

3. Yona S, Kim KW, Wolf Y, Mildner A, Varol D, Breker M, et al. Fate Mapping Reveals Origins and Dynamics of Monocytes and Tissue Macrophages under Homeostasis. Immunity. 2013 Jan;38(1):79–91.

4. Guilliams M, Thierry GR, Bonnardel J, Bajenoff M. Establishment and Maintenance of the Macrophage Niche. Immunity. 2020 Mar;52(3):434–51.

5. Gordon S, Plüddemann A. Tissue macrophages: heterogeneity and functions. BMC Biol. 2017 Dec 29;15(1):53.

6. Gordon S, Plüddemann A, Martinez Estrada F. Macrophage heterogeneity in tissues: phenotypic diversity and functions. Immunol Rev. 2014 Nov 15;262(1):36–55.

7. Gersuk GM, Underhill DM, Zhu L, Marr KA. Dectin-1 and TLRs Permit Macrophages to Distinguish between Different *Aspergillus fumigatus* Cellular States. The Journal of Immunology. 2006 Mar 15;176(6):3717–24.

8. Luther K, Torosantucci A, Brakhage AA, Heesemann J, Ebel F. Phagocytosis of Aspergillus fumigatus conidia by murine macrophages involves recognition by the dectin-1 beta-glucan receptor and Toll-like receptor 2. Cell Microbiol. 2007 Feb;9(2):368–81.

9. Hashimoto D, Chow A, Noizat C, Teo P, Beasley MB, Leboeuf M, et al. Tissue-Resident Macrophages Self-Maintain Locally throughout Adult Life with Minimal Contribution from Circulating Monocytes. Immunity. 2013 Apr;38(4):792–804.

10. Mehrotra P, Ravichandran KS. Drugging the efferocytosis process: concepts and opportunities. Nat Rev Drug Discov. 2022 Aug 1;21(8):601–20.

11. Kim SY, Kim S, Bae DJ, Park SY, Lee GY, Park GM, et al. Coordinated balance of Rac1 and RhoA plays key roles in determining phagocytic appetite. PLoS One. 2017 Apr 4;12(4):e0174603.

12. Brancewicz J, Wójcik N, Sarnowska Z, Robak J, Król M. The Multifaceted Role of Macrophages in Biology and Diseases. Int J Mol Sci. 2025 Feb 27;26(5):2107.

13. Mantovani A, Allavena P, Marchesi F, Garlanda C. Macrophages as tools and targets in cancer therapy. Nat Rev Drug Discov. 2022 Nov 16;21(11):799–820.

14. Ghamangiz S, Jafari A, Maleki-Kakelar H, Azimi H, Mazloomi E. Reprogram to heal: Macrophage phenotypes as living therapeutics. Life Sci. 2025 Jun;371:123601.

15. Peng M, Li N, Wang H, Li Y, Liu H, Luo Y, et al. Macrophages: Subtypes, Distribution, Polarization, Immunomodulatory Functions, and Therapeutics. MedComm (Beijing). 2025 Aug 25;6(8).

16. Ni D, Zhou H, Wang P, Xu F, Li C. Visualizing Macrophage Phenotypes and Polarization in Diseases: From Biomarkers to Molecular Probes. Phenomics. 2023 Dec 24;3(6):613–38.

17. Kadl A, Meher AK, Sharma PR, Lee MY, Doran AC, Johnstone SR, et al. Identification of a Novel Macrophage Phenotype That Develops in Response to Atherogenic Phospholipids via Nrf2. Circ Res. 2010 Sep 17;107(6):737–46.

18. Shapiro H, Lutaty A, Ariel A. Macrophages, Meta-Inflammation, and Immuno-Metabolism. The Scientific World JOURNAL. 2011;11:2509–29.

19. Buckley CD, Gilroy DW, Serhan CN. Proresolving Lipid Mediators and Mechanisms in the Resolution of Acute Inflammation. Immunity. 2014 Mar;40(3):315–27.

20. Buckley CD, Gilroy DW, Serhan CN, Stockinger B, Tak PP. The resolution of inflammation. Nat Rev Immunol. 2013 Jan 30;13(1):59–66.

21. Soliman AM, Soliman M, Shah SSH, Baig HA, Gouda NS, Alenezi BT, et al. Molecular dynamics of inflammation resolution: therapeutic implications. Front Cell Dev Biol. 2025 May 8;13.

22. Zuccolo J, Bau J, Childs SJ, Goss GG, Sensen CW, Deans JP. Phylogenetic Analysis of the MS4A and TMEM176 Gene Families. PLoS One. 2010 Feb 23;5(2):e9369.

23. Tedder TF, Streuli M, Schlossman SF, Saito H. Isolation and structure of a cDNA encoding the B1 (CD20) cell-surface antigen of human B lymphocytes. Proceedings of the National Academy of Sciences. 1988 Jan;85(1):208–12.

24. Kinet JP, Blank U, Ra C, White K, Metzger H, Kochan J. Isolation and characterization of cDNAs coding for the beta subunit of the high-affinity receptor for immunoglobulin E. Proceedings of the National Academy of Sciences. 1988 Sep;85(17):6483–7.

25. Adra CN, Lelias JM, Kobayashi H, Kaghad M, Morrison P, Rowley JD, et al. Cloning of the cDNA for a hematopoietic cell-specific protein related to CD20 and the beta subunit of the high-affinity IgE receptor: evidence for a family of proteins with four membrane-spanning regions. Proceedings of the National Academy of Sciences. 1994 Oct 11;91(21):10178–82.

26. Ishibashi K, Suzuki M, Sasaki S, Imai M. Identification of a new multigene four-transmembrane family (MS4A) related to CD20, HTm4 and β subunit of the high-affinity IgE receptor. Gene. 2001 Feb;264(1):87–93.

27. Levy S, Shoham T. Protein-protein interactions in the tetraspanin web. Physiology (Bethesda). 2005 Aug;20:218–24.

28. Hemler ME. Tetraspanin functions and associated microdomains. Nat Rev Mol Cell Biol. 2005 Oct;6(10):801–11.

29. Eon Kuek L, Leffler M, Mackay GA, Hulett MD. The MS4A family: counting past 1, 2 and 3. Immunol Cell Biol. 2016 Jan 19;94(1):11–23.

30. Hemler ME. Tetraspanin proteins promote multiple cancer stages. Nat Rev Cancer. 2014 Jan 23;14(1):49–60.

31. Liang Y, Tedder TF. Identification of a CD20-, FcεRIβ-, and HTm4-Related Gene Family: Sixteen New MS4A Family Members Expressed in Human and Mouse. Genomics. 2001 Mar;72(2):119–27.

32. Mattiola I, Mantovani A, Locati M. The tetraspan MS4A family in homeostasis, immunity, and disease. Trends Immunol. 2021 Sep;42(9):764–81.

33. Bellenguez C, Küçükali F, Jansen IE, Kleineidam L, Moreno-Grau S, Amin N, et al. New insights into the genetic etiology of Alzheimer's disease and related dementias. Nat Genet. 2022 Apr 4;54(4):412–36.

34. Silva-Gomes R, Mapelli SN, Boutet MA, Mattiola I, Sironi M, Grizzi F, et al. Differential expression and regulation of MS4A family members in myeloid cells in physiological and pathological conditions. J Leukoc Biol. 2022 Mar 25;111(4):817–36.

35. Mattiola I, Tomay F, De Pizzol M, Silva-Gomes R, Savino B, Gulic T, et al. The macrophage tetraspan MS4A4A enhances dectin-1-dependent NK cell–mediated resistance to metastasis. Nat Immunol. 2019 Aug 1;20(8):1012–22.

36. Cruse G, Beaven MA, Music SC, Bradding P, Gilfillan AM, Metcalfe DD. The CD20 homologue MS4A4 directs trafficking of KIT toward clathrin-independent endocytosis pathways and thus regulates receptor signaling and recycling. Mol Biol Cell. 2015 May;26(9):1711–27.

37. Bennett FC, Bennett ML, Yaqoob F, Mulinyawe SB, Grant GA, Hayden Gephart M, et al. A Combination of Ontogeny and CNS Environment Establishes Microglial Identity. Neuron. 2018 Jun;98(6):1170-1183.e8.

38. Schmieder A, Schledzewski K, Michel J, Tuckermann JP, Tome L, Sticht C, et al. Synergistic activation by p38MAPK and glucocorticoid signaling mediates induction of M2-like tumor-associated macrophages expressing the novel CD20 homolog MS4A8A. Int J Cancer. 2011 Jul 28;129(1):122–32.

39. Bubien JK, Zhou LJ, Bell PD, Frizzell RA, Tedder TF. Transfection of the CD20 cell surface molecule into ectopic cell types generates a Ca2+ conductance found constitutively in B lymphocytes. J Cell Biol. 1993 Jun 1;121(5):1121–32.

40. Polyak MJ, Li H, Shariat N, Deans JP. CD20 Homo-oligomers Physically Associate with the B Cell Antigen Receptor. Journal of Biological Chemistry. 2008 Jul;283(27):18545–52.

41. Koslowski M, Sahin U, Dhaene K, Huber C, Türeci O. MS4A12 Is a Colon-Selective Store-Operated Calcium Channel Promoting Malignant Cell Processes. Cancer Res. 2008 May 1;68(9):3458–66.

42. Segovia M, Louvet C, Charnet P, Savina A, Tilly G, Gautreau L, et al. Autologous Dendritic Cells Prolong Allograft Survival Through Tmem176b-Dependent Antigen Cross-Presentation. American Journal of Transplantation. 2014 May;14(5):1021–31.

43. Arthur GK, Ehrhardt-Humbert LC, Snider DB, Jania C, Tilley SL, Metcalfe DD, et al. The FcεRIβ homologue, MS4A4A, promotes FcεRI signal transduction and store-operated Ca2+ entry in human mast cells. Cell Signal. 2020 Jul;71:109617.

44. Huang X, Feng Z, Jiang Y, Li J, Xiang Q, Guo S, et al. VSIG4 mediates transcriptional inhibition of *Nlrp3* and *Il-1* β in macrophages. Sci Adv. 2019 Jan 4;5(1).

45. Deming Y, Filipello F, Cignarella F, Cantoni C, Hsu S, Mikesell R, et al. The *MS4A* gene cluster is a key modulator of soluble TREM2 and Alzheimer's disease risk. Sci Transl Med. 2019 Aug 14;11(505).

46. Sanyal R, Polyak MJ, Zuccolo J, Puri M, Deng L, Roberts L, et al. MS4A4A: a novel cell surface marker for M2 macrophages and plasma cells. Immunol Cell Biol. 2017 Aug 11;95(7):611–9.

47. Li Y, Shen Z, Chai Z, Zhan Y, Zhang Y, Liu Z, et al. Targeting MS4A4A on tumour-associated macrophages restores CD8+ T-cell-mediated antitumour immunity. Gut. 2023 Dec;72(12):2307–20.

48. Sui Y, Zeng W. MS4A4A Regulates Arginase 1 Induction during Macrophage Polarization and Lung Inflammation in Mice. Eur J Immunol. 2020 Oct 29;50(10):1602–5.

49. Shao G, Cui X, Wang Y, Luo S, Li C, Jiang Y, et al. Targeting MS4A4A: A novel pathway to improve immunotherapy responses in glioblastoma. CNS Neurosci Ther. 2024 Jul;30(7):e14791.

50. Aletaha D, Smolen JS. Diagnosis and Management of Rheumatoid Arthritis. JAMA. 2018 Oct 2;320(13):1360.

51. Doumen M, Pazmino S, Bertrand D, Westhovens R, Verschueren P. Glucocorticoids in rheumatoid arthritis: Balancing benefits and harm by leveraging the therapeutic window of opportunity. Joint Bone Spine. 2023 May;90(3):105491.

52. Luo X, Luo B, Fei L, Zhang Q, Liang X, Chen Y, et al. MS4A superfamily molecules in tumors, Alzheimer's and autoimmune diseases. Front Immunol. 2024 Dec 9;15.

53. Edwards JCW, Szczepański L, Szechiński J, Filipowicz-Sosnowska A, Emery P, Close DR, et al. Efficacy of B-Cell–Targeted Therapy with Rituximab in Patients with Rheumatoid Arthritis. New England Journal of Medicine. 2004 Jun 17;350(25):2572–81.

54. Brown GC, St George-Hyslop P. Does Soluble TREM2 Protect Against Alzheimer's Disease? Front Aging Neurosci. 2022 Jan 28;13.

55. Rosner D, Sun J, Yee A, Wagh C, Rychkova A, Cacace R, et al. The Alzheimer's Disease Risk Genes MS4A4A And MS4A6A Cooperate to Negatively Regulate Trem2 and Microglia states. 2024.

56. Mantovani A, Marchesi F, Malesci A, Laghi L, Allavena P. Tumour-associated macrophages as treatment targets in oncology. Nat Rev Clin Oncol. 2017 Jul;14(7):399–416.

57. Molgora M, Esaulova E, Vermi W, Hou J, Chen Y, Luo J, et al. TREM2 Modulation Remodels the Tumor Myeloid Landscape Enhancing Anti-PD-1 Immunotherapy. Cell. 2020 Aug;182(4):886-900.e17.

58. Ratnadiwakara M, Änkö ML. mRNA Stability Assay Using Transcription Inhibition by Actinomycin D in Mouse Pluripotent Stem Cells. Bio Protoc. 2018;8(21).

59. Ernst JA, Li H, Kim HS, Nakamura GR, Yansura DG, Vandlen RL. Isolation and characterization of the B-cell marker CD20. Biochemistry. 2005 Nov 22;44(46):15150–8.

60. Greer PL, Bear DM, Lassance JM, Bloom ML, Tsukahara T, Pashkovski SL, et al. A Family of non-GPCR Chemosensors Defines an Alternative Logic for Mammalian Olfaction. Cell. 2016 Jun;165(7):1734–48.

61. You SF, Brase L, Filipello F, Iyer AK, Del-Aguila J, He J, et al. MS4A4A modifies the risk of Alzheimer disease by regulating lipid metabolism and immune response in a unique microglia state. 2023.

62. Cruse G, Beaven MA, Music SC, Bradding P, Gilfillan AM, Metcalfe DD. The CD20 homologue MS4A4 directs trafficking of KIT toward clathrin-independent endocytosis pathways and thus regulates receptor signaling and recycling. Mol Biol Cell. 2015 May;26(9):1711–27.

63. Couper KN, Blount DG, Riley EM. IL-10: The Master Regulator of Immunity to Infection. The Journal of Immunology. 2008 May 1;180(9):5771–7.

64. Saraiva M, O'Garra A. The regulation of IL-10 production by immune cells. Nat Rev Immunol. 2010 Mar 15;10(3):170–81.

65. Teixeira-Coelho M, Guedes J, Ferreirinha P, Howes A, Pedrosa J, Rodrigues F, et al. Differential post-transcriptional regulation of <scp>IL</scp> -10 by <scp>TLR</scp> 2 and <scp>TLR</scp> 4-activated macrophages. Eur J Immunol. 2014 Mar 16;44(3):856–66.

66. Shurety W, Merino-Trigo A, Brown D, Hume DA, Stow JL. Localization and Post-Golgi Trafficking of Tumor Necrosis Factor-alpha in Macrophages. Journal of Interferon & Cytokine Research. 2000 Apr;20(4):427–38.

67. Murray RZ, Stow JL. Cytokine Secretion in Macrophages: SNAREs, Rabs, and Membrane Trafficking. Front Immunol. 2014 Oct 27;5.

68. Seyhan AA, Gregory B, Cribbs AP, Bhalara S, Li Y, Loreth C, et al. Novel biomarkers of a peripheral blood interferon signature associated with drug-naïve early arthritis patients distinguish persistent from self-limiting disease course. Sci Rep. 2020 Jun 1;10(1):8830.

69. Boutet MA, Mattiola I, Silva-Gomes R, Nerviani A, Sironi M, Ghirardi GM, et al. Synovial MS4A4A correlates with inflammation and counteracts response to corticosteroids in arthritis. Proceedings of the National Academy of Sciences. 2025 Sep 16;122(37).

70. Greer PL, Bear DM, Lassance JM, Bloom ML, Tsukahara T, Pashkovski SL, et al. A Family of non-GPCR Chemosensors Defines an Alternative Logic for Mammalian Olfaction. Cell. 2016 Jun;165(7):1734–48.

71. Saraiva M, O'Garra A. The regulation of IL-10 production by immune cells. Nat Rev Immunol. 2010 Mar 15;10(3):170–81.

72. Stoolman JS, Grant RA, Billingham LK, Poor TA, Weinberg SE, Harding MC, et al. Mitochondria complex III–generated superoxide is essential for IL-10 secretion in macrophages. Sci Adv. 2025 Jan 24;11(4).

73. Carlini V, Noonan DM, Abdalalem E, Goletti D, Sansone C, Calabrone L, et al. The multifaceted nature of IL-10: regulation, role in immunological homeostasis and its relevance to cancer, COVID-19 and post-COVID conditions. Front Immunol. 2023 Jun 8;14.

74. Supino D, Davoudian S, Silva-Gomes R, Piovani D, Garuti R, Desai A, et al. Monocyte-macrophage membrane expression of IL-1R2 is a severity biomarker in sepsis. Cell Death Dis. 2025 Apr 10;16(1):269.

75. Magnusson SE, Wennerberg E, Matt P, Lindqvist U, Kleinau S. Dysregulated Fc receptor function in active rheumatoid arthritis. Immunol Lett. 2014 Nov;162(1):200–6.

76. Zuo Y, Deng GM. Fc Gamma Receptors as Regulators of Bone Destruction in Inflammatory Arthritis. Front Immunol. 2021 Jun 23;12.

LIST OF FIGURES AND TABLES

Figure 1. Origin and development of macrophages. Created with BioRender. 9
Figure 2. Classical transport pathways used to secrete macrophage cytokines. (A) Three major transport pathways for cytokine secretion have been identified to date. The first involves direct transport to the cell surface (IL-10) from the TGN, the second pathways routes cytokines via the recycling endosome and the out to the cell surface (TNF, IL-6 and IL-10), and the 3 rd pathway occurs during phagocytosis where cytokine (TNF) is routed from the recycling endosome to the phagocytic cup. (B) Trafficking machinery that regulate cytokine secretion in macrophages. 11
Figure 3. Spectrum of macrophage polarization from M0 to M1 and M2 phenotype. Created with BioRender. 13
Figure 4. The tetraspanins structure. The full-length protein adopts a compact, rod-like conformation composed of four transmembrane (TM) helices (shown in light and dark grey, labelled 1–4). Connecting TM domains 3 and 4 is a large extracellular loop (spanning 70–130 amino acids), which includes a conserved helical segment (comprising helices A, B, and E, shown in blue) and a variable region (depicted in dark red, located between helices B and E). This variable region often plays a key role in interacting specifically with partner proteins. Although not illustrated, this segment is usually stabilized by two to four conserved disulfide bonds. A smaller extracellular loop (13–30 amino acids) links TM helices 1 and 2. Tetraspanins generally feature short cytoplasmic tails at both the amino and carboxy termini (6–19 amino acids) and possess a small intracellular loop of approximately 4 amino acids (30). Created with BioRender. 16
Figure 5. Expression pattern of membrane-spanning 4A (MS4A) proteins in different leukocyte subsets (32). 17
Figure 6. Multifaceted functions of hematopoietic cell-restricted membrane-spanning 4A (MS4A) proteins (32). 19
Figure 7. Intrinsic Disorder Profile and Predicted 3D Structure of MS4A4A Protein. (A) IUPRED (black) and ANCHOR (red) profiles of disorder, i.e., disorder probability index (DPI, ranging from 0 to 1), are reported as function of the protein sequence. The difference between the two curves (DDPI) is reported in green. (B) MS4A4A structure predicted by AlphaFold. The location of membrane polar surfaces is schematically represented with dashed lines. 37
Figure 8. Predicted binding interface on MS4A4A structure for lipids and for polypeptide chains. The colour coding goes from red to blue, i.e., respectively from highest to lowest propensity for each class of molecules. 38
Figure 9. PrankWeb based prediction of the potential ligand binding regions of MS4A4A structure modelled using AlphaFold (A) and SwissModel (B). For each putative binding site the following parameters are reported: i) Pocket score: solvent accessibility based index of druggability (0-100); ii) Probability score: the knowledge based probability of a pocket to be real (0-1); iii) AA

count: number of residues constituting the pocket; iv) Conservation: degree of evolutive conservation of the pocket among the experimental structures of complexed (0-4)..... 39
Figure 10. Docking simulation between MS4A4A and dexamethasone metasulfobenzoate. 40
Figure 11. Molecular dynamics simulations of MS4A4A structure. Molecular dynamics simulations of MS4A4A in a model membrane have been performed to monitor its ability to act as a channel for water molecules (left) as well as for calcium divalent ion (right). The simulations revealed that the system can transport water molecules (violet spheres) across the membrane and that calcium (orange spheres) can penetrate the inner core of MS4A4A but lacking the ability to cross the membrane..... 42
Figure 12. MS4A4A does not affect basal or ionomycin-induced calcium flux. Calcium fluxes were evaluated in WT and MS4A4A KO BMDMs by plate reader system in macrophages treated and not with ionomycin 10 μM. (A) Measurements are given in relative fluorescent units (RFU); one experiment representative of n=4. (B) The area under the curve (AUC) from 90 to 240 seconds, corresponding to the period following ionomycin addition and subsequent EDTA treatment, is shown (n=4). (C) Data are represented as difference between AUC(ionomycin) and AUC(vehicle) (n=4). Statistical analysis was performed using Paired t-test; p≤0.05 was considered significant. 43
Figure 13. MS4A4A does not affect basal or ionomycin-induced calcium flux but may enhance β-ionone-induced calcium signaling. Calcium fluxes were evaluated in WT and MS4A4A KO BMDMs by FACS in the following conditions: (A) basal level; (B) after stimulation with Ionomycin 10 μM; (C) after stimulation with β-ionone 100 μM. Data are represented as Mean ± SEM and each symborepresentts a different biological replicate (n=4-6). Statistical analysis was performed using Paired t-test compared to non-treated cells; p≤0.05 was considered significant. 44
Figure 14. MS4A4A partially co-localizes with phalloidin, Rab11 and Rab7 in resting and LPS-treated macrophages. Co-localization analysis of MS4A4A with phalloidin, Rab11 and Rab7 in resting and LPS-treated BMDM for 24 h. (A) shows images referring to one experiment representative of 3 analysed. (B) Data are shown as mean ± SEM of the colocalization rate in 20÷30 cells analysed in the experiments showed in panel A. 47
Figure 15. Identification of potential partners for MS4A4A by yeast split-ubiquitin. MS4A4A interactors has been identified by DUAL membrane Plus screening technology based on the split-ubiquitin system. Homo sapiens - MS4A4A (aa 1-239) has been used as reference bait fragment. For each interaction, a Predicted Biological Score (PBS) is computed to assess interaction reliability. Several thresholds have been arbitrarily defined to rank the results in 4 categories from A (the highest confidence rank) to D: A) Very high; B) High; C) Good; D) Moderate (including possible false positive). 48
Figure 16. MS4A4A affect TLR2 surface expression but not total protein level. TLR2 protein expression was analysed in resting BMDMs WT and MS4A4A KO at membrane level by flow cytometry (n=5) (A); and by Western Blot (n=3) (B); total protein level of TLR2 was normalised on

housekeeping protein levels. Data are represented as Mean ± SEM and each symbol represent a different biological replicate. Statistical analysis was performed using Paired t-test; p≤0.05 was considered significant. 50
Figure 17. LPS induce up-regulation of MS4A4A at mRNA and protein level. (A) Ms4a4a qPCR on WT BMDM treated or not with LPS. (B) Western Blot on WT BMDM treated with or without LPS or DEX for 24h. TLR2 protein expression was analysed in resting BMDMs WT and MS4A4A KO at membrane level by flow cytometry (n=5) (A); and by Western Blot (n=3) (B); total protein level of TLR2 was normalised on housekeeping protein levels. Data are represented as Mean ± SEM and each symbol represent a different biological replicate. Statistical analysis was performed using Paired t-test; p≤0.05 was considered significant..... 52
Figure 18. MS4A4A immunofluorescence after LPS and Dex treatment. MS4A4A immunofluorescence (IF) on WT BMDMs stimulated with LPS or DEX for 24h. (A) 10X IF images referring to one experiment representative of 3 analysed. (B) IL-10 IF quantification referred to panel A. Each symbol represents a field. (C) Number of MS4A4A positive BMDMs normalized on number of total cells. Data are represented as Mean ± SEM and each symbol represent a different biological replicate. Statistical analysis was performed using Mann-Withney test; p≤0.05 was considered significant..... 53
Figure 19. MS4A4A does not affect macrophage basal phenotype. (A) % F4/80 positive BMDMs by Flow cytometry (n=10). Statistical analysis was performed using Paired t-test; p≤0.05 was considered significant. (B) Volcano plots display log_2 fold-change on the x-axis and $-log_{10}$(FDR) on the y-axis for WT vs KO BMDMs in resting condition. 54
Figure 20. RNAseq samples cluster mainly by treatment and time point. PCA on all samples using the top 2000 most variable genes assesses samples similarities and visualizes the separation of experimental groups in a 2-Dimensional space. 55
Figure 21. Differential expression genes (DEGs) between WT versus KO BMDMs. Volcano plots display log_2 fold-change on the x-axis and $-log_{10}$(FDR) on the y-axis for each contrast: LPS-treated vs vehicle both WT ad KO BMDMs at timepoint 2h, 8h and 24h. 55
Figure 22. Differential expression genes (DEGs) between LPS versus vehicle. (A) Schedule of comparison analysis. (B) Barplot summarizing results of differential expression analysis: number of Up- and Down-regulated genes per each of the 24 contrasts obtained by filtering genes having FDR < 0.01 and log2FC > 1. (C) Heatmap of DEGs; values are scaled by row and each column represent one replicate (three replicates for sample). 56
Figure 23. Pathway enrichment analysis on LPS-stimulated macrophages. Pathways enrichment analysis in WT and KO BMDMs. Rows report pathways significantly modulated (|z-score | ≥ 2) in at least one comparison. Colour intensity bar indicates the level of positive (in green) or negative (in blue) enrichment. The most up and down regulated pathway are reported, as

representative on macrophage phenotype. Asterisks appear only when pathways are significantly enriched. Gray indicates no modulation. 58
Figure 24. Gene intersections between WT and KO BMDMs. Venn-diagram of DEGs with a |logFC|≥2 in the two comparisons (green = LPS_WT vs vehicle_WT; pink= LPS_KO vs vehicle_KO). 58
Figure 25. Pathway enrichment analysis comparison between WT and KO LPS-stimulated macrophages. Pathways enrichment analysis in WT and KO BMDMs. (A) Comparison at 2h. (B) Comparison at 8h. (C) Comparison at 24h. (D) Pathways differentially modulated In WT or KO macrophages maintained across time points. Rows report pathways significantly modulated (|z-score | ≥ 2) in at least one comparison. Colour intensity bar indicates the level of positive (in green) or negative (in blue) enrichment. Asterisks appear only when pathways are significantly enriched; gray indicates no modulation..... 61
Figure 26. MS4A4A affect IL-10 but not IL-6 and TNF-α secretion after LPS stimulation. Cytokine productions were analysed by ELISA on WT and MS4A4A KO BMDMs treated or not with LPS 100ng/ml for, 2h, 8h and 24h. IL-6 and TNF-α secretion is showed: (A) in pg/ml; (B) as FOLD CHANGE (pg/ml KO versus pg/ml WT). IL-10 secretion is showed: (C) in pg/ml (D) as FOLD CHANGE (pg/ml KO versus pg/ml WT). Data are represented as Mean ± SEM and each symbol represent a different biological replicate (n=8); nd= not detectable. (A-C) statistical analysis was performed using Mann-Withney test LPS versus vehicle (*,**,***) or KO versus WT (°); (B-D) statistical analysis was performed using One sample t test KO versus WT; p≤0.05 was considered significant..... 63
Figure 27. Dose-dependent IL-10 impairment in MS4A4A KO Macrophages. IL-10 cytokine release was analysed by ELISA on WT and MS4A4A KO BMDMs after LPS for 24h. LoD = ELISA Limit Of Detection. Data are represented as Mean ± SEM (n=3). (B) Statistical analysis was performed using One sample t test KO versus WT; p≤0.05 was considered significant..... 63
Figure 28. MS4A4A effect on IFN-β release. IFN-β production were analysed by ELISA on WT and MS4A4A KO BMDMs treated or not with LPS 100ng/ml for, 2h, 8h and 24h. (A) Data are represented in pg/ml. (B) Data are represented as FOLD CHANGE (pg/ml KO versus pg/ml WT) as Mean ± SEM. (A-B) each symbol represents a different biological replicate (n=3-6); nd= not detectable. (A) Statistical analysis was performed using Mann-Withney test LPS versus vehicle; (B) statistical analysis was performed using One sample t test KO versus WT; p≤0.05 was considered significant. 64
Figure 29. Kinetic and magnitude differences in TLR-induced IL-10 production. (A-B) IL-10 production was analysed by ELISA on WT BMDMs treated with different TLRs agonist for, 2h, 8h and 24h. Data are represented as Mean ± SEM (n=4-6). (A) Statistical analysis was performed using Mann-Withney test stimulated versus vehicle; p≤0.05 was considered significant..... 66

Figure 30. TLR-induced IL-10 production IN WT and MS4A4A KO macrophages. (A-B) IL-10 production was analysed by ELISA on WT and KO BMDMs treated with different TLRs agonist for 2h, 8h and 24h. (A) IL-10 release is represented in pg/ml. (B) IL-10 release is represented as FOLD CHANGE (pg/ml KO versus pg/ml WT). Data are represented as Mean ± SEM and each symbol represent a different biological replicate (n=3); nd= not detectable. (A) Statistical analysis was performed using Mann-Withney test; (B) Statistical analysis was performed using One sample t test; p≤0.05 was considered significant..... 68
Figure 31. MS4A4A does not affect Il10 mRNA expression and stability. (A) Gene expression of IL10 in BMDMs WT and KO after treatment with vehicle and LPS 100 ng/ml for 2h, 8h and 24h. Data are represented as Mean ± SEM and each symbol represent a different biological replicate (n=3). Statistical analysis was performed using Mann-Withney test; p≤0.05 was considered significant. (B) Il10 mRNA decay in WT and KO MDMs after LPS + Actinomycin D treatment. 68
Figure 32. Impact of microtubule disruption and PKA inhibition on IL-10 Secretion. WT and KO BMDMs were stimulated with 100 ng/ml LPS for 2 h prior to treatment with nocodazole (10 μM) or the PKA inhibitor H89 (40 μM) for the final 1 h. (A-B) Effect of nocodazole on IL-10 ELISA. (C-D) Effect of H89 on IL-10 ELISA. Data are represented as Mean ± SEM and each symbol represent a different biological replicate (n=3-5). Statistical analysis was performed using Mann-Withney test; p≤0.05 was considered significant..... 69
Figure 33. MS4A4A impairs IL-10 accumulation in LPS-stimulated macrophages. IL-10 ELISA on protein lysates from WT and KO BMDMs stimulated or not with LPS ± Brefeldin for 2h or 8h. Data are represented as Mean ± SEM and each symbol represent a different biological replicate (n=3). Statistical analysis was performed using unpaired t test; p≤0.05 was considered significant..... 70
Figure 34. Reduced intracellular IL-10 in MS4A4A KO Macrophages by immunofluorescence. IL-10 immunofluorescence (IF) on WT and KO BMDMs stimulated with 100 ng/ml LPS ± Brefeldin A for 8h. (A) 10X IF images referring to one experiment representative of 2 analysed. (B) IL-10 IF quantification referred to panel A. Data are represented as Mean ± SEM. Statistical analysis was performed using Mann-Withney test; p≤0.05 was considered significant..... 71
Figure 35. Identification of an IL-10 storage pool in resting macrophages by immunofluorescence. (A) IL-10 IF on untreated WT BMDMs. 10X IF images referring to one experiment representative of 2 analysed. (B) IL-10 IF quantification referred to panel A. (C) IL-10 IF quantification on WT BMDMs treated or not with LPS ± Brefeldin for 8h. (B-C) Data are represented as Mean ± SEM and quantification is representative of one experiment of 2 analysed. Statistical analysis was performed using Mann-Withney test; p≤0.05 was considered significant..... 73
Figure 36. Validation of MS4A4A knockdown by siRNA in human macrophages. WB on total protein lysates for MS4A4A and vinculin. Panel (A) shows image referring to one experiment representative of 6 analysed. (B) Quantification of MS4A4A normalised on housekeeping (vinculin). Bars represent mean ± SEM and each symbol represent a different biological replicate (n=6).

Statistical analysis was performed using two-tailed unpaired (Mann-Whitney) Student's t test; p≤0.05 was considered significant. 73
Figure 37. MS4A4A silencing impairs IL-10 release in LPS-stimulated human macrophages. IL-10 production was analysed by ELISA on human macrophages ± LPS. Bars represent mean ± SEM and each symbol represent a different biological replicate (n=3). LoD = ELISA Limit Of Detection. Statistical analysis was performed using two-tailed unpaired (Mann-Whitney) Student's t test; p≤0.05 was considered significant. 74
Figure 38. MS4A4A expression correlates with joint inflammation and RA progression. MS4A4A transcript expression in synovial tissues presenting an F, M, or L pathotype, assessed by RNA-sequencing. P-values were calculated using the Kruskal–Wallis test with Dunn's post test, **P < 0.01, ****P < 0.0001. (D) Percentage of MS4A4A+cells in synovial tissues presenting an F, M, or L pathotype, assessed by immunohistochemistry (IHC) and quantified by digital image analysis. P-values were calculated using the Kruskal–Wallis test with Dunn's post test, *P < 0.05, **P < 0.01. Correlation between Ms4a4a relative expression and arthritis score (/4) for each individual paw (n = 33, distributed across day 2, day 6, and day 12 timepoints). P-value and r coefficient were calculated according to the Spearman correlation test (69). 76
Figure 39. MS4A4A expression in macrophages limits the CS therapeutic activity in arthritis. (A) Clinical score assessing forepaws and hind paws inflammation after STIA induction in WT and KO mice, injected intraperitoneally daily from D2 with 10 µg Dex or its vehicle. N = 20 to 22 animals per group. Scores of the KO+Dex group are significantly lower compared WT+Dex from day 3 (P < 0.01, as assessed by the two-way ANOVA test followed by Tukey's multiple comparisons). (B) Clinical score after STIA induction in WT KO mice, injected intraperitoneally 25 µg MTX or with PBS every 2 d from D2. N = 5 to 12 animals per group. Scores of the WT+MTX and KO+MTX groups do not statistically differ from untreated corresponding animals (as assessed by the two-way ANOVA test followed by Tukey's multiple comparisons). (C) Clinical score after STIA induction in WT and KO mice treated with a single intraperitoneal injection at day 2 of 2 mg/kg IVIg or with PBS. N = 5 to 12 animals per group. WT+IVIg and KO+IVIg scores are similarly and significantly reduced compared to untreated WT and KO from day 8 (P < 0.05, as assessed by the two-way ANOVA test followed by Tukey's multiple comparisons). (D) Ms4a4a transcript expression in BMDM stimulated with IL-4 alone (CT) or in combination with 1 µM of Dex, 5 ng/mL of MTX or 80 µg of IVIg for 18 h. n = 3 per group. P- values were assessed using the Mann–Whitney test, ***P < 0.001 (69). 77
Figure 40. Dexamethasone affect specifically Fcg3a and Fcer1g expression. (A) Correlation between MS4A4A transcript expression and FCGR3A (Left panel) orFCER1G (Right panel). P-value and r coefficient were calculated according to the Spearman correlation test. (B) FCGR3A transcript expression in synovial tissues presenting a pauci-immunefibroid (F), diffuse-myeloid (M), or lympho-myeloid (L) pathotype, assessed by RNA-sequencing. P-values were calculated using the Kruskal–Wallis test with Dunn'sposttest, **P < 0.01, ***P < 0.001. (C) Fcgr3a, Fcgr1, Fcgr2b Fcgr4 and

transcript expression in BMDM from WT and KO mice treated or not with 1 μM of Dex. Data are represented as Mean ± SEM and each symbol represent a different biological replicate. Statistical analysis was performed using the Mann–Whitney test; p≤0.05 was considered significant (69). ... 79
Figure 41. MS4A4A affect Dex effect on TNF-α and CXCL2 during Fcγ-mediated inflammatory response. (A) TNFα and CXCL2 cytokine production were analysed by ELISA on WT and MS4A4A KO BMDMs treated or not with 500 μg/mL of Agg-IVIG or 100 ng/mL LPS for 8h. 1 μM Dex was added 1 h before Agg-IVIg or LPS stimulation (n=4-10). (B) Tnfα and Cxcl2 transcript expression was assessed by RT-qPCR in the ankles of WT and KO mice treated with PBS or Dex at day 6 after STIA induction (n=6). Data are represented as Mean ± SEM and each symbol represents a different biological replicate. Statistical analysis was performed using the Kruskal–Wallis test with Dunn's post test; p≤0.05 was considered significant (69). ... 80
Figure 42.Transcriptional profiling of WT and MS4A4A KO macrophages revealed no difference in response to Dex. (A) Experimental design of bulk RNAseq: WT and MS4A4A KO BMDMs were treated with/without Dex (1 μM) for 2, 8 and 24 h. This experimental design generated 14 different experimental conditions investigated by RNAseq in biological triplicates. Schedule of performed comparison analysis is reported. (B) PCA on all samples using the top 2000 most variable genes assesses samples similarities and visualizes the separation of experimental groups in a 2-Dimensional space. (C-D) Volcano plots display $\log_2$ fold-change on the x-axis and $-\log_{10}$(FDR) on the y-axis for each contrast: (C) Dex-treated WT vs Dex-treated KO BMDMs at timepoint 2h, 8h and 24h; (D) Dex-treated vs vehicle both WT ad KO BMDMs at timepoint 2h, 8h and 24h; significantly up- and down-regulated genes (FDR < 0.01, $|\log_2 FC| \geq 2$) are highlighted in orange and blue, respectively. (E) Differential expression of selected genes in WT and MS4A4A KO BMDMs. For each gene, the table reports the $\log_2$ fold-change (logFC) in WT and KO (Dex-treated vs vehicle), the corresponding direction of regulation (Up, Down or NS = Not Significant), and the ΔlogFC, defined as the difference in logFC between WT and KO. The final column ("intersection") indicates the specific contrast(s) in which the gene was identified as significantly modulated. For example, "Dex_WT_24h" indicates the gene was significantly differentially expressed in WT at 24h, while "Dex_KO_24h | Dex_WT_24h" indicates the gene was regulated in both genotypes at the 24h timepoint (69). ... 82
Figure 43. MS4A4A does not interact with γ-chain of FcγRs. WT and KO BMDMs were stimulated or not with Agg-IVIg 500 μg/ml for 15 and 15 minutes. Cells were lysed, γ-chain and ms4a4a were immunoprecipitated (IP). (A) IP samples and total protein samples were immunoblotted (IB) for γ-chain, ms4a4a, FcγRIII and vinculin (housekeeping protein). (B) WB on total protein lysates that were immunoprecipitated as positive control of the IP. Panels show images referring to one experiment representative of 3 analysed (n=3). ... 83
Figure 44. Agg-IVIg induces pSyk activation independent of MS4A4A regulation. WT and KO BMDMs were stimulated or not with Agg-IVIg 500 μg/ml for 5, 15 and 15 minutes. (A) WB on total

protein lysates for pSyk, total Syk and vinculin. Panel shows image referring to one experiment representative of 3-6 analysed. (B) quantification of phosphorylated Syk corrected for total Syk. Bars represent mean ± SEM (n= 3-6). Data are represented as Mean ± SEM and each symbol represent a different biological replicate. Statistical analysis was performed using two-tailed unpaired (Mann-Whitney) Student's t test; p≤0.05 was considered significant; * versus vehicle; # versus 5 minutes. 84

Table 1. Stimuli used for BMDM treatment. 27
Table 2. Knowledge based scores of different ligands docked against MS4A4A and GR1. .. 41
Table 3. Identification of potential partners for MS4A4A by Mass Spectrometry-based Immunoprecipitation Proteomics. List of potential interactors of Ms4a4a in resting macrophages and Dex-treated macrophages. For each protein, the value of peptide spectral matches (PSMs) in each sample analyzed is reported. Frequency in WT (F(WT)) and KO (F(KO)) conditions for ms4a4a express the number of times that a given protein is identified with at least one PSM in each replicate for that condition (n=2). 49

Supplementary Figure 1. Enrichment Analysis (Reactome) of MS4A4A interactome in NT (A) and DEX-treated (B) BMDMs. 109

Supplementary Table 1. Taqman probes used for qPCR. 110
Supplementary Table 2. Syber sequences used for qPCR. 110
Supplementary Table 3. Primary antibodies used for Western Blot. 110
Supplementary Table 4. Commercially available drugs for Pocket2 with score ≥8.5. 111
Supplementary Table 5. List of the genes with ΔlogFC < 0.001 for each time point considered differentially expressed between WT and KO. 112

APPENDIX

Supplementary Figure 1. Enrichment Analysis (Reactome) of MS4A4A interactome in NT (A) and DEX-treated (B) BMDMs.

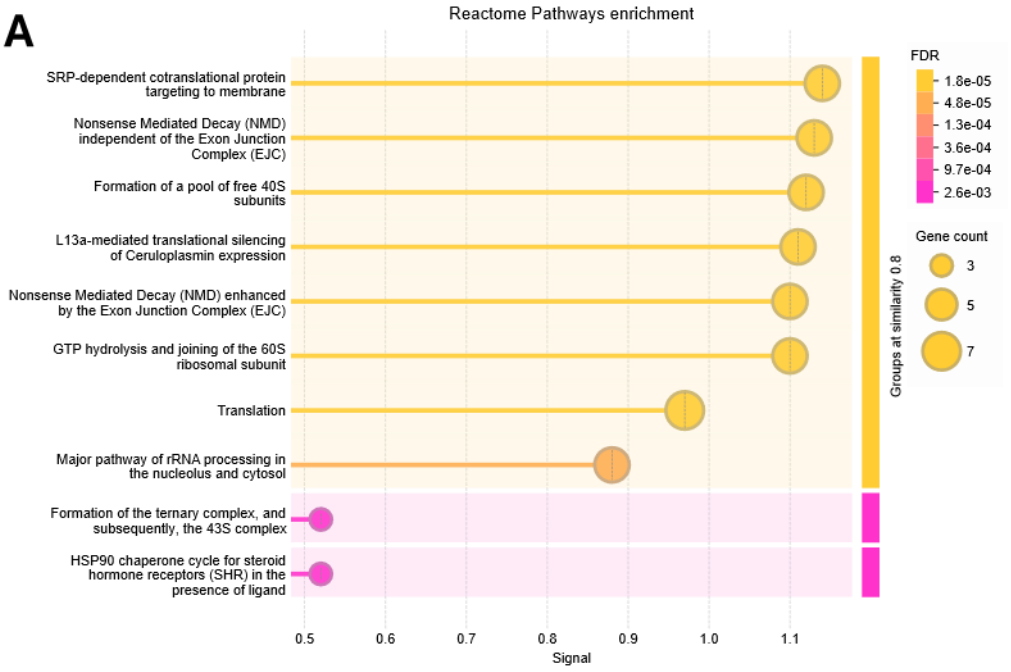

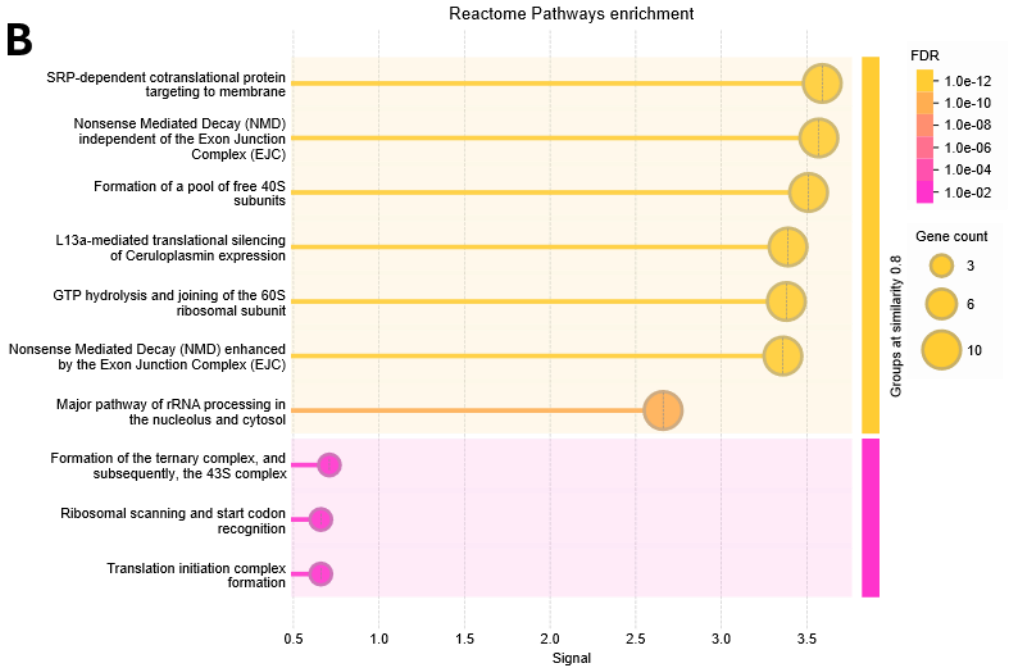

Supplementary Table 1. Taqman probes used for qPCR.

Gene	Assay ID	Company
Il10	Mm00439614	ThermoFisher
Ms4a4a	ARKA763 - custom	ThermoFisher
Ubc	Mm01201237	ThermoFisher

Supplementary Table 2. Syber sequences used for qPCR.

Gene	Primer Forward (5'-3')	Primer Reverse (5'-3')
Ms4a4a	CTGGGAAACATGGCTGTCATA	CTCATCAGGGCAGTCAGAATC
Rplp0	GGCGACCTGGAAGTC CAACT	CCATCAGCACCACAG CCTTC

Supplementary Table 3. Primary antibodies used for Western Blot.

Antibody	Source	Reactivity	Concentration	Company	Cat. N°
CD16/FcγRIII	Rabbit	Mouse	1:1000	Abcam	ab276040
FcεRI chain	Rabbit	Mouse	0.5 µg/ml	Merck	06-727
MS4A4A	Rabbit	human	1:500	Merck	HPA029323
MS4A4A	rat	Mouse	2 µg/ml	Mantovani lab (ICH)	-
Phospho-Syk	Rabbit	Mouse	1:1000	Cell Signaling	2710s
Syk	Rabbit	Mouse	1:1000	Cell Signaling	12358s
TLR2	Rabbit	Mouse	1:1000	Cell Signaling	13744S
vinculin	Rabbit	Mouse/human	1:10 000	Cell Signaling	13901s

Supplementary Table 4. Commercially available drugs for Pocket2 with score ≥8.5.

ID	Name	Formula	CAS	Score
DB01395	Drospirenone	$C_{24}H_{30}O_3$	67392-87-4	-10.0
DB14703	Dexamethasone metasulfobenzoate	$C_{29}H_{33}FO_9S$	16978-57-7	-9.8
DB00693	Fluorescein	$C_{20}H_{12}O_5$	05/07/2321	-8.9
DB11943	Delafloxacin	$C_{18}H_{12}ClF_3N_4O_4$	189279-58-1	-8.9
DB13158	Clobetasone	$C_{22}H_{26}ClFO_4$	54063-32-0	-8.8
DB14568	Ivosidenib	$C_{28}H_{22}ClF_3N_6O_3$	1448347-49-6	-8.8
DB12523	Mizolastine	$C_{24}H_{25}FN_6O$	108612-45-9	-8.7
DB15465	Benzhydrocodone	$C_{25}H_{25}NO_4$	1259440-61-3	-8.7
DB01419	Antrafenine	$C_{30}H_{26}F_6N_4O_2$	55300-29-3	-8.7
DB00209	Trospium	$C_{25}H_{30}NO_3$	47608-32-2	-8.6
DB08907	Canagliflozin	$C_{24}H_{25}FO_5S$	842133-18-0	-8.6
DB14723	Larotrectinib	$C_{21}H_{22}F_2N_6O_2$	1223403-58-4	-8.6
DB00324	Fluorometholone	$C_{22}H_{29}FO_4$	426-13-1	-8.6
DB00685	Trovafloxacin	$C_{20}H_{15}F_3N_4O_3$	147059-72-1	-8.6
DB13953	Estradiol benzoate	$C_{25}H_{28}O_3$	50-50-0	-8.6
DB00972	Azelastine	$C_{22}H_{24}ClN_3O$	58581-89-8	-8.6
DB11614	Rupatadine	$C_{26}H_{26}ClN_3$	158876-82-5	-8.6
DB08827	Lomitapide	$C_{39}H_{37}F_6N_3O_2$	182431-12-5	-8.6
DB06595	Midostaurin	$C_{35}H_{30}N_4O_4$	120685-11-2	-8.5
DB11750	Clobetasol	$C_{22}H_{28}ClFO_4$	25122-41-2	-8.5
DB12825	Lefamulin	$C_{28}H_{45}NO_5S$	1061337-51-6	-8.5
DB00443	Betamethasone	$C_{22}H_{29}FO_5$	378-44-9	-8.5
DB01029	Irbesartan	$C_{25}H_{28}N_6O$	138402-11-6	-8.5
DB08973	Fluclorolone acetonide	$C_{24}H_{29}Cl_2FO_5$	3693-39-8	-8.5
DB00396	Progesterone	$C_{21}H_{30}O_2$	57-83-0	-8.5
DB11260	Diacetyl benzoyl lathyrol	$C_{31}H_{38}O_7$	218916-52-0	-8.5
DB09280	Lumacaftor	$C_{24}H_{18}F_2N_2O_5$	936727-05-8	-8.5

Supplementary Table 5. List of the genes with ΔlogFC < 0.001 for each time point considered differentially expressed between WT and KO.

2h	WT					KO							
gene name	logFC LPS_vs_vehicle	FDR LPS_vs_vehicle	true.diff.exp LPS_ vs_vehicle	LPS MeanLogCPM	vehicle MeanLogCPM	logFC LPS_vs_vehicle	FDR LPS_vs_vehicle	true.diff.exp LPS_ vs_vehicle	LPS MeanLogCPM	vehicle MeanLogCPM	intersection	delta_logFC	FDR_delta
Zfpm1	-0,7	1,78E-01	NS	-0,1	0,6	-2,6	2,91E-05	Down	-1,4	0,9	LPS_KO_2h	1,9	6,37E-08
Tfap4	-1,2	7,01E-03	NS	-1,3	-0,2	-2,8	6,48E-07	Down	-2,1	0,3	LPS_KO_2h	1,5	3,98E-05
Ankrd23	-1,0	1,91E-02	NS	-0,6	0,3	-2,4	2,97E-06	Down	-1,3	0,8	LPS_KO_2h	1,3	1,14E-03
Cgref1	0,9	1,08E-01	NS	0,7	-0,2	2,0	6,20E-04	Up	0,7	-1,4	LPS_KO_2h	-1,2	8,54E-03
Tmem200b	8,0	1,43E-13	Up	3,2	-3,3	6,2	7,67E-13	Up	3,2	-2,4	LPS_KO_2h|LPS_WT_2h	1,8	2,91E-07
Tnn	6,1	8,29E-14	Up	3,6	-2,1	4,5	3,92E-12	Up	3,5	-0,9	LPS_KO_2h|LPS_WT_2h	1,6	1,55E-05
Il12b	9,7	3,95E-13	Up	6,5	-2,6	8,2	9,43E-13	Up	6,4	-1,8	LPS_KO_2h|LPS_WT_2h	1,4	2,19E-04
Etnk2	3,5	6,93E-05	Up	0,5	-2,8	4,8	1,12E-05	Up	0,4	-3,3	LPS_KO_2h|LPS_WT_2h	-1,3	2,28E-03
Nipal1	5,1	6,28E-09	Up	2,4	-2,2	6,4	1,23E-09	Up	2,1	-3,1	LPS_KO_2h|LPS_WT_2h	-1,3	1,28E-03
Tmem56	5,7	2,84E-07	Up	1,0	-3,4	7,0	8,12E-08	Up	0,9	-3,6	LPS_KO_2h|LPS_WT_2h	-1,3	1,28E-03
Fbxo40	3,5	7,49E-08	Up	2,0	-1,3	5,0	2,79E-10	Up	2,4	-2,2	LPS_KO_2h|LPS_WT_2h	-1,5	7,95E-05
Synpo2	3,9	2,17E-06	Up	1,3	-2,2	5,5	7,03E-08	Up	1,4	-3,0	LPS_KO_2h|LPS_WT_2h	-1,6	8,74E-06
Shisa3	6,2	2,01E-10	Up	3,2	-2,7	7,8	1,02E-11	Up	3,6	-3,2	LPS_KO_2h|LPS_WT_2h	-1,7	3,57E-06
Zfp811	3,6	3,60E-05	Up	0,3	-2,9	5,5	3,83E-07	Up	0,6	-3,3	LPS_KO_2h|LPS_WT_2h	-1,9	3,59E-08
Bpifc	2,2	4,72E-05	Up	0,9	-1,2	4,3	1,27E-08	Up	1,1	-2,6	LPS_KO_2h|LPS_WT_2h	-2,0	1,50E-09
Six1	5,2	1,92E-10	Up	2,2	-2,4	7,4	2,00E-11	Up	2,0	-3,5	LPS_KO_2h|LPS_WT_2h	-2,2	2,32E-11
Sele	8,6	5,78E-17	Up	4,9	-3,0	10,9	2,38E-17	Up	4,8	-3,6	LPS_KO_2h|LPS_WT_2h	-2,4	2,80E-13
Htra4	3,0	2,77E-06	Up	0,6	-2,0	1,7	6,04E-04	NS	0,6	-1,0	LPS_WT_2h	1,3	2,18E-03
Il19	5,1	1,47E-06	Up	0,7	-3,3	7,8	1,71E-06	NS	0,1	-3,8	LPS_WT_2h	-2,7	2,78E-17

8h	WT					KO							
gene name	logFC LPS_vs_vehicle	FDR LPS_vs_vehicle	true.diff.exp LPS_ vs_vehicle	LPS MeanLogCPM	vehicle MeanLogCPM	logFC LPS_vs_vehicle	FDR LPS_vs_vehicle	true.diff.exp LPS_ vs_vehicle	LPS MeanLogCPM	vehicle MeanLogCPM	intersection	delta_logFC	FDR_delta
Gemin4	-2,2	1,67E-01	NS	-1,8	2,0	-7,9	2,61E-03	Down	-3,4	3,2	LPS_KO_8h	5,8	1,09E-68
Tbc1d16	-1,8	1,09E-05	NS	-1,0	0,7	-3,9	2,96E-09	Down	-2,6	0,7	LPS_KO_8h	2,0	1,53E-07
Tmem200b	5,7	7,80E-09	NS	0,4	-3,5	4,2	1,98E-08	Up	1,0	-2,7	LPS_KO_8h	1,5	4,79E-04
Cenpp	-1,5	1,54E-05	NS	0,0	1,5	-3,0	5,98E-10	Down	-1,1	1,8	LPS_KO_8h	1,5	6,26E-04
Gm10134	2,2	3,99E-05	NS	0,6	-1,3	3,5	2,79E-07	Up	0,9	-2,2	LPS_KO_8h	-1,3	7,38E-03
Tcp10b	8,6	1,23E-08	Up	0,9	-3,8	4,9	6,44E-08	Up	1,5	-2,8	LPS_KO_8h|LPS_WT_8h	3,7	7,42E-28
Acot1	-5,6	8,70E-09	Down	-3,3	0,9	-9,1	3,05E-10	Down	-3,8	1,3	LPS_KO_8h|LPS_WT_8h	3,5	6,31E-24
Gm4841	11,5	1,75E-13	Up	3,7	-3,8	8,2	4,89E-13	Up	4,0	-3,3	LPS_KO_8h|LPS_WT_8h	3,3	6,46E-21
Tnfaip8l3	8,0	2,62E-12	Up	3,8	-3,1	6,0	6,25E-11	Up	3,6	-2,0	LPS_KO_8h|LPS_WT_8h	1,9	6,39E-07
Il2ra	8,8	1,06E-14	Up	5,0	-2,9	6,9	1,14E-13	Up	4,9	-1,5	LPS_KO_8h|LPS_WT_8h	1,9	1,02E-06
Rnf225	7,6	7,71E-13	Up	2,2	-3,5	5,7	1,55E-11	Up	2,2	-2,7	LPS_KO_8h|LPS_WT_8h	1,9	1,37E-06
Dll1	8,7	1,10E-17	Up	2,6	-3,6	6,8	1,24E-16	Up	2,6	-3,1	LPS_KO_8h|LPS_WT_8h	1,9	1,46E-06
Chrna5	7,7	9,05E-10	Up	1,5	-3,6	5,9	2,59E-08	Up	1,3	-3,4	LPS_KO_8h|LPS_WT_8h	1,8	5,80E-06
Nos2	14,7	2,08E-19	Up	10,7	-3,0	12,9	4,24E-19	Up	10,9	-1,7	LPS_KO_8h|LPS_WT_8h	1,8	5,89E-06
Ccl17	7,7	1,13E-11	Up	2,4	-3,5	6,0	2,10E-10	Up	2,3	-3,0	LPS_KO_8h|LPS_WT_8h	1,8	7,46E-06
U90926	7,0	2,85E-07	Up	0,9	-3,6	5,3	4,49E-06	Up	0,6	-3,3	LPS_KO_8h|LPS_WT_8h	1,7	1,52E-05
Mycl	8,4	7,23E-15	Up	4,4	-3,0	6,7	6,21E-14	Up	4,5	-2,0	LPS_KO_8h|LPS_WT_8h	1,7	4,77E-05
Gm29094	4,6	4,71E-09	Up	2,8	-1,7	3,0	1,94E-06	Up	2,6	-0,3	LPS_KO_8h|LPS_WT_8h	1,6	6,44E-05
Gm14403	-2,1	1,94E-05	Down	-1,0	1,0	-3,6	6,85E-08	Down	-2,5	0,9	LPS_KO_8h|LPS_WT_8h	1,5	2,76E-04
Fam83d	-3,1	2,07E-07	Down	-0,9	2,1	-4,6	1,41E-09	Down	-2,0	2,3	LPS_KO_8h|LPS_WT_8h	1,5	4,56E-04
110032F04R	9,5	1,13E-09	Up	1,8	-3,8	8,1	1,07E-09	Up	2,2	-3,6	LPS_KO_8h|LPS_WT_8h	1,4	1,04E-03
Rragb	-2,6	2,21E-09	Down	-0,9	1,5	-3,9	2,19E-11	Down	-2,2	1,3	LPS_KO_8h|LPS_WT_8h	1,3	3,28E-03
Kif14	-2,0	1,12E-03	Down	-1,4	0,6	-3,3	1,10E-05	Down	-2,1	0,9	LPS_KO_8h|LPS_WT_8h	1,3	3,52E-03
Srpk3	-2,5	2,33E-06	Down	-1,2	1,1	-3,8	5,03E-09	Down	-1,9	1,5	LPS_KO_8h|LPS_WT_8h	1,3	3,72E-03
Ankle1	-5,8	4,50E-11	Down	-3,0	2,0	-7,1	3,70E-12	Down	-3,3	2,4	LPS_KO_8h|LPS_WT_8h	1,3	8,46E-03
Synpo2	5,9	4,34E-11	Up	3,4	-2,0	7,2	2,42E-12	Up	4,2	-2,6	LPS_KO_8h|LPS_WT_8h	-1,4	2,89E-03
Rgs11	-3,9	2,53E-08	Down	-2,5	0,9	-2,5	9,51E-06	Down	-1,8	0,5	LPS_KO_8h|LPS_WT_8h	-1,4	2,78E-03
Dgat2	3,9	7,74E-14	Up	3,6	-0,1	5,3	6,29E-16	Up	3,9	-1,2	LPS_KO_8h|LPS_WT_8h	-1,4	1,43E-03
Lrrc4	5,4	5,83E-12	Up	2,5	-2,3	6,8	1,88E-12	Up	2,6	-3,3	LPS_KO_8h|LPS_WT_8h	-1,4	8,81E-04
Nuak1	-3,7	1,41E-07	Down	-2,1	1,3	-2,3	1,42E-04	Down	-1,4	0,7	LPS_KO_8h|LPS_WT_8h	-1,5	5,04E-04
Rtn2	4,3	1,66E-08	Up	1,9	-2,3	5,8	3,58E-10	Up	2,5	-2,7	LPS_KO_8h|LPS_WT_8h	-1,5	4,68E-04
Il17rd	4,1	2,87E-07	Up	1,8	-2,0	5,6	7,19E-09	Up	2,5	-2,7	LPS_KO_8h|LPS_WT_8h	-1,5	2,77E-04
Tmem151a	-5,3	2,00E-08	Down	-3,0	1,5	-3,8	2,46E-06	Down	-2,5	1,0	LPS_KO_8h|LPS_WT_8h	-1,5	2,41E-04
Gfi1	6,7	6,63E-13	Up	1,8	-3,3	8,3	8,51E-14	Up	2,4	-3,6	LPS_KO_8h|LPS_WT_8h	-1,6	1,68E-04
Cacnb3	3,8	1,19E-08	Up	2,8	-1,0	5,4	1,16E-10	Up	3,2	-2,2	LPS_KO_8h|LPS_WT_8h	-1,6	1,37E-04
Slc6a4	8,0	4,41E-17	Up	4,6	-2,7	9,5	1,95E-17	Up	4,9	-3,2	LPS_KO_8h|LPS_WT_8h	-1,6	1,36E-04
Gbp10	6,8	2,62E-12	Up	5,3	-1,8	8,4	6,21E-13	Up	5,5	-2,6	LPS_KO_8h|LPS_WT_8h	-1,6	7,19E-05
Bpifc	4,6	3,91E-09	Up	1,0	-2,8	6,2	5,15E-10	Up	1,1	-3,4	LPS_KO_8h|LPS_WT_8h	-1,7	3,39E-05
Edn1	10,0	9,33E-19	Up	6,7	-2,6	11,7	1,59E-18	Up	6,6	-3,5	LPS_KO_8h|LPS_WT_8h	-1,7	1,83E-05
Shisa3	8,5	2,87E-14	Up	5,0	-2,7	10,3	6,52E-15	Up	5,6	-3,2	LPS_KO_8h|LPS_WT_8h	-1,8	9,13E-06
Lrrc14b	-9,8	1,55E-10	Down	-3,5	4,7	-8,1	8,59E-11	Down	-2,6	5,1	LPS_KO_8h|LPS_WT_8h	-1,8	8,83E-06
Pif1	-6,9	5,05E-11	Down	-3,6	1,3	-5,0	6,25E-10	Down	-2,9	1,3	LPS_KO_8h|LPS_WT_8h	-1,9	2,84E-06
Frat2	-7,1	9,41E-16	Down	-3,3	2,4	-5,3	8,87E-15	Down	-2,4	2,4	LPS_KO_8h|LPS_WT_8h	-1,9	2,84E-06
Gm17296	-4,2	2,55E-06	Down	-3,0	1,0	-2,2	3,32E-04	Down	-0,9	1,2	LPS_KO_8h|LPS_WT_8h	-2,0	4,69E-07
Btla	6,1	4,19E-09	Up	1,6	-3,3	8,0	3,55E-10	Up	2,1	-3,6	LPS_KO_8h|LPS_WT_8h	-2,0	3,60E-07
Macc1	6,5	5,54E-09	Up	1,2	-3,5	8,6	2,01E-08	Up	0,8	-3,8	LPS_KO_8h|LPS_WT_8h	-2,1	5,52E-08
Tlr11	4,0	1,66E-07	Up	0,7	-2,8	6,1	4,05E-09	Up	1,0	-3,4	LPS_KO_8h|LPS_WT_8h	-2,2	1,35E-08
Ifnb1	6,7	5,55E-11	Up	2,9	-2,9	8,9	5,65E-11	Up	3,0	-3,6	LPS_KO_8h|LPS_WT_8h	-2,2	9,48E-09
Ppm1n	6,3	4,42E-09	Up	1,0	-3,5	8,6	6,11E-09	Up	0,9	-3,8	LPS_KO_8h|LPS_WT_8h	-2,3	4,78E-10
Il23r	9,3	1,65E-15	Up	3,9	-3,5	12,0	1,21E-15	Up	4,2	-3,8	LPS_KO_8h|LPS_WT_8h	-2,7	8,60E-14
Sectm1a	7,7	1,63E-10	Up	2,8	-3,3	10,6	1,71E-10	Up	2,8	-3,8	LPS_KO_8h|LPS_WT_8h	-2,9	6,87E-16
Asprv1	6,2	9,19E-11	Up	2,2	-3,2	10,0	2,91E-11	Up	2,2	-3,8	LPS_KO_8h|LPS_WT_8h	-3,8	2,49E-29
Pald1	-11,0	4,50E-09	Down	-3,8	3,2	-6,7	2,11E-08	Down	-2,8	3,2	LPS_KO_8h|LPS_WT_8h	-4,3	2,25E-37
Galnt9	-4,6	1,57E-08	Down	-3,1	0,5	-6,1	2,72E-09	NS	-3,5	0,5	LPS_WT_8h	1,4	1,25E-03
Anp32a	3,2	2,16E-07	Up	5,4	2,5	1,9	3,50E-04	NS	4,6	2,6	LPS_WT_8h	1,3	4,68E-03
Stab2	-2,6	1,46E-04	Down	-1,1	1,4	-1,3	3,65E-02	NS	-0,3	0,9	LPS_WT_8h	-1,3	3,31E-03
Angptl6	-2,8	4,74E-07	Down	-1,7	0,8	-1,2	4,41E-03	NS	-1,0	0,4	LPS_WT_8h	-1,5	2,53E-04
Timd4	7,9	7,32E-08	Up	3,6	-3,3	9,7	5,46E-06	NS	0,6	-3,8	LPS_WT_8h	-1,8	5,89E-06
Tgfb3	-3,4	1,32E-06	Down	-2,0	1,1	-1,5	3,39E-03	NS	-0,6	0,8	LPS_WT_8h	-1,8	3,43E-06
Nr1d1	-3,7	3,32E-09	Down	-1,8	1,7	-1,9	2,71E-05	NS	-0,4	1,6	LPS_WT_8h	-1,9	2,68E-06
Gm21985	-3,3	9,99E-03	Down	-2,3	2,2	-1,0	4,02E-01	NS	-1,2	-0,1	LPS_WT_8h	-2,3	2,42E-10
Hist1h2bq	-4,1	6,73E-04	Down	-2,9	1,0	-1,7	7,78E-02	NS	-1,1	0,4	LPS_WT_8h	-2,4	4,04E-11

24h	WT					KO							
gene name	logFC LPS_vs_vehicle	FDR LPS_vs_vehicle	true.diff.exp LPS_ vs_vehicle	LPS MeanLogCPM	vehicle MeanLogCPM	logFC LPS_vs_vehicle	FDR LPS_vs_vehicle	true.diff.exp LPS_ vs_vehicle	LPS MeanLogCPM	vehicle MeanLogCPM	intersection	delta_logFC	FDR_delta
U90926	8,8	2,33624E-07	NS	0,8	-3,8	6,0	1,49E-07	Up	1,7	-3,2	LPS_KO_24h	2,8	7,22E-11
Slit1	-1,0	2,28E-02	NS	-0,5	0,9	-3,3	3,29E-07	Down	-2,0	1,2	LPS_KO_24h	2,3	5,43E-07
Rnf225	5,9	4,23E-09	NS	0,5	-3,4	3,8	3,02E-07	Up	0,6	-2,8	LPS_KO_24h	2,0	2,08E-05
Rasgrf1	3,0	1,15E-05	NS	-0,1	-2,6	6,4	4,56E-09	Up	0,6	-3,6	LPS_KO_24h	-3,4	1,46E-16
Lrrc14b	-8,0	1,96E-08	Down	-3,3	3,0	-11,1	9,63E-09	Down	-3,8	3,3	LPS_KO_24h|LPS_WT_24h	3,2	4,68E-14
Csf3	10,0	2,83E-10	Up	2,2	-3,8	7,0	7,62E-10	Up	2,4	-3,3	LPS_KO_24h|LPS_WT_24h	3,0	3,18E-12
Meikin	8,7	7,39E-09	Up	0,9	-3,8	6,1	3,85E-08	Up	1,0	-3,4	LPS_KO_24h|LPS_WT_24h	2,6	1,37E-09
Plekhh2	-3,6	3,96E-08	Down	-2,2	1,5	-5,7	5,72E-10	Down	-3,2	1,6	LPS_KO_24h|LPS_WT_24h	2,2	3,87E-06
Cd163	-2,0	3,09E-04	Down	-0,4	2,0	-4,0	1,37E-07	Down	-1,6	2,4	LPS_KO_24h|LPS_WT_24h	2,0	4,94E-05
Styk1	6,6	1,36E-08	Up	0,6	-3,6	4,7	1,00E-07	Up	0,8	-2,9	LPS_KO_24h|LPS_WT_24h	1,9	1,42E-04
Ankrd66	4,7	6,13E-07	Up	0,6	-3,1	3,0	4,85E-05	Up	0,6	-2,1	LPS_KO_24h|LPS_WT_24h	1,7	1,57E-03
Tgfb3	-2,4	2,64E-05	Down	-1,2	1,0	-4,0	4,98E-08	Down	-2,0	1,4	LPS_KO_24h|LPS_WT_24h	1,6	3,74E-03
Slco2b1	-5,8	2,35E-11	Down	-3,2	1,8	-7,4	3,68E-11	Down	-3,6	1,5	LPS_KO_24h|LPS_WT_24h	1,6	6,90E-03
Nrcam	-4,0	4,31E-09	Down	-1,4	2,2	-5,5	1,32E-10	Down	-2,6	2,5	LPS_KO_24h|LPS_WT_24h	1,5	9,49E-03
Gbp2b	6,3	5,02E-08	Up	2,2	-3,0	7,9	7,21E-08	Up	1,7	-3,6	LPS_KO_24h|LPS_WT_24h	-1,5	9,26E-03
Car2	5,7	5,56E-13	Up	3,9	-1,7	7,3	1,23E-13	Up	3,9	-2,6	LPS_KO_24h|LPS_WT_24h	-1,6	6,17E-03
Fam3b	7,7	2,35E-14	Up	3,8	-3,0	9,2	6,79E-15	Up	4,1	-3,5	LPS_KO_24h|LPS_WT_24h	-1,6	6,17E-03
Il6	9,0	1,01E-12	Up	4,6	-3,0	10,6	1,71E-13	Up	5,4	-3,4	LPS_KO_24h|LPS_WT_24h	-1,6	3,48E-03
Antxr1	3,1	3,70E-09	Up	1,7	-1,1	4,7	2,79E-11	Up	1,7	-2,5	LPS_KO_24h|LPS_WT_24h	-1,6	3,40E-03
Slc6a4	5,3	9,63E-12	Up	2,1	-2,4	7,0	9,20E-13	Up	2,4	-3,2	LPS_KO_24h|LPS_WT_24h	-1,7	1,59E-03
Gm16181	4,3	3,76E-08	Up	1,2	-2,7	6,1	2,87E-10	Up	2,0	-3,1	LPS_KO_24h|LPS_WT_24h	-1,8	7,29E-04
Cxcl3	7,0	4,56E-12	Up	5,0	-1,8	9,0	1,74E-12	Up	4,9	-3,0	LPS_KO_24h|LPS_WT_24h	-2,0	8,44E-05
Syt7	4,4	6,34E-08	Up	1,6	-2,3	6,4	2,79E-09	Up	1,8	-3,3	LPS_KO_24h|LPS_WT_24h	-2,0	3,58E-05
Rtn4rl1	-6,6	2,15E-10	Down	-3,4	1,4	-4,6	1,42E-08	Down	-3,1	1,2	LPS_KO_24h|LPS_WT_24h	-2,0	2,91E-05
Il23r	10,5	3,23E-17	Up	5,7	-3,4	13,2	8,97E-17	Up	5,4	-3,8	LPS_KO_24h|LPS_WT_24h	-2,7	1,16E-09
Gstt4	8,0	5,41E-10	Up	1,8	-3,6	10,7	2,65E-11	Up	2,9	-3,8	LPS_KO_24h|LPS_WT_24h	-2,7	5,12E-10
Apol9a	6,8	1,63E-13	Up	4,6	-2,0	10,7	2,49E-14	Up	4,7	-3,6	LPS_KO_24h|LPS_WT_24h	-3,8	8,45E-21
Olr1	4,6	1,98E-10	Up	1,5	-2,6	9,2	1,93E-11	Up	1,4	-3,8	LPS_KO_24h|LPS_WT_24h	-4,6	1,02E-30
Amica1	2,0	1,61E-03	Up	2,2	0,2	0,4	5,22E-01	NS	1,3	0,7	LPS_WT_24h	1,6	3,84E-03
0I0109I03Ri	3,9	1,13E-06	Up	0,4	-2,9	2,3	3,49E-04	NS	-0,1	-1,9	LPS_WT_24h	1,6	6,17E-03
Galnt9	-6,3	8,10E-10	Down	-3,6	0,4	-4,6	5,09E-08	NS	-3,3	0,1	LPS_WT_24h	-1,7	1,40E-03
Hist1h2ae	-3,3	2,23E-06	Down	-2,4	0,4	-0,4	5,17E-01	NS	-0,7	-0,4	LPS_WT_24h	-2,9	1,00E-11
Rpgrip1	-3,8	2,08E-08	Down	-1,7	1,7	-0,9	4,81E-02	NS	0,5	1,6	LPS_WT_24h	-2,9	8,38E-12

Part of the results of this were published in the following manuscript: *Boutet MA, Mattiola I, Silva-Gomes R, Nerviani A, Sironi M, Ghirardi GM, Troilo A et al. Synovial MS4A4A correlates with inflammation and counteracts response to corticosteroids in arthritis. Proceedings of the National Academy of Sciences. 2025 Sep 16;122(37);* ***doi: 10.1073/pnas.2504529122***

DISSEMINATION OF RESULTS

The results of this PhD research have been periodically disseminated during internal events (e.g. Report Days and PhD Retreat) as well as through presentations at both national and international scientific conferences. These opportunities have allowed for the early sharing of data and feedback within the scientific community. In the coming months, the final experiments are expected to be completed, and the study will be submitted for publication in a peer-reviewed journal. This step is intended to promote the transfer of knowledge to the broader scientific community and to foster the widest possible integration and collaboration among researchers in the field. Additionally, data described in paragraph 4, titled *"Role of MS4A4A in modulating dexamethasone response in rheumatoid arthritis"*, have been partially published (69): *Boutet MA, Mattiola I, Silva-Gomes R, Nerviani A, Sironi M, Ghirardi GM, Troilo A et al. Synovial MS4A4A correlates with inflammation and counteracts response to corticosteroids in arthritis. Proceedings of the National Academy of Sciences. 2025 Sep 16;122(37).*

Short lay summary - Italian

Il nostro sistema immunitario è composto da molte cellule diverse che ci proteggono da infezioni e malattie. Una di queste cellule, chiamata macrofago, ha un ruolo fondamentale nel controllare l'infiammazione e aiutare il corpo a guarire. Il mio progetto di dottorato si è occupato di studiare una proteina chiamata MS4A4A, presente soprattutto nei macrofagi, che potrebbe essere importante per il loro corretto funzionamento. MS4A4A sembra aiutare a ridurre l'infiammazione e potrebbe interagire con altre proteine coinvolte nella risposta immunitaria. Modificazioni a carico di questa proteina sono state associate a malattie come l'artrite reumatoide, il cancro e l'Alzheimer ma il suo ruolo non è ancora del tutto chiaro.
In questo progetto ho studiato MS4A4A al fine di capire la sua struttura e dove si trova nella cellula, scoprire con quali altre proteine interagisce e capire come influisce sulla risposta immunitaria. Una migliore comprensione di come funziona questa proteina nel macrofago potrebbe aiutare a sviluppare nuovi modi per controllare l'infiammazione e curare malattie legate al sistema immunitario.

Short lay summary - English

Our immune system is made up of many different cells that protect us from infections and diseases. One of these cells, called a macrophage, plays a fundamental role in controlling

inflammation and helping the body heal. My PhD project focused on studying a protein called MS4A4A, which is mainly expressed in macrophages and may be important for their proper function. MS4A4A appears to help reduce inflammation and may interact with other proteins involved in the immune response. Changes in this protein have been linked to diseases such as rheumatoid arthritis, cancer and Alzheimer’s disease, although its exact role is still not fully understood. In this project, I studied MS4A4A to understand its structure and cellular localization, to identify with which other proteins it interacts, and to explore how it affects the immune response. A better understanding of how this protein works in macrophages could help develop new ways to control inflammation and treat diseases related to the immune system.